Joint Radar-Communication Systems: Modulation Schemes and System Design

Lucas Giroto de Oliveira, *Graduate Student Member, IEEE*, Benjamin Nuss, *Graduate Student Member, IEEE*, Mohamad Basim Alabd, *Graduate Student Member, IEEE*, Axel Diewald, *Graduate Student Member, IEEE*, Mario Pauli, *Senior Member, IEEE*, and Thomas Zwick, *Fellow, IEEE*

***Abstract*—The joint radar-communication (RadCom) concept has been continuously gaining interest due to the possibility of integrating radar sensing and communication functionalities in a same radio-frequency hardware platform. Besides a number of challenges in terms of hardware design and signal processing, the choice of suitable modulation schemes plays a significant role in driving the performance of RadCom systems. In this sense, this article presents an overview of state-of-the-art modulation schemes for RadCom systems, namely chirp sequence, phase-modulated continuous wave, orthogonal frequency-division multiplexing, and orthogonal chirp-division multiplexing. For each of them, a detailed system model is outlined and parameters for quantifying both radar and communication performances are presented. Finally, a comparative analysis of the aforementioned RadCom modulation schemes is carried out to illustrate the presented discussion.**

***Index Terms*—Chirp sequence (CS), orthogonal chirp-division multiplexing (OCDM), orthogonal frequency-division multiplexing (OFDM), phase-modulated continuous wave (PMCW), radar-communication (RadCom).**

I. Introduction

DUE to the growing number of applications that occupy frequency spectra at steadily increasing carrier frequencies as well as their need for connectivity and sensing capabilities [1], there has been a growing interest in the convergence of radar sensing and communication systems [2], [3]. Not only the coexistence of both systems has been investigated, but also their radar-centric, communication-centric, or multiobjective co-design [4]–[7], e.g., both applications sharing the same hardware platform and therefore having common transmit and/or receive signals, while distinct processing strategies are adopted to obtain communication data and estimate parameters of radar targets. The concept of co-existing and co-designed systems supporting both radar sensing and communication is, for example, known as joint communication and sensing (JCAS), also named joint wireless communication and radar sensing or joint communication and radar/radio sensing and abbreviated as JC&S, JCS, JCR, or JCRS [6], [8]–[11], joint radar-communications (JRC) [4], [12], [13], wireless communication and radar sensing (C&R) [7], depending on whether the system design is radar- or communication-centric. In the particular case where the same signal is used for both applications, the joint system is known as a dual-functional radar-communication (DFRC) [14]–[16], dual-functional communication and radar sensing (DFCS) [17], or joint radar-communication (RadCom) system [18], [19]. Since the proposal of what is known as the world's first RadCom system in 1963 [20], through the introduction of a RadCom system based on orthogonal frequency-division multiplexing (OFDM) in 2009 [21], until efforts towards the convergence of radar sensing and communication in the context of beyond fifth-generation (5G) and sixth-generation (6G) networks [2], significant advances have been made in the RadCom field as thoroughly described in [15].

In a radar-centric perspective, a possible application of the RadCom concept is in the context of highly automated driving (HAD) [22], where vehicle-to-vehicle (V2V) and vehicle-to-infrastructure (V2I) communication can be achieved by embeddeding communication symbols into the radar signal and used, e.g., for traffic coordination and interference avoidance among radar sensors [23]–[25]. Such tasks can be performed by approaches such as coordination on physical and link layer levels among devices serving as a shared platform in a protocol-based approach to alternate radar and communication operation [26], [27] , or by a RadCom approach consisting of the transmission of radar signals with embedded communication symbols [28]–[31]. A further radar-centric application of the RadCom concept is in the context of radar networks [32], where hybrid active-passive radars can use the same signal to perform bistatic measurements as well as to extract communication data which aims to coordinate and synchronize radar nodes within the network.

Focusing on the use of already-existing communication platforms for, e.g., providing radar as a service (RaaS) [33], [34], the application of the RadCom concept in a communication-centric approach enables a wide range of possibilities for beyond 5G and 6G networks. Those include accurate detection and tracking of unmanned aerial vehicles (UAVs) based on echoes of communication signals emitted by base stations [6], [35] and environment mapping by user equipments (UEs) via radar processing on received echoes from communication signals [36], [37]. Another possible communication-centric RadCom application is the use of multiple 5G New Radio

Manuscript received May 1st, 2021; revised September 1st, 2021; accepted September 22nd, 2021. This work was supported by the Federal Ministry of Education and Research (BMBF), Germany, through the Project "ForMikro-REGGAE", under Grant 16ES1061. The work of L. Giroto de Oliveira was financed by the German Academic Exchange Service (DAAD) - Funding program number 57440921. *(Corresponding author: Lucas Giroto de Oliveira.)*

The authors are with the Institute of Radio Frequency Engineering and Electronics (IHE), Karlsruhe Institute of Technology (KIT), 76131 Karlsruhe, Germany (e-mail: lucas.oliveira@kit.edu, benjamin.nuss@kit.edu, mohamad.alabd@kit.edu, axel.diewald@kit.edu, mario.pauli@kit.edu, and thomas.zwick@kit.edu).

(NR) demodulation reference signals (DMRSs) on the UE side as bistatic radar measurements of a multistatic network [11] for accurate target localization.

In both aforementioned RadCom approaches, efficient modulation schemes must be adopted, in which appropriate communication performance can be achieved and the influence of transmitted data on ultimately obtained radar images can be minimized or removed. On the one hand, radar-centric applications can be supported by RadCom systems based on, e.g., chirp sequence (CS) [29], [38] or the digital phase-modulated continuous wave (PMCW) [39], [40], which jointly enable radar sensing and reliable, low-latency communication at low data rates. In the radar literature, the first modulation scheme is also known as fast-chirp frequency-modulated continuous wave (FMCW) [28], while the latter is alternatively named code-modulated, spread spectrum, or pseudo-noise (PN) radar [22], [29]. On the other hand, digital multicarrier modulation schemes such as OFDM [41], [42] and orthogonal chirp-division multiplexing (OCDM) [43], [44] are preferred in communication-centric applications where higher data rate and spectral efficiency are required.

In this context, the present article provides an overview of the four aforementioned state-of-the-art modulation schemes for RadCom systems, being its main contributions as follows:

- A literature review on state-of-the-art research on enablement of RadCom systems, ranging from hardware requirements to signal processing algorithms.
- A discussion on both radar and communication aspects for the considered modulation schemes, including analog and digital processing steps, system architectures, as well as radar and communication performances and trade-offs.
- Closed-form expressions for as accurate as possible system modeling and parameters for efficient system design and performance prediction of RadCom systems are presented.
- A radar-centric comparative performance analysis based on simulation and measurement results to support the carried-out discussion.

The remainder of this article is organized as follows. Section II presents a literature review on state-of-the-art research on enablement of RadCom systems. Next, Section III outlines a generic RadCom system model and presents specific system design and performance aspects assuming the use of CS, PMCW, OFDM, and OCDM modulation schemes. Section IV then presents a comparative performance analysis of the four considered RadCom modulation schemes assuming a radar-centric parameterization, and concluding remarks are finally given in Section V.

Notation

Throughout this article, t denotes time in seconds, f denotes frequency in Hertz, and $\mathrm{rect}(t)$ is the rectangular function that takes the value 1 for $t \in [0, 1)$ and 0 otherwise. Additionally, $(\cdot)^*$ is the complex conjugate operator, $(\cdot)^T$ is the transpose operator, and $\langle\cdot\rangle_\upsilon$ is the modulo υ operator, $\upsilon \in \mathbb{N}_+$. Furthermore, $\Re\{\cdot\}$ and $\Im\{\cdot\}$ denote the real and imaginary parts of a complex number, respectively, $\mathcal{A}_\varphi\{\cdot\}$ aliases back high-frequency components of a signal into the $[-\varphi/2, \varphi/2]$ frequency range, $\varphi \in \mathbb{R}_+$, and $Q(\cdot)$ is the Q-function defined as $Q(\chi) = \left(1/\left(2\pi\right)^{1/2}\right) \int_\chi^\infty \mathrm{e}^{-\psi^2/2}\, d\psi$ for $\chi \in \mathbb{R}$.

II. State-of-the-art research on joint radar-communication systems

For an appropriate operation of RadCom systems, a number of aspects must be considered. In this context, some of the main defining factors that have been investigated in the technical literature are hardware challenges, analog and digital signal processing and the choice for a modulation scheme, which are addressed in Subsections II-A to II-C, respectively.

A. Hardware challenges

Some of the main hardware constraints that are common to both radar- and communication-centric RadCom systems [33] are (i) linearity and efficiency of power amplifiers (PAs), (ii) in-band full duplex (IBFD) operation of transmit and receive channels with enough isolation, (iii) low noise figure, high gain and compression point in low-noise amplifiers (LNAs), as well as (iv) digital-to-analog converters (DACs) and analog-to-digital converters (ADCs) with high resolutions in all-digital RadCom systems. Those constraints are mainly imposed by radar sensing requirements, and are described as follows.

Regarding (i), both radar and communication applications demand increasing bandwidths, which makes the PA design considerably more challenging. Furthermore, typical modulation schemes for radar-centric RadCom systems such as CS and PMCW usually impose low PA linearity requirements [39]. However, if one adopts modulation schemes that yield significantly higher peak-to-average power ratios (PAPRs) such as OFDM [42] and OCDM [43], the PA efficiency suffers a fair reduction since a back-off from the PA compression point is necessary.

The required isolation for appropriate IBFD operation mentioned in (ii) is a long-known problem in radar and radar-centric RadCom systems. Usually, isolation of several tens of decibels are mandatory for extending the maximum detectable range [33], since the self-interference (SI) power from transmit to receive channels defines the LNA compression point mentioned in (iii) and may limit the RadCom system sensitivity to targets at far ranges. In communication-centric RadCom systems, however, this is a new challenge to be faced either via self-interference cancellation (SIC) and decoupling techniques [45] or by solely performing bistatic measurements, in which the transmit and receive channels are not collocated [11].

Besides the aforementioned issues related to (ii) and (iii), the maximum detectable range in a RadCom system is also limited by the quantization noise [40]. While this may not necessarily a problem in communication-centric RadCom networks where radar sensing is only provided as an additional feature, the need for high-resolution ADCs and DACs mentioned in (iv) becomes a critical issue in radar-centric RadCom systems based on digital modulation schemes such as PMCW, OFDM, and OCDM due to the required high sampling rates. In this context, a typically required sampling rate of $1\,\mathrm{GSa/s}$

at a bit resolution of 14 bits yields a data rate of $28\,\mathrm{Gbit/s}$ per transmit or receive channel with one in-phase/quadrature (I/Q) channel each to be handled by a field programmable gate array (FPGA), e.g., in a simple single-input single-output (SISO) configuration of a RadCom system [46]. The aforementioned high data rates in fully-digital radar systems result in the challenging task of handling the many digital signal processing operations, whose computational complexity can be estimated similarly to the OFDM and OCDM cases in [47], in a short time interval, as well as in the requirement for storages ranging from about 35 to $70\,\mathrm{MB}$ for typical receive data frame durations between $10\,\mathrm{ms}$ and $20\,\mathrm{ms}$ would be required, which becomes even higher in multiple-input multiple-output (MIMO) configurations. To overcome those issues, bandwidth enlargement and/or sampling rate reduction techniques can be adopted for radar-centric, OFDM-based RadCom systems. Due to the compatibility between OFDM and OCDM modulation schemes [43], such techniques can in principle also be applied to OCDM-based RadCom systems. Bandwidth enlargement methods comprise techniques such as the use of frequency combs [48], [49], linear frequency-modulated carriers [50], and stepped carrier frequencies [51]–[53]. As a sampling rate reduction technique, compressed sensing can also be employed with the drawback of increased computational complexity for radar processing [54].

In the specific case of radar-centric RadCom systems based on chirp signals, time-frequency ramp generators using phase-locked loops (PLLs) that lock over wide bandwidths while presenting appropriate linearity and low phase noise [33] face additional requirements. Furthermore, the PLL-controlled oscillator must run coherently to ensure that phase-modulated communication symbols can be correctly identified at the receiver of other communication or RadCom systems, which is usually not a constrain in chirp-based, radar-only systems. In case data modulation strategies such as frequency-shift keying (FSK) are adopted, non-coherent setups can be alternatively adopted as in the proposed chirp-based RadCom system implementation in [55]. In all of the aforementioned cases, however, the complex design of fully integrated transmit and receive analog front-ends is a constant challenge to be faced [56], [57].

In the context of fully-digital RadCom systems, however, recent advances show the possibility of modularizing the hardware design with independent front- and back-end blocks [46]. An example is the scalable MIMO platform presented in [58], which supports the implementation of PMCW-based systems. In the aforementioned design, the presence of binary phase-shift keying (BPSK) modulators enables the transmission of pseudorandom binary sequences (PRBSs) carrying binary data symbols for simultaneous radar and communication operation. For flexible fully-digital RadCom systems, however, general-purpose front-ends as the one described in [59] can be adopted. Consequently, the necessary system adjustments for enabling the implementation of RadCom systems based on any digital modulation scheme rely on adjustments of the baseband processing, e.g., on an FPGA back-end. In the specific case of [59], a real time implementation of a $76\,\mathrm{GHz}$ OFDM radar, which inherently supports RadCom operation, has been reported. It is finally worth highlighting that, to alleviate requirements in front-ends for fully-digital RadCom systems and efficiently deal with the high experienced data rates in such systems, recent studies in the literature make use of platforms such as the Xilinx RFSoCs [60], which have features as, e.g., flexible digital up and down converters.

B. Analog and digital signal processing

A further research field in the state-of-the-art literature on RadCom systems comprises analog and digital signal processing techniques to either alleviate some of the hardware requirements discussed in Subsection II-A or complement them in enabling the operation of RadCom systems [7].

In terms of digital signal processing, a number of techniques has been proposed for both radar- and communication-centric RadCom systems. Those include, e.g., interference cancellation (IC) techniques for both enabling coexistence of radar, communication, and RadCom systems [61], among which are the use of stepped-carrier OFDM [30], [62] mentioned in Subsection II-A. Additionally, techniques for compensating the influence of received communication signals on the radar sensing performance play a significant role in RadCom systems [63], [64], especially in radar-centric applications. In the context of communication-centric RadCom systems, where the available bandwidth for communication and sensing may not cover an uninterrupted frequency range, techniques based on, e.g., compressed sensing for extracting radar target parameters from RadCom signals have also been proposed [65]. Aiming not only to enable RadCom operation, but also to optimize it, studies as [66] propose joint signal optimization having, e.g., sum rate as an optimization parameter for communication and mutual information or the Cramer-Rao bound for radar sensing, while observing constraints such as multi-user interference and effective channel gain.

Another main topic in this field is the optimization of omnidirectional and directional beam patterns [67]–[69] via analog [70], digital [71] or hybrid beamforming [72]. In this context, hardware limitations such as quantized phase shifters and non-ideal beam pattern of antenna arrays [17] are taken into account at a transmit beamforming stage to optimize the fractions of power from the same RadCom signal that are transmitted towards either radar targets to be sensed or communication and RadCom receivers [71]. Additionally, receive beamforming can yield spatial filtering of interference and clutter from directions that are not of interest, which also results in a reduction of the overall receive power and therefore alleviates hardware requirements. A joint beamforming optimization at both RadCom transmitter and receiver can be performed, having, e.g., the optimization of the radar target detection and SIC for enabling IBFD operation as the main goals and communication link requirements as constraints [72]–[76]. Lastly, the joint use of beamforming and orthogonal signals has also been investigated for scenarios where data is embedded on signals that are used for jointly serving multiple communication users and performing radar sensing [77], [78].

C. Modulation schemes

Besides satisfying basic hardware and signal processing requirements, a suitable modulation scheme must be adopted to enable efficient communication and radar sensing in a RadCom system. Straightforward approaches to enable RadCom operation include embedding communication data onto any type of radar signal, e.g., via beam-pattern modulation. However, the choice of more elaborate modulation schemes [28], [29] that are both compatible with existing radar and communication technologies and allow efficient system parameterization to yield desired performance in both tasks of RadCom systems is preferred. In this sense, the already-mentioned CS, PMCW, OFDM, and OCDM modulation schemes have been perceived as attractive solutions in the RadCom literature.

In the CS context, a number of RadCom modulation scheme variants has been proposed in the literature. Among those, partial modulation of chirps [79] and phase coding of chirps [80] allow the transmission of several modulation symbols per chirp, which on the one hand increases the achievable data rate, but on the other hand degrade the range sidelobe level in obtained radar images and may cause intersymbol interference (ISI) and prevent appropriate equalization under multipath conditions. A further approach is the modulation of the time-frequency chirp pattern [24], [81]. In this case, however, the required pre-processing of the receive radar signal to compensate the influence of transmit data onto range sidelobes is very sensitive to eventual phase rotations of the signal. Alternative solutions to the joint RadCom signal include time-division duplexing (TDD) between signals for radar sensing and communication, which may, e.g., consist of a sequence of unmodulated chirps that serves as radar sensing signal and communication preamble followed by a sequence of modulated, overlapping chirps for communication with higher spectral efficiency [25], [34], [82]. In this context, a digital signal generation at the transmitter is demanded, which is an additional requirement w.r.t. currently available CS-based radar devices. Additionally, simultaneous radar sensing and communication is not possible, and a balance between both tasks must be carefully found.

Regarding binary PMCW, a considerably lower number of RadCom approaches has been reported in the literature. A possible approach is the binary phase-modulation of PRBSs adopting BPSK or its differential variant, which attains low data rates but sufficiently preserves the radar sensing performance [83]–[86]. The low data rate yielded by the use of BPSK could be compensated by using information bits to be transmitted to generate the PRBS, e.g, by defining the initial state of a linear-feedback shift register (LFSR) that generates maximum-length sequences (MLSs) [83]. At the PMCW-based RadCom system, however, multiple correlators for the various possible MLSs would be necessary.

Usually, CS and PMCW modulation schemes are mainly intended for radar-centric applications where the hardware platform must be kept relatively simple. In contrast, digital multicarrier modulation schemes such as OFDM [21], [59], [87]–[91] and OCDM [47], [92] are preferred in both radar-centric RadCom applications where more flexibility for, e.g., MIMO operation and in communication-centric RadCom applications where high spectral efficiency and data rates are targeted. The first modulation scheme is based on the transmission of orthogonal subcarriers and offers the possibility of achieving quasi-unbiased radar estimation via a zero forcing (ZF)-like radar channel estimation to remove the influence of transmit modulation symbols [21], [63], [64], [89], [93]. In its turn, the latter modulation scheme uses orthogonal subchirps to perform transmission of data belonging to digital modulation constellations, and uses a correlation-based receiver that yields range sidelobes depending on the transmit modulation symbols [47]. Further processing approaches for OCDM-based systems that yield unbiased channel estimation for sensing purposes have already been proposed, e.g., in [94], but no extension to the RadCom concept has been reported in the literature yet. In terms of communication performance, however, OCDM-based systems tend to achieve better results compared to their OFDM counterpart [95] if no further measures such as frequency-selective bit and power allocation [96] are taken, since OCDM cannot straightforwardly profit from such techniques due to its spread spectrum nature. This is mainly due to their greater robustness against a number of impairments, including multipath propagation, Doppler shifts, ISI even under reduced cyclic prefix (CP) lengths [97], and narrowband interference (NBI) [98], which is associated with their spread spectrum characteristic and can be explained, e.g., by the discrete Fresnel transform (DFnT) circular convolution theorem [99]. Alternative digital multicarrier modulation schemes that have already been investigated in the RadCom context comprise generalizations of OFDM and OCDM such as orthogonal time-frequency space (OTFS) [100], filter bank multicarrier (FBMC) [101], generalized frequency-division multiplexing (GFDM) [102], which achieve somewhat similar trade-offs between radar sensing and communication performances as the two aforementioned modulation schemes. An important similarity among the aforementioned OFDM- and OCDM-based modulation schemes in a RadCom context is the possibility of applying the index modulation (IM) principle [14] to jointly transmit modulated data and limit the occupancy of frequency tones within the considered bandwidth [103]. While the application of IM may not be straightforward in all OFDM and OCDM variations, the concept has been increasingly gaining attention in recent studies in the literature as an approach to avoid interference in highly populated scenarios.

Given this background, Section III presents a detailed description of the system models as well as radar and communication performance parameters for RadCom systems based on variants of CS, PMCW, OFDM, and OCDM that allow appropriate RadCom operation. Although specific modulation schemes are presented, the carried-out discussions are easily extendable to other RadCom system based on the four aforementioned modulation schemes.

III. Modulation schemes for joint radar-communication

Let a SISO RadCom system be based on an IBFD radio-frequency (RF) device that transmits signals jointly used for

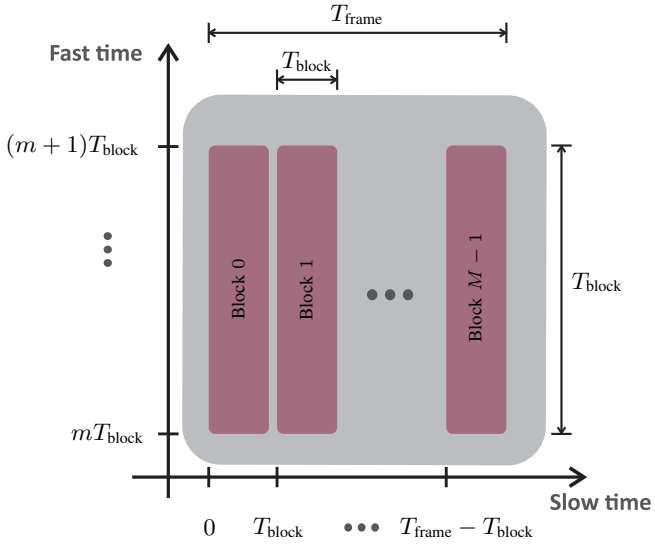

Fig. 1. RadCom frame structure. The fast time axis comprises the time interval in which every mth block is transmitted, having a total duration T_{block}. For the sake of simplicity, no time granularity is defined for the fast time axis since it depends on the sampling period that changes with the adopted modulation scheme. In its turn, the slow time axis marks the start of each mth block, having therefore time granularity equal to T_{block} and total duration T_{frame}.

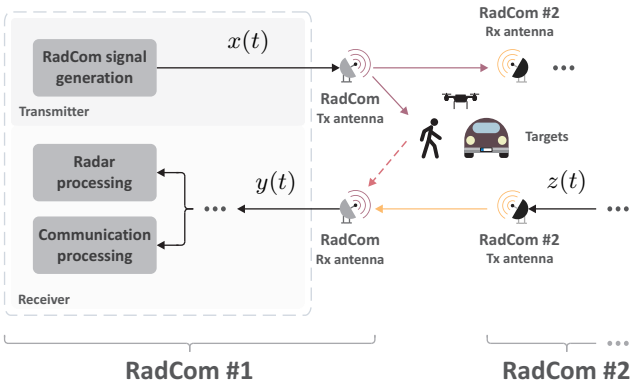

Fig. 2. Basic RadCom system representation.

radar sensing and carrying modulated data for communicating with other RadCom or communication systems. Moreover, the considered RadCom system is also capable of performing both radar parameter estimation and extracting modulated data coming from other RadCom or communication systems from its receive signal. It is further assumed that this RadCom system performs transmission based on frames of time duration T_{frame}, which are comprised of $M \in \mathbb{N}_+$ consecutive blocks of time duration T_{block}, resulting in $T_{\text{frame}} = MT_{\text{block}}$. A serial representation of the RadCom frame structure is depicted in Fig. 1, where the blocks within the frame have index $m \in \{0, 1, \ldots, M-1\}$, fast time is the continuous time axis within the duration of a block and slow time is the discrete time axis with time step equal to T_{block}. At the transmitter of the RadCom system, each block is individually modulated with data belonging to a modulation constellation. Similarly, the blocks are individually evaluated at the receiver of the RadCom system. While the communication processing at the RadCom receiver consists of extracting modulated data from each block individually, the radar processing consists of estimating one range profile per block, based on which a range-velocity radar image is finally computed.

In this context, the system model depicted in Fig. 2 comprises the considered RadCom system, represented as RadCom #1, radar targets, and another RadCom system, which is represented as RadCom #2. It is assumed that the signals $x(t) \in \mathbb{R}$ and $z(t) \in \mathbb{R}$, where $t \in [0, T_{\text{frame}})$, carry frames transmitted by RadCom #1 and RadCom #2, respectively, besides occupying the frequency band $f \in [f_{\text{c}} - B/2, f_{\text{c}} + B/2]$. Consequently, both RadCom #1 and #2 occupy an RF bandwidth B centered at the carrier frequency $f_{\text{c}} \gg B$.

The analog signal $x(t)$ containing a transmit frame of the RadCom #1 in the form of a serial burst of blocks is transmitted with the power $P_{\text{Tx}} \in \mathbb{R}_{\geq 0}$ by the transmit antenna of RadCom #1, propagates through the medium and: (i) travels through a total of $P \in \mathbb{N}_+$ paths, labeled as $p \in \{0, 1, \ldots, P-1\}$, and is captured by the receive antenna of RadCom #2; and (ii) is reflected off a total of $H \in \mathbb{N}_+$ radar point targets, labeled as $h \in \{0, 1, \ldots, H-1\}$, and is captured by the receive antenna of RadCom #1 itself. For the sake of simplicity, it is assumed that RadCom #1 and RadCom #2 have quasi-collocated transmit and receive antennas and identical hardware so that the wireless communication channel between them is reciprocal, and that multipath-free propagation of reflections off radar point targets takes place. Although those assumptions neglect some aspects of the dominant scattering behavior in radar scenarios, they result in a simplified system model that allows fair assessment of the influence of adopted modulation schemes and processing strategies on the radar performance and have been also made in other studies in the literature [18], [35], [64]. Furthermore, it is considered that changes in the positions and velocities of scatterers are negligible, so that the only changes in the experienced radar and communication channels within the measurement time are Doppler-shift induced phase rotations. Based on those assumptions, the captured signal $y(t) \in \mathbb{R}$ by the receive antenna of RadCom #1 can be expressed as

$$\begin{aligned} y(t) \approx & \sum_{h=0}^{H-1} \alpha_h^{\text{rad}} x(t - \tau_{\text{target},h}) \mathrm{e}^{\mathrm{j}2\pi f_{\text{D,target},h} t} \\ & + \sum_{p=0}^{P-1} \alpha_p^{\text{com}} z(t - \tau_{\text{path},p} - \tau_{\Delta}) \mathrm{e}^{\mathrm{j}2\pi f_{\text{D,path},p} t} \mathrm{e}^{\mathrm{j}2\pi f_{\Delta} t} \\ & + n(t). \end{aligned} \tag{1}$$

The first term in (1) represents the quasi-monostatic radar reflections suffered by $x(t)$ off H radar point targets and captured by the receive antenna of RadCom #1, accounting for the attenuation factor α_h^{rad}, the delay $\tau_{\text{target},h}$, and the Doppler shift $f_{\text{D,target},h}$. In this term, the attenuation factor α_h^{rad} results from the propagation through the overall traveled path of length $2R_h$ by $x(t)$ to the hth target and back to RadCom #1, being $R_h = c_0 \tau_{\text{target},h}/2$ the range of the hth target w.r.t. RadCom #1, the reflection off the hth target and other factors,

and can be expressed as [63]

$$\alpha_h^{\text{rad}} = \sqrt{\frac{G_{\text{Tx}}\ G_{\text{Rx}}\ \lambda_0^2\ \sigma_{\text{RCS},h}}{(4\pi)^3\ R_h^4}}. \tag{2}$$

In (2), G_{Tx} and G_{Rx} are the transmit and receive antenna gains, respectively, that are equal for both RadCom #1 and RadCom #2, $\lambda_0 = c_0/f_{\text{c}}$ is the wavelength associated with the carrier frequency f_{c}, and $\sigma_{\text{RCS},h}$ is the radar cross section (RCS) of the hth target. Additionally, the delay $\tau_{\text{target},h}$ from the first term in (1) is associated with the overall traveled path of length $2R_h$ by $x(t)$, while the Doppler shift $f_{\text{D,target},h} = 2v_{\text{target},h}/\lambda_0$ results from the relative radial velocity $v_{\text{target},h}$ of the hth target w.r.t. RadCom #1. It is worth highlighting that carrier phases due to reflection off radar targets are neglected for simplicity since they are only relevant for direction of arrival (DoA) estimation, which would only be possible in a MIMO RadCom system.

In its turn, the second term in (1) represents the P versions of the transmit signal $z(t)$ of RadCom #2 after travelling through P paths and being captured by the receive antenna of RadCom #1. This term accounts for: (i) the attenuation factor α_h^{com}, (ii) the delay $\tau_{\text{path},p}$, and (iii) the Doppler shift $f_{\text{D,path},p}$ suffered by $z(t)$ due to its propagation and reflection off scatterers through the pth path between the transmit antenna of RadCom #2 and the receive antenna of RadCom #1, as well as (iv) the time offset τ_Δ and (v) the frequency offset f_Δ between RadCom #1 and #2. It is worth highlighting that both τ_Δ and f_Δ, as well as resulting phase rotations, are affected by relative motion between RadCom #1 and #2, which ultimately leads to the need of more frequent channel state information (CSI) estimation at the receiving RadCom system for both communication and IC purposes and can be achieved by similar strategies to, e.g., the one introduced in [104]. Assuming for simplicity that $z(t)$ suffers a single reflection while traveling through the the pth path, the attenuation factor α_p^{com} can be expressed as [27]

$$\alpha_p^{\text{com}} = \sqrt{\frac{G_{\text{Tx}}\ G_{\text{Rx}}\ \lambda_0^2 \rho_p^2}{(4\pi)^2\ R_{\text{path},p}^2}}, \tag{3}$$

where ρ_p is the reflection coefficient associated with the pth path, and $R_{\text{path},p} = c_0\tau_{\text{path},p}/2$ is the overall path length traveled by $z(t)$ from RadCom #2 to RadCom #1.

After the reception by RadCom #1, the signal $y(t)$ undergoes analog conditioning, down-conversion to the baseband, and digital-to-analog (D/A) conversion. Next, two distinct processing strategies are performed on $y(t)$ to estimate radar parameters of the H targets and extract communication symbols transmitted by RadCom #2. Assuming that ideal separation of the radar and communication contributions of $y(t)$ is achieved and that all target reflections are clearly separated from each other according to the range resolution ΔR and relative radial velocity resolution Δv, besides being constrained to the maximum tolerable range R_{max} and relative radial velocity v_{max}, the radar processing ultimately yields a range-velocity radar image, in which the hth point target appears as a peak with signal-to-noise ratio (SNR) w.r.t. the resulting additive white Gaussian noise (AWGN) after signal processing given by

$$SNR_{\text{image},h} = \frac{P_{\text{Tx}}\ G_{\text{Tx}}\ G_{\text{Rx}}\ \sigma_{\text{RCS},h}\ \lambda_0^2\ G_{\text{p}}}{(4\pi)^3\ R_h^4\ k_{\text{B}}\ B\ T_{\text{therm}}\ NF}, \tag{4}$$

where G_{p} is the modulation-scheme-dependent radar processing gain resulting from operations to form the range and relative radial velocity profiles, k_{B} is the Boltzmann constant, T_{therm} is the standard room temperature in Kelvin, and NF is the overall receiver noise figure. In the denominator of (4), the term $k_{\text{B}}\ B\ T_{\text{therm}}\ NF$ accounts for the power of the sampled version of the AWGN $n(t)$. Besides influencing the ultimately experienced SNR, the considered parameters in (4) also play a role in defining the required ADC dynamic range and the corresponding number of ADC bits $N_{\text{bit}}^{\text{ADC}} \in \mathbb{N}_+$. Assuming that an analog compensation of coupling between transmit and receive antennas takes place, which is, e.g., the case in CS-based RadCom systems, the required *effective* ADC dynamic range after radar signal processing $\mathcal{D}_{\text{image}}$ so that the quantization noise and the thermal noise are at the same level in the ultimatelly obtained range-velocity radar image is

$$\mathcal{D}_{\text{image}} = \frac{P_{\text{Tx}}\ G_{\text{Tx}}\ G_{\text{Rx}}\ \sigma_{\text{RCS,max}}\ \lambda_0^2\ G_{\text{p}}}{(4\pi)^3\ R_{\text{min}}^4\ k_{\text{B}}\ B\ T_{\text{therm}}\ NF}, \tag{5}$$

where $\sigma_{\text{RCS,max}}$ is the maximum expected target RCS and R_{min} is the minimum expected target range. In fully-digital radars such as PMCW, OFDM, OCDM, the aforementioned analog compensation of the coupling is not always possible, which can lead to a high coupling level between the transmit and receive antennas. Assuming that the coupled signal has much higher power than any received target reflection and defining a power coupling factor $C_{\text{Tx,Rx}}$, the required *effective* ADC dynamic range becomes

$$\mathcal{D}_{\text{image}} = \frac{P_{\text{Tx}} C_{\text{Tx,Rx}} G_{\text{p}}}{k_{\text{B}}\ B\ T_{\text{therm}}\ NF}. \tag{6}$$

Since the processing gain G_{p} in (5) and (6) increases the power of the target peak in the radar image w.r.t. to both thermal noise and quantization noise and it is only experienced after radar signal processing, the required *physical* ADC dynamic range is equal to $\mathcal{D}_{\text{image}}/G_{\text{p}}$. Consequently, the required number of ADC bits $N_{\text{bit}}^{\text{ADC}} \in \mathbb{N}_+$ can finally be calculated based on the approximate relationship assumed in [105], i.e.,

$$10\log_{10}(\mathcal{D}_{\text{image}}/G_{\text{p}}) = 1.76 + 6.02 N_{\text{bit}}^{\text{ADC}}. \tag{7}$$

For the sake of conciseness, it is henceforth assumed that the sufficient number of ADC bits is adopted so that the aforementioned dynamic range requirement are satisfied.

For communication purposes, the SNR measure of interest is the E_{b}/N_0, which denotes energy per bit to noise power spectral density ratio that is jointly influenced by all P paths and depends on both the adopted modulation scheme and modulation constellation. It is worth highlighting that IC must be performed before further communication processing in case RadCom #1 receives signals from other RadCom or communication systems besides RadCom #2. As the power of received radar target reflections is typically much lower than that of communication signals, IC for the radar contribution to the

receive signal $y(t)$ is henceforth not considered. Furthermore, no additional constraints on the calculated ADC dynamic ranges according to (5) or (6) apply since radar operation of the considered RadCom system typically demands much higher number of bits $N_{\text{bit}}^{\text{ADC}}$ than required for communication purposes.

A more detailed analysis of both radar sensing and communication performances depends significantly on particular aspects of the adopted RadCom modulation scheme. In this sense, Subsections III-A to III-D present an overview of RadCom systems based on CS, PMCW, OFDM, and OCDM modulation schemes, providing further details on their respective block-frame structures, processing steps, and performance metrics for radar sensing and communication.

A. Chirp Sequence

In the considered SISO CS-based RadCom system, the frame of the joint RadCom transmit signal is a chirp sequence that comprises $M^{\text{CS}} \in \mathbb{N}_+$ blocks of time duration $T_{\text{block}}^{\text{CS}}$. Each of those blocks comprise (i) a linear chirp of time duration $T_{\text{chirp}}^{\text{CS}}$ that sweeps the frequency band $f \in [f_{\text{c}} - B^{\text{CS}}/2, f_{\text{c}} + B^{\text{CS}}/2]$, where B^{CS} is the RF bandwidth occupied by the CS-based RadCom system, with a chirp rate $\mu = B^{\text{CS}}/T_{\text{chirp}}^{\text{CS}}$ and is modulated by symbols belonging to a quadrature phase-shift keying (QPSK) constellation, and (ii) a guard interval of time duration $T_{\text{guard}}^{\text{CS}}$. The resulting time duration of a block is therefore $T_{\text{block}}^{\text{CS}} = T_{\text{chirp}}^{\text{CS}} + T_{\text{guard}}^{\text{CS}}$, while the resulting frame duration is expressed as $T_{\text{frame}}^{\text{CS}} = M^{\text{CS}} T_{\text{block}}^{\text{CS}} = M^{\text{CS}}(T_{\text{chirp}}^{\text{CS}} + T_{\text{guard}}^{\text{CS}})$.

The processing chain of the considered CS-based RadCom system is depicted in Fig. 3. At the transmitter side, the chirp belonging to the mth block, $m \in \{0, 1, \ldots, M^{\text{CS}} - 1\}$, is modulated with the mth QPSK symbol from the modulated data stream $\mathbf{d}_{\text{Tx}}^{\text{CS}} \in \mathbb{C}^{M^{\text{CS}} \times 1}$. Taking the architecture of the commercially-available radar sensor AWR1843 from TI [106] as a reference, the linear chirps are generated with the combination of an oscillator with direct digital synthesis (DDS) or a PLL, the QPSK modulation is achieved via a programmable analog phase shifter. It is also worth highlighting that, since information is modulated by altering the phase of transmit chirps, the oscillator must run coherently to avoid distorting the QPSK symbols. Next, the modulated chirp sequence undergoes amplification by a PA, which has low linearity requirements due to its chirp-like input signals, and the resulting signal $x^{\text{CS}}(t) \in \mathbb{R}$ is transmitted by the transmit antenna. Omitting power factors for the sake of simplicity, the continuous time domain signal containing the mth block of the transmit frame can be expressed for $t \in \left[mT_{\text{block}}^{\text{CS}}, (m+1)T_{\text{block}}^{\text{CS}}\right)$ as in (8). In this equation, $S_m^{\text{CS}} \in \mathbb{C} | S_m^{\text{CS}} = \mathrm{e}^{\mathrm{j}\phi_m^{\text{CS}}}$ denotes the mth QPSK symbol carried by the transmit frame in the CS-based RadCom system, which is modulated in the form of the phase $\phi_m^{\text{CS}} \in \{\pi/4, 3\pi/4, 5\pi/4, 7\pi/4\}$. The continuous-time signal $x^{\text{CS}}(t)$ containing the frame comprising M^{CS} blocks transmitted by the CS-based RadCom system can therefore be expressed as

$$x^{\text{CS}}(t) = \sum_{m=0}^{M^{\text{CS}}-1} s_m^{\text{CS}}(t) \ \text{rect}\left(\frac{t - mT_{\text{block}}^{\text{CS}}}{T_{\text{block}}^{\text{CS}}}\right). \tag{9}$$

Based on the presented concepts, Fig. 4 depicts a serial representation of the frame in the considered CS-based RadCom system, where non-linear sections of the chirps outside the frequency band of interest are not depicted for simplicity.

At the receiver of the CS-based RadCom system, the signal $y^{\text{CS}}(t) \in \mathbb{R}$, which according to (1) contains the output version of $x^{\text{CS}}(t)$ by the radar channel, the output version of the signal $z^{\text{CS}}(t) \in \mathbb{R}$ transmitted by another RadCom system from the communication, and additive noise, is captured by the receive antenna. It is then amplified by an LNA and mixed with copies of the unmodulated transmit chirps in an I/Q receiver, which returns a signal containing beat frequencies associated with reflections off radar targets and received communication signals. It is worth highlighting that, although an I/Q receiver is not mandatory for CS-based radar sensing [38], some studies on CS radar adopt it [107] and, in the considered system, this receiver architecture is necessary for correctly identifying the QPSK symbols contained in receive signals that have been transmitted by other CS-based RadCom systems. The resulting signal then undergoes further analog conditioning, including high-pass (HP) filtering to discard the low beat frequencies resulting from the spillover between transmit and receive antennas, amplification, and low-pass (LP) filtering. Alternatively, the three last stages can be interpreted as a band-pass (BP) filtering. The ultimately obtained analog signal undergoes analog-to-digital (A/D) conversion with sampling rate F_{s}^{CS} and corresponding sampling period $T_{\text{s}}^{\text{CS}} = 1/F_{\text{s}}^{\text{CS}}$. Compared to the sampling rate required at the ADCs of digital RadCom systems, F_{s}^{CS} can assume much lower values since it will only limit the maximum unambiguous range [38], [107] and the processing gain, without degrading further radar sensing performance parameters. Consequently, a rather simple and cost-effective RadCom hardware platform can be used for the considered CS-based RadCom system.

Next, the resulting samples from both I and Q channels are converted into the real and imaginary parts of a serial vector. The aforementioned vector then undergoes serial-to-paralell (S/P) conversion to form a frame with M_{CS} columns, each of them containing blocks of length $N_{\text{block}}^{\text{CS}}$, where $N_{\text{block}}^{\text{CS}} \in \mathbb{N}_+ | N_{\text{block}}^{\text{CS}} = T_{\text{block}}^{\text{CS}}/T_{\text{s}}^{\text{CS}}$ is the number of samples resulting from A/D conversion with sampling rate F_{s}^{CS} of a single block consisting of a modulated linear chirp and a guard interval. Subsequently, the frame of size $N_{\text{block}}^{\text{CS}} \times M_{\text{CS}}$ undergoes sample selection, which is denoted as SS in Fig. 3 and

$$s_m^{\text{CS}}(t) = \begin{cases} \cos\left(2\pi\left(f_{\text{c}} - B^{\text{CS}}/2\right)\left(t - mT_{\text{block}}^{\text{CS}}\right) + \pi\mu\left(t - mT_{\text{block}}^{\text{CS}}\right)^2 + \phi_m^{\text{CS}}\right), & t \in \left[mT_{\text{block}}^{\text{CS}}, mT_{\text{block}}^{\text{CS}} + T_{\text{chirp}}^{\text{CS}}\right) \\ 0, & t \in \left[mT_{\text{block}}^{\text{CS}} + T_{\text{chirp}}^{\text{CS}}, (m+1)T_{\text{block}}^{\text{CS}}\right) \end{cases} \tag{8}$$

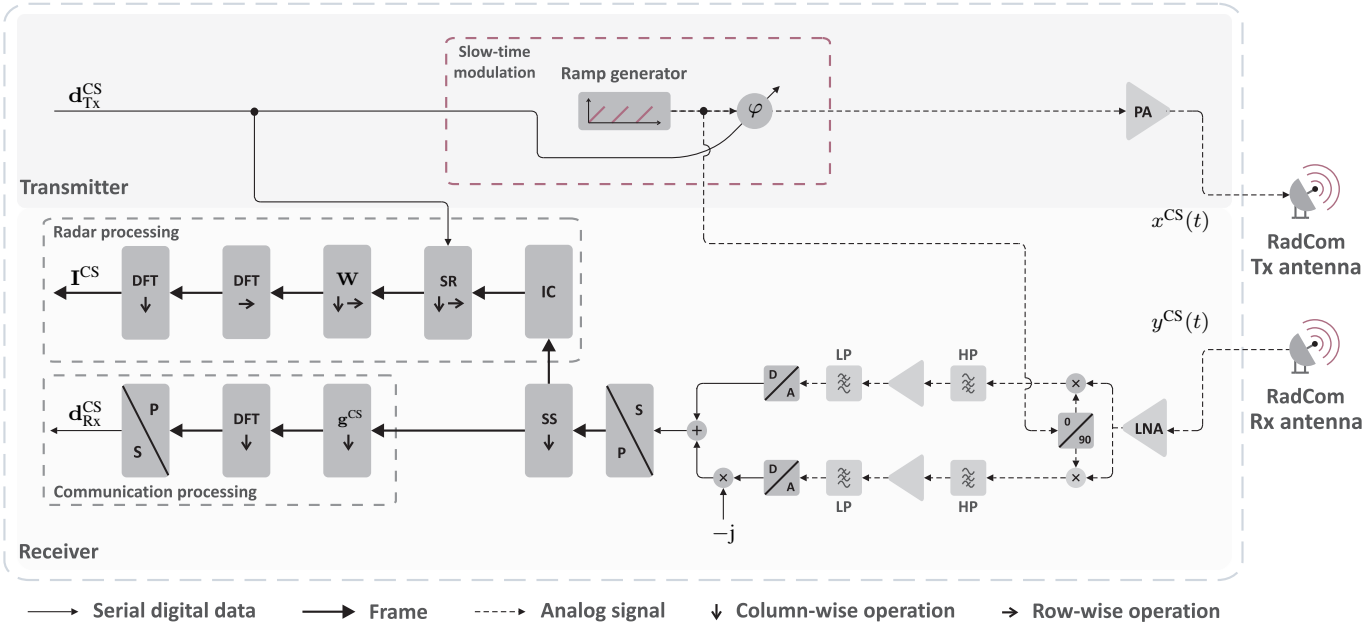

Fig. 3. SISO CS-based RadCom system representation.

consists of discarding the $N_{\text{guard}}^{\text{CS}} \in \mathbb{N}_+ | N_{\text{guard}}^{\text{CS}} = T_{\text{guard}}^{\text{CS}}/T_{\text{s}}^{\text{CS}}$ last samples associated with the guard interval of each block. It is worth highlighting that additional samples at the beginning and end of the remaining $N_{\text{chirp}}^{\text{CS}} \in \mathbb{N}_+ | N_{\text{chirp}}^{\text{CS}} = N_{\text{block}}^{\text{CS}} - N_{\text{guard}}^{\text{CS}}$ samples are usually discarded since they only contain noise and products of non-linear parts of transmit and receive chirps. From this point, different processing steps are performed to generate a radar image and extract data from communication signals originally contained in $y^{\text{CS}}(t)$. The remaining radar and communication processing steps are detailed in Subsections III-A1 and III-A2, respectively, while multiplexing schemes for MIMO or multiuser operation of the considered CS-based RadCom system are discussed in Subsection III-A3.

1) Radar processing: The remaining radar processing steps in the considered CS-based RadCom system start with IC, which consists of removing the influence of communication signals, which are originally transmitted by other RadCom or communication systems, from the output frame from the sample selection processing. Next, the resulting frame undergoes symbol removal, which is denoted in Fig. 3 as SR and consists of multiplying each column with the complex conjugate of the QPSK symbol used to modulate the corresponding transmit chirp. The resulting matrix then undergoes range and velocity windowing in fast- and slow-time directions, respectively. Subsequently, discrete Fourier transforms (DFTs) are performed in the slow-time direction to convert Doppler-shift-induced phase rotations of each chirp within the chirp sequence [38], [40], [107] into Doppler shift estimates, which can be translated into relative radial velocity estimates. The last radar processing step consists of performing DFTs in the fast-time direction to estimate beat frequencies, which can be translated into range estimates.

Based on the aforementioned radar processing steps, the ultimately obtained range-velocity radar image $\mathbf{I}^{\text{CS}} \in \mathbb{C}^{N_{\text{chirp}}^{\text{CS}} \times M^{\text{CS}}}$ experiences a processing gain G_{p}^{CS} and has a range resolution ΔR^{CS} and a maximum unambiguous range $R_{\text{max,unamb}}^{\text{CS}}$. The latter is defined based on the maximum detectable beat frequency that is assumed to be equal to F_{s}^{CS}. Since the sampling frequency F_{s}^{CS} only allows to dectect frequencies from $-F_{\text{s}}^{\text{CS}}/2$ to $F_{\text{s}}^{\text{CS}}/2$ in baseband, the actual beat frequencies from $F_{\text{s}}^{\text{CS}}/2$ to F_{s}^{CS} can be simply extracted from the negative frequencies of the sampled spectrum since no actual negative beat frequencies are experienced. Additionally, $\mathbf{I}^{\text{CS}}$ has a relative radial velocity resolution Δv^{CS} and a maximum unambiguous relative radial velocity $v_{\text{max,unamb}}^{\text{CS}}$. Based on [38], [40], [107], the aforementioned radar parameters are shown in Table I at the end of Section III. Since the symbol removal indicated in Fig. 3 must be appropriately performed, consecutive modulated chirps cannot have significant overlap at the CS-based RadCom receiver. As a tolerance to such overlaps is application-dependent, no restriction on maximum tolerable range is defined in Table I. Also, a maximum tolerable relative radial velocity must be defined according to the tolerable range bias due to the range-Doppler coupling effect [107]. Since it is application dependent and there is no common rule in the literature, no maximum tolerable relative radial is listed in Fig. 3 for the considered CS-based RadCom system.

2) Communication processing: First, the time, frequency and phase offsets from the second term in (1) are assumed to be removed via synchronization based on a preamble, e.g., consisting of unmodulated chirps as in [24], [25], [33], [34]. The remaining communication processing steps in the considered CS-based RadCom system start with a ZF time-domain equalization (TDE) via element-wise multiplication of each block by the vector $\mathbf{g}^{\text{CS}} \in \mathbb{C}^{N_{\text{chirp}}^{\text{CS}} \times 1}$ that contains the multiplicative inverse of an estimate of the experienced communication channel $\mathbf{h}^{\text{CS}} \in \mathbb{C}^{N_{\text{chirp}}^{\text{CS}} \times 1}$. Based on the DFT theorems, the aforementioned division in the discrete-time domain leads to a deconvolution in the discrete-frequency do-

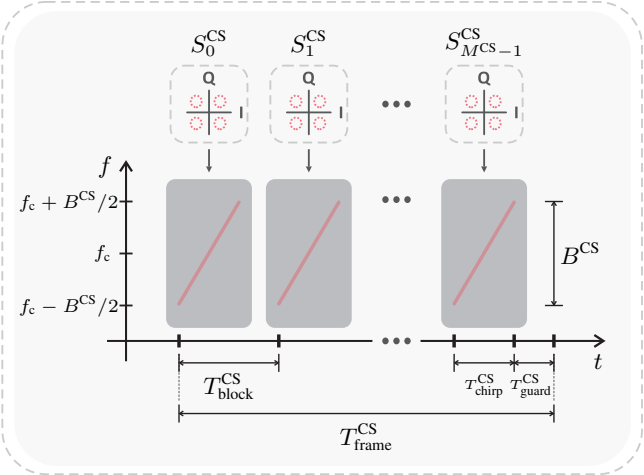

Fig. 4. CS frame serial representation.

main, which removes the effects of the communication channel on the beat frequencies associated with the contribution of $z^{\mathrm{CS}}(t)$ to the receive signal $y^{\mathrm{CS}}(t)$ in the CS-based RadCom system. It is worth highlighting that the channel impulse response (CIR) estimate must be updated periodically via the use of unmodulated pilot chirps to account for phase rotations introduced by Doppler shifts of scatterers indicated in (1). Subsequently, DFTs are performed in the slow-time direction, which together with the previous processing steps constitutes a matched-filter-like communication receiver. The resulting matrix finally undergoes paralell-to-serial (P/S) conversion, having the receive QPSK symbols extracted from the peak at the first samples of its columns to generate the receive modulated data stream $\mathbf{d}_{\mathrm{Rx}}^{\mathrm{CS}} \in \mathbb{C}^{M^{\mathrm{CS}}\times 1}$. Based on the presented communication processing steps in the considered CS-based RadCom system, the resulting data rate $\mathcal{R}_{\mathrm{QPSK}}^{\mathrm{CS}}$, energy per bit to noise power spectral density ratio $(E_\mathrm{b}/N_0)_{\mathrm{QPSK}}^{\mathrm{CS}}$ and bit error ratio (BER) denoted by $\mathrm{BER}_{\mathrm{QPSK}}^{\mathrm{CS}}$ assuming QPSK modulation are presented in Table I at the end of Section III, where $h_n^{\mathrm{CS}} \in \mathbb{C}$ is the nth element of $\mathbf{h}^{\mathrm{CS}}$.

3) Multiplexing for MIMO and multiuser scenarios: In case MIMO or multiuser operation of the CS-based RadCom system is to be enabled, an adequate multiplexing strategy must be adopted so that the transmit signals of $N_{\mathrm{Tx}} \in \mathbb{N}_+$ MIMO transmit channels or users are orthogonal to each other.

A commonly used approach, e.g., in commercially available MIMO-CS radars is time-division multiplexing (TDM), which consists of allocating interleaved time slots of duration $T_{\mathrm{chirp}}^{\mathrm{CS}} + T_{\mathrm{guard}}^{\mathrm{CS}}$ so that each of the N_{Tx} transmitters transmits its block consisting of a chirp and a pause without interference of any of the other $N_{\mathrm{Tx}} - 1$ transmitters. One of the main implications of TDM in a CS-based RadCom system is therefore higher susceptibility to the well-known range migration issue [108], [109] and to phase errors, besides a reduction of the relative radial velocity unambiguity. Although those effects are intensified in the MIMO case where different transmit channels should ideally estimate the same ranges and relative radial velocities so that DoA estimation can be adequately performed later on, compensation techniques have already been investigated in the literature [110], [111]. Additionally, the use of TDM changes the maximum unambiguous velocity listed in Table I to $v_{\mathrm{max,unamb}}^{\mathrm{CS}} = c_0/[4f_\mathrm{c}N_{\mathrm{Tx}}(T_{\mathrm{chirp}}^{\mathrm{CS}} + T_{\mathrm{guard}}^{\mathrm{CS}})]$ due to the longer required time to transmit each block, which becomes $T_{\mathrm{block}}^{\mathrm{CS}} = N_{\mathrm{Tx}}(T_{\mathrm{chirp}}^{\mathrm{CS}} + T_{\mathrm{guard}}^{\mathrm{CS}})$. It is worth highlighting that, although the processing gain expression remains the same as the one listed in Table I, the effectively experienced processing gain tends to be $10\log_{10}(\mathrm{N_{Tx}})$ dB smaller than in the SISO case due to the necessary reduction of M^{CS} by a factor of N_{Tx} to keep the overall measurement time $T_{\mathrm{frame}}^{\mathrm{CS}}$ constant. Finally, no change of the communication performance parameters from Table I is experienced if TDM is used for enabling MIMO operation, since the orthogonal signals experience the same communication channel and can carry different modulation symbols. In the multiuser case, however, the achieved data rate assuming QPSK modulation is reduced by a factor of N_{Tx} to $\mathcal{R}_{\mathrm{QPSK}}^{\mathrm{CS}} = 2/[N_{\mathrm{Tx}}(T_{\mathrm{chirp}}^{\mathrm{CS}} + T_{\mathrm{guard}}^{\mathrm{CS}})]$.

A second possible multiplexing approach for CS-based RadCom systems is frequency-division multiplexing (FDM). The most straightforward FDM approach for the multiplexing of N_{Tx} transmitters consists of applying a frequency shift equal to $F_\mathrm{s}^{\mathrm{CS}}/2$ to the chirp associated with a given transmitter w.r.t. the chirp associated with the previous transmitter. The simplest example of such approach would be for $N_{\mathrm{Tx}} = 2$, where the chirp associated with the first transmitter remains unaltered, while the chirp associated with the second transmitter is frequency-shifted by $F_\mathrm{s}^{\mathrm{CS}}/2$. The aforementioned frequency shifts result in an RF bandwidth of $B^{\mathrm{CS}} + (N_{\mathrm{Tx}} - 1)F_\mathrm{s}^{\mathrm{CS}}/2$ in the range $f \in [f_\mathrm{c} - B^{\mathrm{CS}}/2, f_\mathrm{c} + B^{\mathrm{CS}}/2 + (N_{\mathrm{Tx}} - 1)F_\mathrm{s}^{\mathrm{CS}}/2]$. At the receiver side, the beat frequencies associated with each transmitter would then be in interleaved bands that are shifted by $F_\mathrm{s}^{\mathrm{CS}}$ in the positive frequency axis. To enable such FDM approach, either strongly selective filters that are able to individually capture the beat frequencies associated with each transmitter would be required, which is very challenging to realize, or an ADC sampling rate of $N_{\mathrm{Tx}}F_\mathrm{s}^{\mathrm{CS}}$ and additional post processing would be required. Besides the more challenging implementation and the required wider RF bandwidth and higher ADC sampling rate of a CS-based RadCom system adopting the described FDM multiplexing approach, no further radar or communication performance parameters listed in Table I are changed.

Finally, a further multiplexing strategy for enabling MIMO or multiuser operation in CS-based RadCom systems is code-division multiplexing (CDM). Such a strategy can be implemented by an additional phase coding to the one performed for embedding QPSK modulation symbols in the considered CS-based RadCom system [112]. A possible approach in this context is, e.g., the use of an outer coding, which can be a binary Hadamard code with N_{Tx} codewords of length N_{Tx} [40], [113], [114]. In this approach, each of the N_{Tx} codewords is assigned to a different transmitter, which transmits N_{Tx} copies of each block modulated with the corresponding binary element of its codeword. The simplest example would be for $N_{\mathrm{Tx}} = 2$, in which the first transmitter transmits two copies of the same block, both with 0° phase shifts since the first transmitter is associated with the Hadamard codeword $[1\ 1]^T$. Similarly, the second transmitter transmits one copy

of the block with 0° phase shift and another one with 180° phase shift following its Hadamard codeword $[1\ -1]^T$. At the receiver side, the receive blocks are decoded via phase-shifting by corresponding element of the codeword of the evaluated transmitter and summed. Ideally, this should result in the block transmitted by the evaluated transmitted with a processing gain of $10\log_{10}(\mathrm{N_{Tx}})\,\mathrm{dB}$ due to the averaging-like effect of the decoding. The described CDM multiplexing approach increases $T^{\mathrm{CS}}_{\mathrm{block}}$ by a factor of N_{Tx} and consequently decreases $v^{\mathrm{CS}}_{\mathrm{max,unamb}}$ by a factor of N_{Tx} as in the TDM case. Additionally, the processing gain is changed to $G^{\mathrm{CS}}_{\mathrm{p}} = N_{\mathrm{Tx}} N^{\mathrm{CS}}_{\mathrm{chirp}} M^{\mathrm{CS}}$, although it may assume the same value as in the SISO case due to the necessary reduction of M^{CS} by a factor of N_{Tx} to keep $T^{\mathrm{CS}}_{\mathrm{frame}}$ constant as in the TDM case. In terms of communication performance, the only change w.r.t. to the listed parameters in Table I is the same described data rate reduction by a factor of N_{Tx} for the TDM case in multiuser scenarios. Further CDM-based approaches for CS-based RadCom systems include intra-chirp coding [115], as opposed to the previously described inter-chirp coding approach based on Hadamard codes. Since such approaches demand more complex practical implementation and lead to degradation of range sidelobes, they are not further discussed in this article.

B. Phase-Modulated Continuous Wave

The transmit frame of the considered SISO PMCW-based RadCom system contains $M^{\mathrm{PMCW}} \in \mathbb{N}_+$ blocks of time duration $T^{\mathrm{PMCW}}_{\mathrm{block}}$, each of them containing $A^{\mathrm{PMCW}} \in \mathbb{N}_+$ repetitions of a same BPSK-modulated version of a PRBS. The aforementioned PRBS has $N^{\mathrm{PMCW}}_{\mathrm{PRBS}} \in \mathbb{N}_+$ chips that are updated with a chip rate $F^{\mathrm{PMCW}}_{\mathrm{s}}$, which results in a PRBS time duration $T^{\mathrm{PMCW}}_{\mathrm{PRBS}} = N^{\mathrm{PMCW}}_{\mathrm{PRBS}}/F^{\mathrm{PMCW}}_{\mathrm{s}}$. Alternatively, the chips and the chip rate can be respectively interpreted as samples and sampling rate. Consequently, the frame duration is $T^{\mathrm{PMCW}}_{\mathrm{frame}} = M^{\mathrm{PMCW}} T^{\mathrm{PMCW}}_{\mathrm{block}} = M^{\mathrm{PMCW}}(A^{\mathrm{PMCW}} T^{\mathrm{PMCW}}_{\mathrm{PRBS}})$.

To choose an appropriate PRBS, aspects such as achievable sidelobe level and robustness against Doppler shifts must be investigated [116], besides requirements for sequence generation. A possible PRBS generation strategy is the use of a LFSR, which allows simpler and more cost-effective generation of, e.g., MLSs, also known as m-sequences, than employing a DAC with the drawback of not supporting interpolation at the D/A conversion and therefore causing out-of-band (OOB) emission due to the sinc-shaped repetitions of the PRBS spectral content at the first Nyquist zone. This ultimately results in a wider occupied RF bandwidth, which according to [39] can be defined as $B^{\mathrm{PMCW}} = 2F^{\mathrm{PMCW}}_{\mathrm{s}}$ as shown in Fig. 5 for a single PRBS repetition assuming the use of an MLS. To suppress OOB emission, one can adopt strategies such as the spectral sidelobe supression proposed in [39], which is based on 3rd harmonic rejection and LP filtering before modulation of the RF carrier.

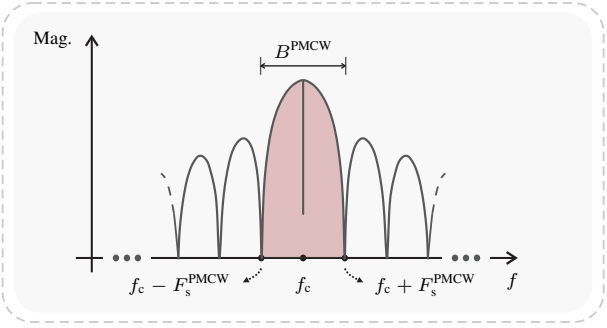

Fig. 5. Evaluated RF spectrum without LP or BP filtering for a single PRBS repetition, which is an MLS in the considered example.

Although PMCW-based systems can adopt polyphase sequences, the use of PRBSs is preferred to avoid the need for an I/Q transmitter and to have higher energy efficiency, since the resulting transmit signal of a PRBS-based PMCW system is a continuous wave (CW), which allows operating the PA in compression [39]. As for the choice for BPSK modulation, it is intended to keep the resulting modulated copies of the PRBS binary and consequently profit from the typical characteristics from binary PMCW radar systems.

The processing chain of the considered PMCW-based RadCom system with the previously described transmit signal characteristics is depicted in Fig. 6. At the transmitter side, the mth BPSK symbol, $m \in \{0, 1, \ldots, M^{\mathrm{PMCW}} - 1\}$, from the modulated data stream $\mathbf{d}^{\mathrm{PMCW}}_{\mathrm{Tx}} \in \mathbb{C}^{M^{\mathrm{PMCW}} \times 1}$ is modulated in the slow-time with the adopted PRBS [83]–[86]. The resulting BPSK-modulated PRBS is then repeated A^{PMCW} times to allow accumulation at the receive side of the PMCW-based RadCom system [39], [113], [114], which is denoted in Fig. 6 as $A^{\mathrm{PMCW}}\times$ REP. It is worth highlighting that the A^{PMCW}-time repetition at the transmit side and the accumulation of each A^{PMCW} repetitions of the BPSK-modulated PRBS are complementary operations, which are optional in PMCW-based radar systems where no modulation of PRBSs take place. Next, the modulated frame consisting of M^{PMCW} blocks carrying a total of M^{PMCW} BPSK symbols modulates the RF carrier of frequency f_{c}, which results in a CW of frequency f_{c} that is phase-modulated by both PRBS chips and BPSK symbols, hence the name PMCW. The aforementioned signal then undergoes amplification by a PA, which can operate in compression since its input signal is a CW, and the resulting signal $x^{\mathrm{PMCW}}(t) \in \mathbb{R}$ is transmitted by the transmit antenna. If power factors are omitted for the sake of simplicity, then the continuous-time domain signal containing the mth block transmitted within the transmit frame of the PMCW-based RadCom system can be expressed for $t \in \left[mT^{\mathrm{PMCW}}_{\mathrm{block}}, (m+1)T^{\mathrm{PMCW}}_{\mathrm{block}}\right)$ as in (10).

$$s^{\mathrm{PMCW}}_m(t) = \left[\sum_{a=0}^{A^{\mathrm{PMCW}}-1} S^{\mathrm{PMCW}}_m\ \psi\left(t - aT^{\mathrm{PMCW}}_{\mathrm{PRBS}} - mT^{\mathrm{PMCW}}_{\mathrm{block}}\right) \mathrm{rect}\left(\frac{t - aT^{\mathrm{PMCW}}_{\mathrm{PRBS}} - mT^{\mathrm{PMCW}}_{\mathrm{block}}}{T^{\mathrm{PMCW}}_{\mathrm{PRBS}}}\right)\right] \cos\left(2\pi f_{\mathrm{c}} t\right) \tag{10}$$

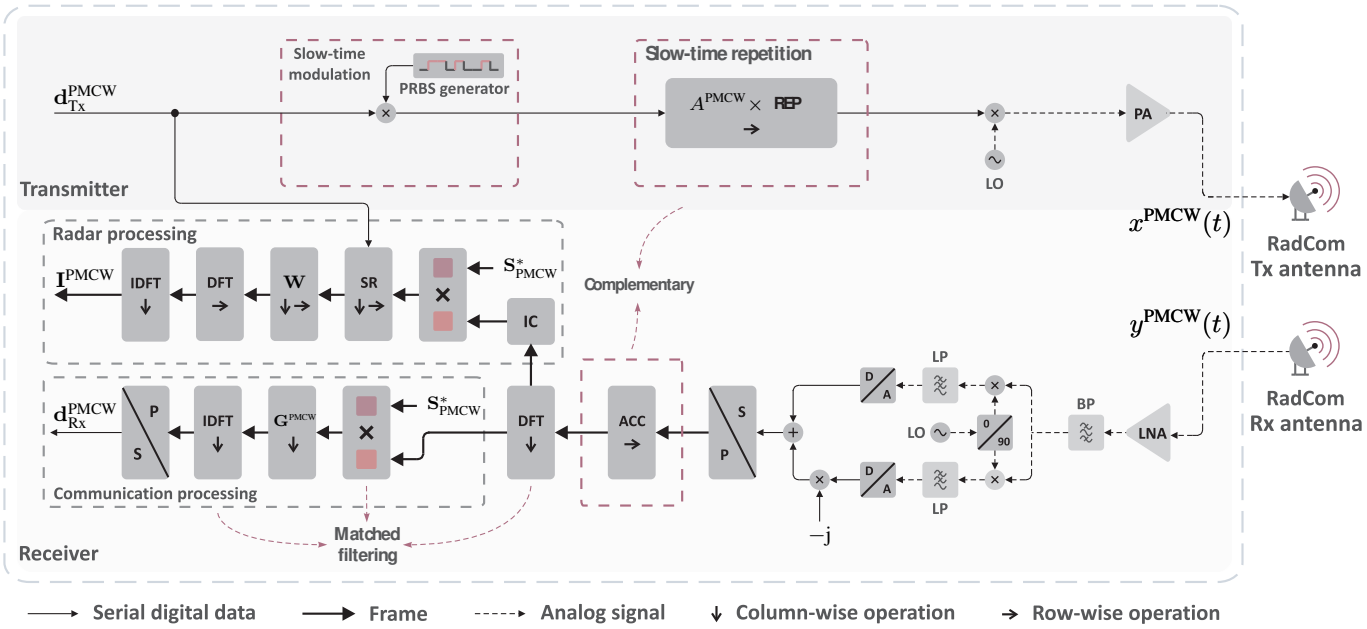

Fig. 6. SISO PMCW-based RadCom system representation.

In this equation, $S_m^{\mathrm{PMCW}} \in \mathbb{C} | S_m^{\mathrm{PMCW}} = \mathrm{e}^{\mathrm{j}\phi_m^{\mathrm{PMCW}}}$ denotes the mth BPSK symbol carried by the transmit frame, which has phase $\phi_m^{\mathrm{PMCW}} \in \{0, \pi\}$. Additionally, $\psi(t) \in \{-1, 1\}$ is the adopted PRBS defined for $t \in [0, T_{\mathrm{PRBS}}^{\mathrm{PMCW}})$. The continuous-time domain transmit signal $x^{\mathrm{PMCW}}(t)$ containing the frame comprising M^{PMCW} blocks transmitted by the PMCW-based RadCom system can be therefore expressed as

$$x^{\mathrm{PMCW}}(t) = \sum_{m=0}^{M^{\mathrm{PMCW}}-1} s_m^{\mathrm{PMCW}}(t) \ \mathrm{rect}\left(\frac{t - mT_{\mathrm{block}}^{\mathrm{PMCW}}}{T_{\mathrm{block}}^{\mathrm{PMCW}}}\right). \quad (11)$$

Based on the presented concepts, Fig. 7 depicts a serial representation of the frame in the considered PMCW-based RadCom system.

At the receiver of the PMCW-based RadCom system, the receive signal $y^{\mathrm{PMCW}}(t) \in \mathbb{R}$ containing the output version of $x^{\mathrm{PMCW}}(t)$ by the radar channel, the output version of the transmit signal $z^{\mathrm{PMCW}}(t) \in \mathbb{R}$ of another RadCom system by the communication channel, and additive noise according to (1) is captured by the receive antenna. $y^{\mathrm{PMCW}}(t)$ then undergoes analog conditioning in an I/Q receiver and A/D conversion with sampling rate $F_{\mathrm{s}}^{\mathrm{PMCW}}$ and corresponding sampling period $T_{\mathrm{s}}^{\mathrm{PMCW}} = 1/F_{\mathrm{s}}^{\mathrm{PMCW}}$, being the samples from both I and Q channels into the real and imaginary parts of a serial vector. After S/P conversion on the aforementioned vector, accumulation of A^{PMCW} PRBS repetitions, each modulated with the same BPSK symbol, is optionally performed in the slow-time direction. Since there may be phase breaks between consecutive blocks modulated with different BPSK symbols S_m^{PMCW}, the first out of the A^{PMCW} PRBS repetitions of each block must be discarded before accumulation. The aforementioned processing is similar to what happens in outer-code-based MIMO-PMCW radar systems [113], and intends to avoid an effect that can be compared to the well-known ISI in communication systems [42]. Furthermore, A^{PMCW} must in principle assume the highest value possible to avoid processing gain loss due to the discarded sequence repetition at the beginning of each block. However, very high A^{PMCW} values may lead to incoherence of the accumulation due to Doppler-shift-induced phase rotations, which also leads to processing gain reduction and data rate reduction.

After slow-time accumulation, DFTs are finally performed in the fast-time direction, i.e., along the chips of each PMCW block and different processing strategies are adopted for radar sensing and communication, which are respectively detailed in Subsections III-B1 and III-B2. Additionally, typical multiplexing schemes for MIMO or multiuser operation of the considered PMCW-based RadCom system are described in Subsection III-B3.

1) Radar processing: After IC, the remaining radar processing steps in the considered PMCW-based RadCom system comprises an element-wise multiplication of each block by the vector $\mathbf{S}_{\mathrm{PMCW}}^{*} \in \mathbb{C}^{N_{\mathrm{PRBS}}^{\mathrm{PMCW}} \times 1}$, which is the complex-conjugate version of the DFT of the adopted PRBS. The resulting frame undergoes symbol removal by multiplying each of its columns with the respective BPSK symbols used to modulate the transmit blocks, which is denoted in Fig. 6 as SR. Next, range and velocity windowing in fast- and slow-time directions, respectively, with the aim of supressing sidelobes in the radar image to be formed. The output matrix from the aforementioned windowing subsequently undergoes row-wise DFTs, i.e., DFTs in the slow-time direction, to convert Doppler-shift-induced phase rotations into Doppler shift estimates, which are translated into relative radial velocities. Finally, column-wise inverse discrete Fourier transforms (IDFTs), i.e., IDFTs in the fast-time direction, are performed to estimate time delays, which are translated into range. Together with the previously element-wise multiplication by $\mathbf{S}_{\mathrm{PMCW}}^{*}$ in the discrete-frequency domain, the IDFT operation yields a matched filtering, which is more computationally efficient and yields the same result as the periodic cross-correlation function

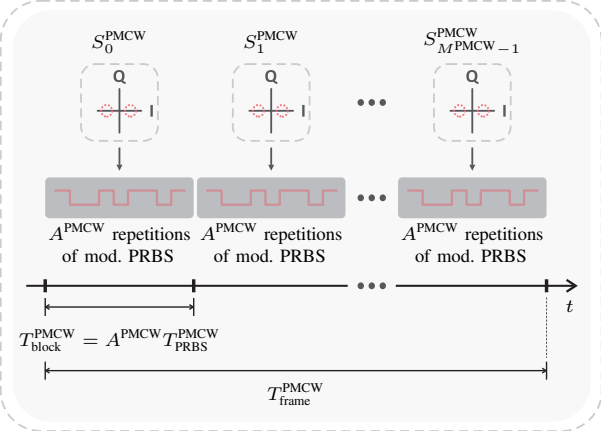

Fig. 7. PMCW transmit signal: frame serial representation.

(PCCF) of the receive blocks with the adopted PRBS [116].

The ultimately obtained range-velocity radar image $\mathbf{I}^{\text{PMCW}} \in \mathbb{C}^{N_{\text{PRBS}}^{\text{PMCW}} \times M^{\text{PMCW}}}$ experiences a processing gain $G_{\text{p}}^{\text{PMCW}}$ and has range resolution ΔR^{PMCW} and a maximum unambiguous range $R_{\text{max,unamb}}^{\text{PMCW}}$, as well as a relative radial velocity resolution Δv^{PMCW} and a maximum unambiguous relative radial velocity $v_{\text{max,unamb}}^{\text{PMCW}}$ as shown in Table I at the end of Section III based on [39], [40], [116]. While no further restrictions on maximum tolerable range apply in the considered PMCW-based RadCom system, the definition of a maximum tolerable relative radial velocity depends on the Doppler shift tolerance of the adopted PRBS [116] and is therefore not defined in Table I.

2) Communication processing: Before starting the communication processing of the considered PMCW-based RadCom system, it is first assumed that the time, frequency and phase offsets from the second term in (1) are removed via synchronization based on a preamble comprised of unmodulated PRBSs. The remaining communication processing steps comprise a joint equalization and matched filtering in the discrete-frequency domain, which shares some similarities with the previously described radar processing. In this sense, each column of the resulting frame from discrete-frequency domain matched filtering undergoes element-wise multiplication by the vector $\mathbf{G}^{\text{PMCW}} \in \mathbb{C}^{N_{\text{PRBS}}^{\text{PMCW}} \times 1}$. Assuming that $\mathbf{G}_{\text{PMCW}}$ contains the multiplicative inverse of the communication channel frequency response (CFR) estimate $\mathbf{H}^{\text{PMCW}} \in \mathbb{C}^{N_{\text{PRBS}}^{\text{PMCW}} \times 1}$, the aforementioned processing yields a ZF frequency-domain equalization (FDE). Similarly to the CS case in Subsection III-A2, the CFR estimate must be periodically updated via unmodulated PRBSs to compensate phase rotation introduced by Doppler shifts indicated in (1). The resulting frame from the joint equalization and matched filtering finally undergoes P/S conversion, which consists of extracting the receive BPSK symbols from the peak at the first samples of the frame columns and forming the receive modulated data stream $\mathbf{d}_{\text{Rx}}^{\text{PMCW}} \in \mathbb{C}^{M^{\text{PMCW}} \times 1}$. The described communication processing steps in the considered PMCW-based RadCom system yield data rate denoted by $\mathcal{R}_{\text{BPSK}}^{\text{PMCW}}$, as well as energy per bit to noise power spectral density ratio $(E_{\text{b}}/N_0)_{\text{BPSK}}^{\text{PMCW}}$ and BER denoted by $\text{BER}_{\text{BPSK}}^{\text{PMCW}}$ assuming BPSK modulation as presented in Table I at the end of Section III, where $H_n^{\text{PMCW}} \in \mathbb{C}$ is the nth element of $\mathbf{H}^{\text{PMCW}}$.

3) Multiplexing for MIMO and multiuser scenarios: For enabling MIMO or multiuser operation in PMCW-based RadCom systems, a common practice is to adopt CDM aiming for interference-free operation of N_{Tx} transmitters. The reason why TDM-based approaches are usually not adopted is the greater flexibility in the design of coded PMCW signals with the possibility of not experiencing the processing gain caused by reduced number of transmitted PRBSs per transmitter that would occur in the TDM case. As for FDM, it is usually not adopted since the design of PRBSs or general pseudorandom sequences is usually not flexible in the discrete-frequency domain, being approaches such as the commonly used interleaved FDM in OFDM systems [117] not suitable for PMCW-based RadCom systems.

In the CDM context, a possible multiplexing approach is based on the use of different PRBSs that are orthogonal to each other by each of the N_{Tx} transmitters [40], [116]. While this approach results in no changes in the radar and communication performance parameters listed in Table I, it requires a total of N_{Tx} different correlators at the receiver side to support the N_{Tx} orthogonal PRBSs. A possible issue with this approach is the relatively high sidelobe level of the PCCFs of orthogonal PRBSs, which tends to limit the radar dynamic range to about $30\,\text{dB}$ for the commonly adopted PRBSs [40].

Alternatively, outer codes [40], [113], [114] can be integrated into the signal structure of the SISO case described earlier in this section. Assuming the use of a Hadamard code as discussed in Subsection III-A3 for the CS case, the required duration $T_{\text{block}}^{\text{PMCW}}$ to transmit a block increases by a factor of N_{Tx}, becoming $N_{\text{Tx}} T_{\text{block}}^{\text{PMCW}}$. Consequently, the maximum unambiguous relative radial velocity listed in Table I decreases by a factor of N_{Tx}, becoming $v_{\text{max,unamb}}^{\text{PMCW}} = F_{\text{s}}^{\text{PMCW}} c_0 / (4 f_{\text{c}} N_{\text{Tx}} N_{\text{PRBS}}^{\text{PMCW}} A^{\text{PMCW}})$. The last parameter from Table I that is changed with the use of CDM based on outer coding is the processing gain, which becomes $G_{\text{p}}^{\text{PMCW}} = N_{\text{Tx}} N_{\text{PRBS}}^{\text{PMCW}} A^{\text{PMCW}} M^{\text{PMCW}}$. However, as discussed for the CS case in in Subsection III-A3, the ultimately experienced $G_{\text{p}}^{\text{PMCW}}$ tends to be the same as in the SISO case due to the necessary reduction of M^{PMCW} by a factor of N_{Tx} if $T_{\text{frame}}^{\text{CS}}$ is to be kept constant. Similarly to the outer-coding based CDM approach described for CS in Subsection III-A3, the only change in the communication performance parameters listed in Table I is the reduction of the achieved data rate assuming BPSK modulation by a factor of N_{Tx} to $\mathcal{R}_{\text{BPSK}}^{\text{PMCW}} = F_{\text{s}}^{\text{PMCW}} / [N_{\text{Tx}} (N_{\text{PRBS}}^{\text{PMCW}} A^{\text{PMCW}})]$.

C. Orthogonal Frequency-Division Multiplexing

The considered SISO OFDM-based RadCom system transmits a frame that comprises of $M^{\text{OFDM}} \in \mathbb{N}_+$ blocks, each containing one OFDM symbol that carries $N_{\text{subc}}^{\text{OFDM}} \in \mathbb{N}_+$ QPSK-modulated subcarriers[1] and a CP to prevent ISI when propagating through both radar and communication channels [42]. The OFDM frame carries therefore data from a modulated data stream $\mathbf{d}_{\text{Tx}}^{\text{OFDM}} \in \mathbb{C}^{N_{\text{subc}}^{\text{OFDM}} M^{\text{OFDM}} \times 1}$ containing a total of

[1]Hence the subscript "subc" in $N_{\text{subc}}^{\text{OFDM}}$.

$N_{\text{subc}}^{\text{OFDM}} M^{\text{OFDM}}$ QPSK symbols, which ultimately leads to a considerably higher data rate as in the SISO CS- and PMCW-based RadCom systems from Subsections III-A and III-B. Although higher-order digital modulations could be adopted for enabling higher data rates, the choice for QPSK is justified by the fact that it is less sensitive to phase rotations and results same allocated power at OFDM subcarriers, which ultimately yields more reliable radar measurements.

Following [18], [63], [89], [93], the processing chain of the considered OFDM-based RadCom system with the previously described transmit signal characteristics is depicted in Fig. 8. The modulated data stream $\mathbf{d}_{\text{Tx}}^{\text{OFDM}} \in \mathbb{C}^{N_{\text{subc}}^{\text{OFDM}} M^{\text{OFDM}} \times 1}$ first undergoes S/P conversion, generating the discrete-frequency domain OFDM frame $\mathbf{S}^{\text{OFDM}} \in \mathbb{C}^{N_{\text{subc}}^{\text{OFDM}} \times M^{\text{OFDM}}}$. The frame $\mathbf{S}^{\text{OFDM}} \in \mathbb{C}^{N_{\text{subc}}^{\text{OFDM}} \times M^{\text{OFDM}}}$ then undergoes column-wise IDFTs along the $N_{\text{subc}}^{\text{OFDM}}$ QPSK-modulated subcarriers of each of its M^{OFDM} OFDM symbols, and the resulting discrete-time domain OFDM frame has CPs of length $N_{\text{CP}}^{\text{OFDM}} \in \mathbb{N}_+$ prepended to each of its M^{OFDM} OFDM symbols. Next, the discrete-time domain OFDM frame with prepended CPs, which has size $(N_{\text{subc}}^{\text{OFDM}} + N_{\text{CP}}^{\text{OFDM}}) \times M^{\text{OFDM}}$, undergoes P/S conversion and the real and imaginary parts of the resulting vector are fed to DACs of sampling rate $F_{\text{s,DAC}}^{\text{OFDM}}$. The output analog signals by the DACs undergo analog conditioning and I/Q modulation to the carrier of frequency f_{c}, producing the analog signal $x^{\text{OFDM}}(t) \in \mathbb{R}$ that is transmitted by the transmit antenna of the OFDM-based RadCom system. It is worth highlighting that, in contrast to the CS- and PMCW-based RadCom systems from Subsections III-A and III-B, respectively, an input power back-off from the PA compression is required in the OFDM-based RadCom system due to the high PAPR experienced in OFDM signals [42], which can be higher than 10 dB depending on the adopted modulation scheme and number of subcarriers $N_{\text{subc}}^{\text{OFDM}}$.

Omitting power factors for simplicity and assuming that no CP is used, the continuous-time domain signal $s_m^{\text{OFDM, w/o CP}}(t,\tau) \in \mathbb{C}$ carrying the mth OFDM symbol, $m \in \{0,1,\ldots,M^{\text{OFDM}}-1\}$, can be expressed for $t \in \left[0, T_{\text{symb}}^{\text{OFDM}}\right)$ and $\tau \in \left[mT_{\text{block}}^{\text{OFDM}}, (m+1)T_{\text{block}}^{\text{OFDM}}\right)$ as in (12). In this equation, $S_{n,m}^{\text{OFDM}} \in \mathbb{C} | S_{n,m}^{\text{OFDM}} = \mathrm{e}^{\mathrm{j}\phi_m^{\text{OFDM}}}$ is the QPSK symbol with phase $\phi_m^{\text{OFDM}} \in \{\pi/4, 3\pi/4, 5\pi/4, 7\pi/4\}$ that is modulated onto the nth subcarrier, $n \in \{0,1,\ldots,N_{\text{subc}}^{\text{OFDM}}-1\}$, of the mth OFDM symbol. Furthermore, $\Delta f^{\text{OFDM}} = 1/T_{\text{symb}}^{\text{OFDM}}$ is the subcarrier frequency spacing defined by the OFDM symbol time duration disregarding CP $T_{\text{symb}}^{\text{OFDM}} = N_{\text{subc}}^{\text{OFDM}}/B^{\text{OFDM}}$, which in turns depends on the RF bandwidth B^{OFDM} occupied by the OFDM signal. It is worth highlighting that B^{OFDM} is defined assuming that the adopted sampling rate $F_{\text{s,DAC}}^{\text{OFDM}}$ is higher than the Nyquist critical sampling rate and that the LP filtering right after D/A conversion is capable to suppress the repetitions of the OFDM signal spectral content outside the first Nyquist zone. Those repetitions are produced by the sample and hold (S&H) circuit in the DACs, which also yields a sinc-shaped attenuation that can be digitally compensated by a inverted sinc filter. The aforementioned interpolation and upconversion of the transmit OFDM signal ultimately result in an RF spectrum for a single OFDM symbol as depicted in Fig. 9 and can be achieved by using extra, inactive subcarriers at the edge of the OFDM symbol in the discrete-frequency domain. Consequently, the continuous-time domain signal $s_m^{\text{OFDM}}(t) \in \mathbb{R}$ carrying the mth OFDM symbol with $N_{\text{CP}}^{\text{OFDM}}$-length CP can be expressed as in (13), where $T_{\text{block}}^{\text{OFDM}} = T_{\text{symb}}^{\text{OFDM}} + T_{\text{CP}}^{\text{OFDM}}$ is the duration of each OFDM block consisting of an OFDM symbol and its corresponding CP of time duration $T_{\text{CP}}^{\text{OFDM}} = N_{\text{CP}}^{\text{OFDM}}/B^{\text{OFDM}}$. The continuous-time domain signal $x^{\text{OFDM}}(t) \in \mathbb{R}$ containing the frame comprising M^{OFDM} blocks transmitted by the OFDM-based RadCom system can be finally expressed as

$$x^{\text{OFDM}}(t) = \sum_{m=0}^{M^{\text{OFDM}}-1} s_m^{\text{OFDM}}(t) \ \text{rect}\left(\frac{t - mT_{\text{block}}^{\text{OFDM}}}{T_{\text{block}}^{\text{OFDM}}}\right). \quad (14)$$

Based on the presented concepts, Figs. 10a and 10b depict serial representations of the frame and a block in the considered OFDM-based RadCom system, respectively.

At the receiver side of the OFDM-based RadCom system, the output version of $x^{\text{OFDM}}(t)$ by the radar channel, the output version of the transmit signal $z^{\text{OFDM}}(t) \in \mathbb{R}$ of another RadCom system by the communication channel, and additive noise according to (1) are combined into the continuous-time domain signal $y^{\text{OFDM}}(t) \in \mathbb{R}$ that is captured by the receive

$$\begin{aligned} s_m^{\text{OFDM, w/o CP}}(t,\tau) =& \Re\left\{\frac{1}{N_{\text{subc}}^{\text{OFDM}}} \sum_{n=0}^{N_{\text{subc}}^{\text{OFDM}}-1} S_{\langle n \rangle_{N/2},m}^{\text{OFDM}} \mathrm{e}^{\mathrm{j}2\pi(n-N/2)\Delta f^{\text{OFDM}} t}\right\} \cos\left(2\pi f_{\text{c}}\tau\right) \\ &+ \Im\left\{\frac{1}{N_{\text{subc}}^{\text{OFDM}}} \sum_{n=0}^{N_{\text{subc}}^{\text{OFDM}}-1} S_{\langle n \rangle_{N/2},m}^{\text{OFDM}} \mathrm{e}^{\mathrm{j}2\pi(n-N/2)\Delta f^{\text{OFDM}} t}\right\} \sin\left(2\pi f_{\text{c}}\tau\right), \\ & t \in \left[0, T_{\text{symb}}^{\text{OFDM}}\right), \tau \in \left[mT_{\text{block}}^{\text{OFDM}}, (m+1)T_{\text{block}}^{\text{OFDM}}\right) \end{aligned} \quad (12)$$

$$s_m^{\text{OFDM}}(t) = \begin{cases} s_m^{\text{OFDM, w/o CP}}\left(t + T_{\text{symb}}^{\text{OFDM}} - T_{\text{CP}}^{\text{OFDM}} - mT_{\text{block}}^{\text{OFDM}}, t\right), & t \in \left[mT_{\text{block}}^{\text{OFDM}}, mT_{\text{block}}^{\text{OFDM}} + T_{\text{CP}}^{\text{OFDM}}\right) \\ s_m^{\text{OFDM, w/o CP}}(t - T_{\text{CP}}^{\text{OFDM}} - mT_{\text{block}}^{\text{OFDM}}, t), & t \in \left[mT_{\text{block}}^{\text{OFDM}} + T_{\text{CP}}^{\text{OFDM}}, (m+1)T_{\text{block}}^{\text{OFDM}}\right) \end{cases} \quad (13)$$

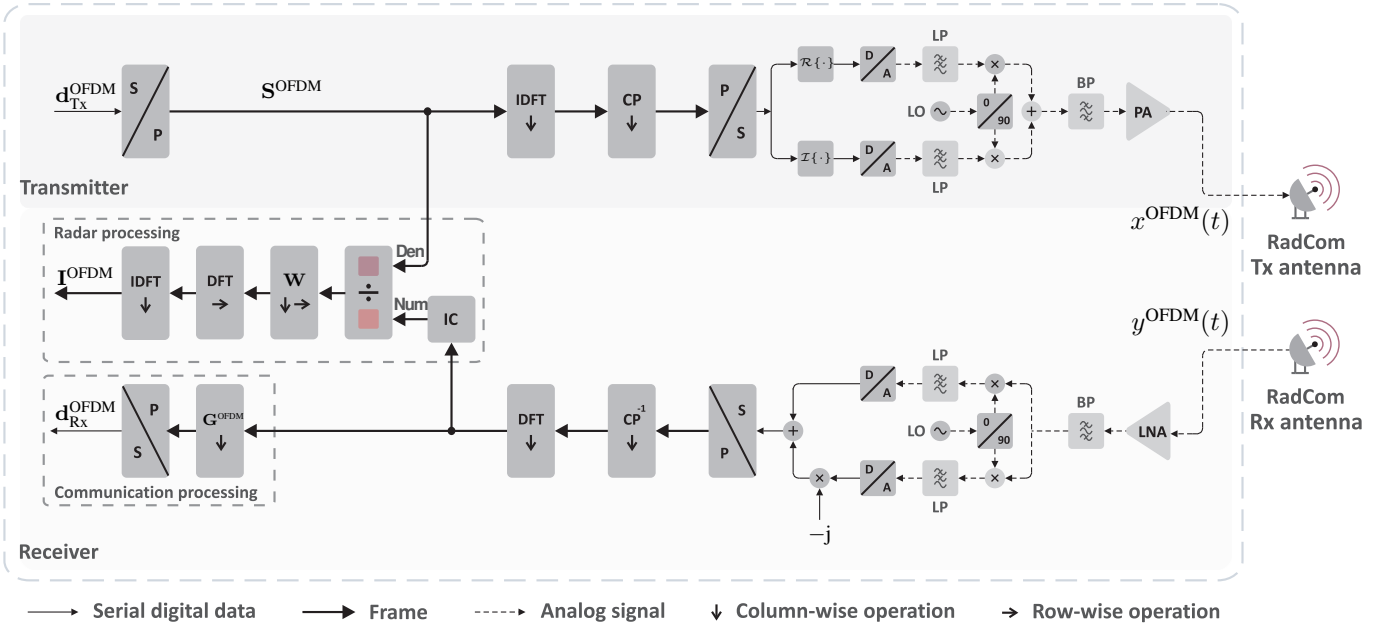

Fig. 8. SISO OFDM-based RadCom system representation.

antenna. After the same analog conditioning, A/D conversion with sampling rate $F_{\mathrm{s}}^{\mathrm{OFDM}} = B^{\mathrm{OFDM}}$ and corresponding sampling period $T_{\mathrm{s}}^{\mathrm{OFDM}} = 1/F_{\mathrm{s}}^{\mathrm{OFDM}}$ is performed for both I and Q channels as described for the PMCW case in Subsection III-B. The resulting complex-valued vector undergoes S/P conversion, forming a discrete-time domain OFDM frame containing M^{OFDM} receive symbols with CP. Next CP removal and DFTs are performed along the M^{OFDM} columns of the aforementioned frame, which produces a discrete-frequency domain receive OFDM frame of size $N_{\mathrm{subc}}^{\mathrm{OFDM}} \times M^{\mathrm{OFDM}}$, on which distinct further processing steps are performed for radar sensing and communication, as respectively detailed in Subsections III-C1 and III-C2. Finally, a multiplexing strategy to enable MIMO or multiuser operation of the OFDM-based RadCom system is discussed in Subsection III-C3.

1) Radar processing: The remaining radar processing steps in the considered OFDM-based RadCom system start with IC, which consists of removing the influence of communication signals originally transmitted by other RadCom or communication systems from the discrete-frequency domain receive OFDM frame. Afterwards, the resulting frame is divided by the frame $\mathbf{S}^{\mathrm{OFDM}}$ that contains the transmit QPSK modulation symbols, which yields one ZF estimate of the radar CFR for each of the M^{OFDM} symbols. The remaining processing steps are the same from the PMCW case in Subsection III-B1, i.e., range and velocity windowing, row-wise DFTs for Doppler shift estimation, and column-wise IDFTs for time delay estimation, being the estimated Doppler shifts and time delays translated into relative radial velocity and range estimates, respectively.

Following [21], [118], [119], the aforementioned processing steps in the OFDM-based RadCom system ultimately yield the range-velocity radar image $\mathbf{I}^{\mathrm{OFDM}} \in \mathbb{C}^{N_{\mathrm{subc}}^{\mathrm{OFDM}} \times M^{\mathrm{OFDM}}}$, which experiences a processing gain $G_{\mathrm{p}}^{\mathrm{OFDM}}$ and is associated with range resolution ΔR^{OFDM}, maximum unambiguous range $R_{\mathrm{max,unamb}}^{\mathrm{OFDM}}$, and maximum tolerable range $R_{\mathrm{max,ISI}}^{\mathrm{OFDM}}$, as well as relative radial velocity resolution, Δv^{OFDM}, maximum unambiguous relative radial velocity $v_{\mathrm{max,unamb}}^{\mathrm{OFDM}}$, and maximum tolerable relative radial velocity $v_{\mathrm{max,ICI}}^{\mathrm{OFDM}}$ values as shown in Table I at the end of Section III.

2) Communication processing: Considering that time, frequency and phase offsets from the second term in (1) have already been compensated via synchronization based on a preamble defined by, e.g., the Schmidl and Cox algorithm [104], the remaining communication processing in the considered OFDM-based RadCom system comprises of a ZF FDE via fast-time, element-wise multiplication of each block by the vector $\mathbf{G}^{\mathrm{OFDM}} \in \mathbb{C}^{N_{\mathrm{subc}}^{\mathrm{OFDM}} \times 1}$ that contains the multiplicative inverse of the estimate of the experienced communication CFR $\mathbf{H}^{\mathrm{OFDM}} \in \mathbb{C}^{N_{\mathrm{subc}}^{\mathrm{OFDM}} \times 1}$. As in the CS and PMCW cases from Subsections III-A2 and III-B2, respectively, the CFR estimate must be updated periodically to compensate for phase rotations introduced by Doppler shifts of scatterers indicated in (1), which is achieved with the use of pilot subcarriers in OFDM-based systems [41], [42], [64]. The resulting frame from the FDE finally undergoes P/S conversion, generating the receive modulated data stream $\mathbf{d}_{\mathrm{Rx}}^{\mathrm{OFDM}} \in \mathbb{C}^{(N_{\mathrm{subc}}^{\mathrm{OFDM}} M^{\mathrm{OFDM}}) \times 1}$.

The communication processing steps in the considered OFDM-based RadCom system result in the overall data rate denoted by $\mathcal{R}_{\mathrm{QPSK}}^{\mathrm{OFDM}}$, as well as energy per bit to noise power spectral density ratio $(E_{\mathrm{b}}/N_0)_{\mathrm{QPSK},n}^{\mathrm{OFDM}}$ and BER denoted by $\mathrm{BER}_{\mathrm{QPSK},n}^{\mathrm{OFDM}}$ for the nth QPSK-modulated subcarrier as presented in Table I at the end of Section III, where $H_n^{\mathrm{OFDM}} \in \mathbb{C}$ is the nth element of $\mathbf{H}^{\mathrm{OFDM}}$.

3) Multiplexing for MIMO and multiuser scenarios: For MIMO and multiuser operation of OFDM-based RadCom systems, the widely adopted multiplexing approach to achieve orthogonality of a total of N_{Tx} transmit signals is FDM based on an interleaved subcarrier assignment scheme [117]. This scheme is adopted to ensure that signals from different

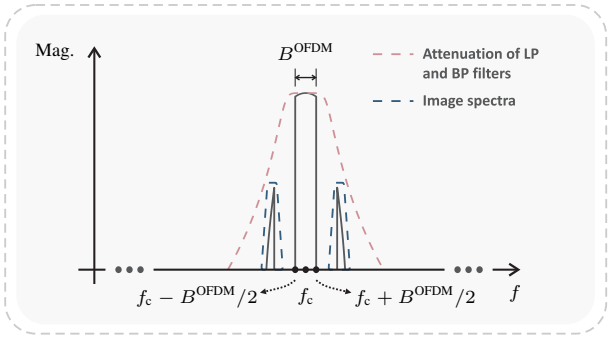

Fig. 9. Evaluated spectrum for one OFDM symbol.

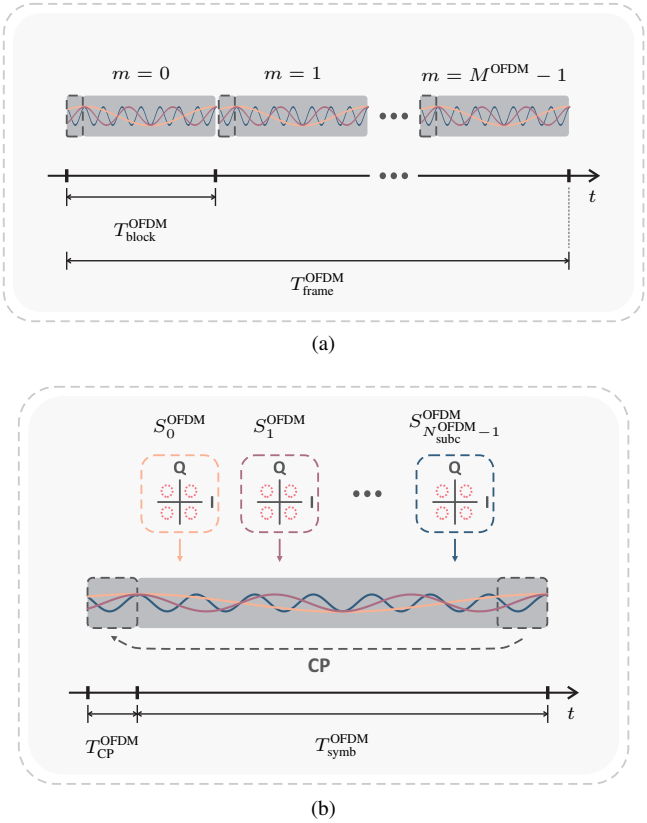

Fig. 10. OFDM transmit signal: (a) frame serial representation and (b) block representation.

transmit channels are orthogonal in the frequency domain as long as tolerable Doppler shifts are experienced, being those assumed to be equal to or less than the same upperbound of $0.1\Delta f^{\text{OFDM}}$ associated with the tolerable intercarrier interference (ICI) in OFDM systems [35], [42], [64], [117]. The simplest example of this approach would be for $N_{\text{Tx}} = 2$ with even $N^{\text{OFDM}}_{\text{subc}}$, where every subcarrier of even index, i.e., $n \in \{0, 2, 4, \ldots, N^{\text{OFDM}}_{\text{subc}} - 2\}$, would be assigned to the first transmitter, while every subcarrier of odd index, i.e., $n \in \{1, 3, 5, \ldots, N^{\text{OFDM}}_{\text{subc}} - 1\}$, would be assigned to the second transmitter. After performing the processing steps until the DFT at the receiver side, the $N^{\text{OFDM}}_{\text{subc}}/N_{\text{Tx}}$ subcarriers assigned to the evaluated transmitter are selected and further processed. Consequently, the processing gain listed in Table I is changed to $G^{\text{OFDM}}_{\text{p}} = (N^{\text{OFDM}}_{\text{subc}}/N_{\text{Tx}})M^{\text{OFDM}}$, which tends to be $10\log_{10}(\text{N}_{\text{Tx}})\,\text{dB}$ lower than in the SISO case. The last changed radar performance parameter w.r.t. the listed ones in Table I is the maximum unambiguous range, which is reduced to $R^{\text{OFDM}}_{\text{max,unamb}} = (N^{\text{OFDM}}_{\text{subc}}/N_{\text{Tx}})c_0/(2B^{\text{OFDM}})$. Finally, it is worth highlighting that no communication performance parameters are changed in this multiplexing approach in the MIMO case if each transmit channel transmits a different payload, whereas the data rate assuming QPSK modulation is reduced by a factor of N_{Tx} to $\mathcal{R}^{\text{OFDM}}_{\text{QPSK}} = 2N^{\text{OFDM}}_{\text{subc}}\text{B}^{\text{OFDM}}/[N_{\text{Tx}}(N^{\text{OFDM}}_{\text{subc}} + N^{\text{OFDM}}_{\text{CP}})]$ in the multiuser case.

Straightforward alternative MIMO strategies for OFDM-based RadCom systems include TDM [41], which is usually not considered for the same reasons as in the PMCW case from Subsections III-B3. A further possibility is CDM based on either the use of uncorrelated OFDM symbols [119], yielding considerably poor isolation among different transmitters, or outer codes [42], which are same as discussed for the CS and PMCW cases from Subsections III-A3 and III-B3, respectively. Since the aforementioned approaches tend to be outperformed by the previously discussed interleaved FDM, they are not discussed in further detail. Although optimized CDM strategies have been recently investigated in the literature [120], this article focuses solely on the widely adopted interleaved FDM for the sake of simplicity.

D. Orthogonal Chirp-Division Multiplexing

OCDM-based systems share many similarities with their OFDM counterparts. Some of their few differences are, e.g., data modulation onto orthogonal subchirps [121] instead of subcarriers and the use of the DFnT and its inverse instead of the DFT-IDFT pair [43]. Similarly to its OFDM counterpart from Subsection III-C, the considered SISO OCDM-based RadCom system transmits a frame that comprises of $M^{\text{OCDM}} \in \mathbb{N}_+$ blocks, each containing one OCDM symbol that carries $N^{\text{OCDM}}_{\text{subch}} \in \mathbb{N}_+$ QPSK-modulated subchirps[2] and a CP. The OCDM frame carries data from a modulated data stream $\mathbf{d}^{\text{OCDM}}_{\text{Tx}} \in \mathbb{C}^{N^{\text{OCDM}}_{\text{subch}}M^{\text{OCDM}}\times 1}$ containing a total of $N^{\text{OCDM}}_{\text{subch}}M^{\text{OCDM}}$ QPSK symbols, achieving the same data rate as an equally parameterized SISO OFDM-based RadCom system.

Based on [47], the processing chain of the considered OCDM-based RadCom system is depicted in Fig. 11. In this figure, the modulated data stream $\mathbf{d}^{\text{OCDM}}_{\text{Tx}} \in \mathbb{C}^{N^{\text{OCDM}}_{\text{subch}}M^{\text{OCDM}}\times 1}$ first undergoes S/P convesion, generating the discrete-Fresnel domain OCDM frame $\mathbf{S}^{\text{OCDM}} \in \mathbb{C}^{N^{\text{OCDM}}_{\text{subch}}\times M^{\text{OCDM}}}$. As opposed to the column-wise IDFTs in the OFDM case described in Subsection III-C, the frame $\mathbf{S}^{\text{OCDM}}$ undergoes column-wise inverse discrete Fresnel transforms (IDFnTs) along the $N^{\text{OCDM}}_{\text{subch}}$ QPSK-modulated subchirps of each of its M^{OCDM} OCDM symbols. According to [43], [44], [47], [92], the aforementioned IDFnTs can be accomplished via element-wise pre-multiplication of every $N^{\text{OCDM}}_{\text{subch}}$-length column of the OCDM frame by the complex conjugate of vector $\mathbf{\Theta}_2 \in \mathbb{C}^{N^{\text{OCDM}}_{\text{subch}}\times 1}$, followed by column-wise IDFTs on the resulting frame and

[2]Hence the subscript "subch" in $N^{\text{OCDM}}_{\text{subch}}$.

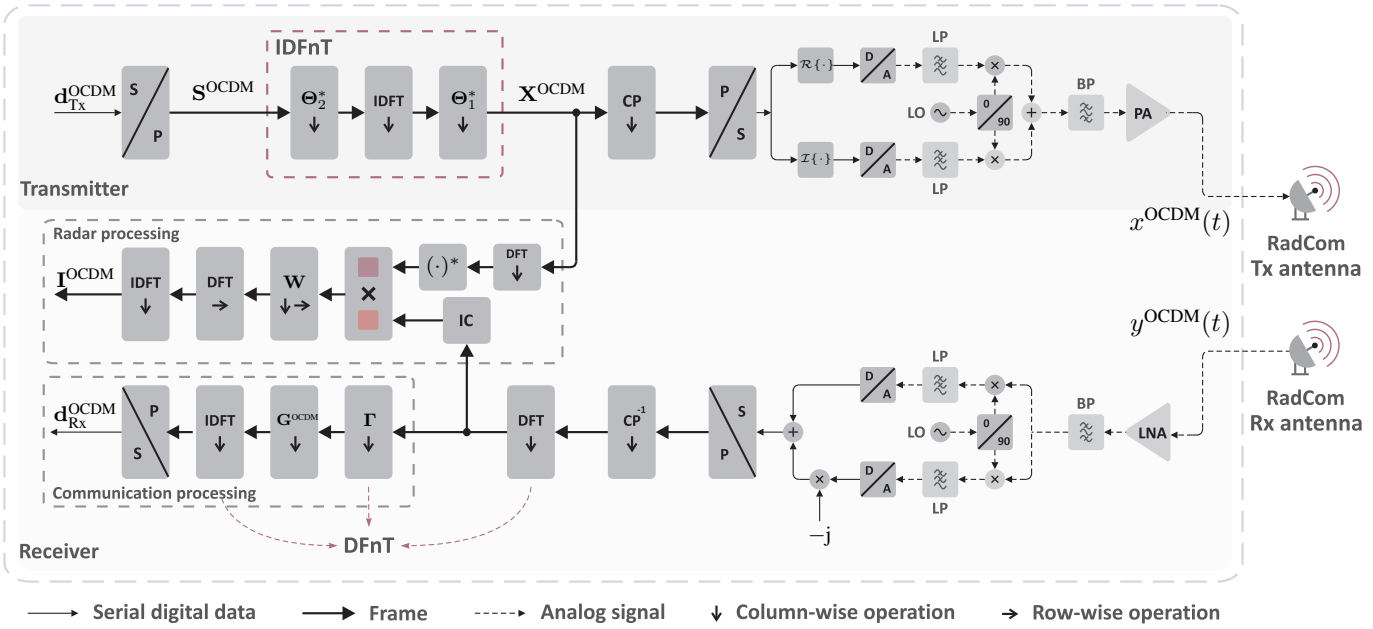

Fig. 11. SISO OCDM-based RadCom system representation.

element-wise multiplication of each of its columns by the complex conjugate of vector $\boldsymbol{\Theta}_1 \in \mathbb{C}^{N_{\text{subch}}^{\text{OCDM}} \times 1}$. Assuming even $N_{\text{subch}}^{\text{OCDM}}$, the nth element of $\boldsymbol{\Theta}_2$, $n \in \{0, 1, \ldots, N_{\text{subch}}^{\text{OCDM}} - 1\}$, is expressed as [43]

$$\Theta_{2,n} = \mathrm{e}^{\mathrm{j}\pi n^2 / N_{\text{subch}}^{\text{OCDM}}}, \tag{15}$$

while the nth element of $\boldsymbol{\Theta}_1$ is

$$\Theta_{1,n} = \mathrm{e}^{-\mathrm{j}\frac{\pi}{4}} \mathrm{e}^{\mathrm{j}\pi n^2 / N_{\text{subch}}^{\text{OCDM}}}. \tag{16}$$

It is worth highlighting that, although the aforementioned operations take place in different domains, the same index n is used for $\Theta_{1,n}$ and $\Theta_{2,n}$ for the sake of simplicity. Next, CPs of length $N_{\text{CP}}^{\text{OCDM}} \in \mathbb{N}_+$ are prepended to each of the M^{OCDM} OCDM symbols of the output discrete-time domain OCDM frame $\mathbf{X}^{\text{OCDM}} \in \mathbb{C}^{N_{\text{subch}}^{\text{OCDM}} \times M^{\text{OCDM}}}$ from the aforementioned IDFnT operation. For communication purposes, shorter CP lengths can be used in OCDM-based systems compared to their OFDM counterparts [43], [95], [122], which results from the fact that ISI is spread over all subchirps and can be explained by the DFnT convolution theorem [99]. However, the use of CPs with shorter length than the radar CIR may bias radar measurements. The following operations are the same as the ones described in Subsection III-C for the OFDM case, and the resulting transmit analog signal $x^{\text{OCDM}}(t) \in \mathbb{R}$ also has a similar PAPR than its OFDM counterpart due to many similarities between the OCDM and OFDM schemes [43].

Based on the aforementioned processing steps and omitting the power factors for simplicity, the continuous-time domain signal $s_m^{\text{OCDM, w/o CP}}(t, \tau) \in \mathbb{R}$ carrying the mth OCDM symbol, $m \in \{0, 1, \ldots, M^{\text{OCDM}} - 1\}$, without CP can be expressed for $t \in \left[0, T_{\text{symb}}^{\text{OCDM}}\right)$ and $\tau \in \left[mT_{\text{block}}^{\text{OCDM}}, (m+1)T_{\text{block}}^{\text{OCDM}}\right)$ as in (17). In this equation, $S_{n,m}^{\text{OCDM}} \in \mathbb{C} | S_{n,m}^{\text{OCDM}} = \mathrm{e}^{\mathrm{j}\phi_m^{\text{OCDM}}}$ is the QPSK symbol with phase $\phi_m^{\text{OCDM}} \in \{\pi/4, 3\pi/4, 5\pi/4, 7\pi/4\}$ that is modulated onto the nth subchirp, $n \in \{0, 1, \ldots, N_{\text{subch}}^{\text{OCDM}} - 1\}$, of the mth OCDM symbol. Additionally, $T_{\text{symb}}^{\text{OCDM}} = N_{\text{subch}}^{\text{OCDM}} / B^{\text{OCDM}}$ is time duration of an OCDM symbol disregarding CP, which depends on the RF bandwidth B^{OCDM} occupied by the OCDM signal. Unlike the subcarriers in the OFDM case from Subsection III-C, all subchirps occupy the whole discrete-frequency domain spectrum of the OCDM signal. However, interpolation of the transmit OCDM signal can still be achieved via frequency-domain zero padding (FDZP) as described in [123], which ultimately results in an RF spectrum for a single OCDM symbol as exemplary depicted in Fig. 12, where $F_{\text{s,DAC}}^{\text{OCDM}}$ is the sampling frequency adopted at the DACs. The continuous-time domain signal $s_m^{\text{OCDM}}(t) \in \mathbb{R}$ carrying

$$\begin{aligned} s_m^{\text{OCDM, w/o CP}}(t, \tau) = &\Re\left\{ \mathcal{A}_{B^{\text{OCDM}}} \left\{ \frac{1}{N_{\text{subch}}^{\text{OCDM}}} \mathrm{e}^{\mathrm{j}\pi/4} \sum_{n=0}^{N_{\text{subch}}^{\text{OCDM}}-1} S_{n,m}^{\text{OCDM}} \mathrm{e}^{-\mathrm{j}\pi \frac{N}{T^2}\left[n\frac{T}{N} - t\right]^2} \right\} \right\} \cos(2\pi f_{\text{c}} \tau) \\ &+ \Im\left\{ \mathcal{A}_{B^{\text{OCDM}}} \left\{ \frac{1}{N_{\text{subch}}^{\text{OCDM}}} \mathrm{e}^{\mathrm{j}\pi/4} \sum_{n=0}^{N_{\text{subch}}^{\text{OCDM}}-1} S_{n,m}^{\text{OCDM}} \mathrm{e}^{-\mathrm{j}\pi \frac{N}{T^2}\left[n\frac{T}{N} - t\right]^2} \right\} \right\} \sin(2\pi f_{\text{c}} \tau), \\ &t \in \left[0, T_{\text{symb}}^{\text{OCDM}}\right), \tau \in \left[mT_{\text{block}}^{\text{OCDM}}, (m+1)T_{\text{block}}^{\text{OCDM}}\right) \end{aligned} \tag{17}$$

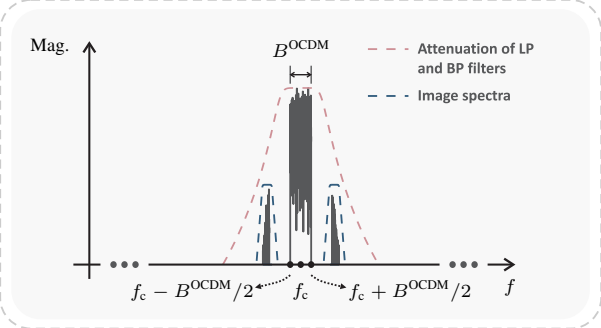

Fig. 12. Evaluated spectrum for one OCDM symbol.

the mth OCDM symbol with $N_{\text{CP}}^{\text{OCDM}}$-length CP can therefore be expressed as in (18), in which $T_{\text{block}}^{\text{OCDM}} = T_{\text{symb}}^{\text{OCDM}} + T_{\text{CP}}^{\text{OCDM}}$ is the duration of each OCDM block comprised of an OCDM symbol and a CP of time duration $T_{\text{CP}}^{\text{OCDM}} = N_{\text{CP}}^{\text{OCDM}}/B^{\text{OCDM}}$. Consequently, the continuous-time domain transmit signal $x^{\text{OCDM}}(t) \in \mathbb{R}$ carrying the frame comprised of M^{OCDM} blocks that is transmitted by the OCDM-based RadCom system can be expressed as

$$x^{\text{OCDM}}(t) = \sum_{m=0}^{M^{\text{OCDM}}-1} s_m^{\text{OCDM}}(t)\ \text{rect}\left(\frac{t - mT_{\text{block}}^{\text{OCDM}}}{T_{\text{block}}^{\text{OCDM}}}\right). \quad (19)$$

Based on the presented concepts, Fig. 13a depicts a serial representation of the frame in the considered OCDM-based RadCom system, while Fig. 13b shows the detailed structure of a single block.

At the receiver side of the OCDM-based RadCom system, the receive antenna captures the continuous-time domain signal $y^{\text{OCDM}}(t) \in \mathbb{R}$, which comprises of the output version of $x^{\text{OCDM}}(t)$ by the radar channel, the output version of the transmit signal $z^{\text{OCDM}}(t) \in \mathbb{R}$ of another RadCom system by the communication channel, and additive noise according to (1). The initial processing steps at the receiver side are similar to the ones from the OFDM case described in Subsection III-C, i.e., analog conditioning, A/D conversion with sampling rate $F_{\text{s}}^{\text{OCDM}} = B^{\text{OCDM}}$ and corresponding sampling period $T_{\text{s}}^{\text{OCDM}} = 1/F_{\text{s}}^{\text{OCDM}}$ is performed for both I and Q channels. After S/P conversion on the sampled complex-valued vector, CP removal, and DFTs are performed along the M^{OCDM} columns of the output frame. The resulting discrete-frequency domain receive frame of size $N_{\text{subch}}^{\text{OCDM}} \times M^{\text{OCDM}}$ finally undergoes distinct processing steps for radar sensing and communication purposes, which are respectively detailed in Subsections III-D1 and III-D2. Furthermore, the application of multiplexing strategies to the considered OCDM-based RadCom system to enable MIMO or multiuser operation is finally discussed in Subsection III-D3.

1) Radar processing: As in the previously presented modulation schemes, the radar processing in the considered OCDM-based RadCom system starts with IC. Next, the resulting frame undergoes element-wise multiplication by the complex conjugate of the output frame from column-wise DFTs on $\mathbf{X}^{\text{OCDM}}$. Similarly to the radar processing in the PMCW case described in Subsection III-B1, the aforementioned operation yields a matched filtering in the discrete-frequency domain, which, after further processing, will ultimately generate radar range profiles whose sidelobes will be defined by the transmit QPSK symbols in the considered OCDM-based RadCom system. Compared to [47], the use of simple DFTs ultimately yields a PCCF between the transmit and receive OCDM symbols, which has less associated computational complexity than the use of zero-padded DFTs in [47] used for performing a linear cross-correlation and introduces no degradation of the range sidelobe level. Furthermore, the reason why a simple element-wise division in the discrete-frequency domain is not performed as in the OFDM case from Subsection III-C1 is that OCDM symbols do not present flat spectral content as their OFDM counterparts and can even have null frequency tones, which prevents estimation of radar CFR [47]. In fact, although alternative radar processing strategies that explore properties of the DFnT could be used, no such approaches have been

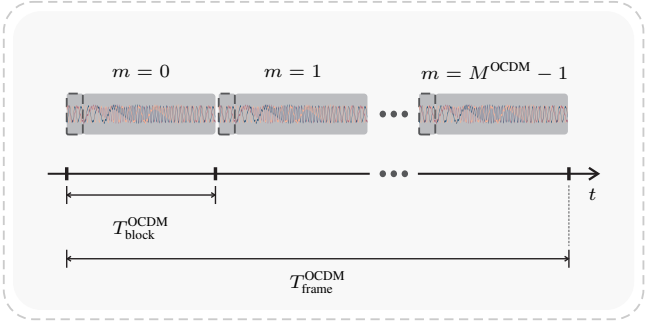

(a)

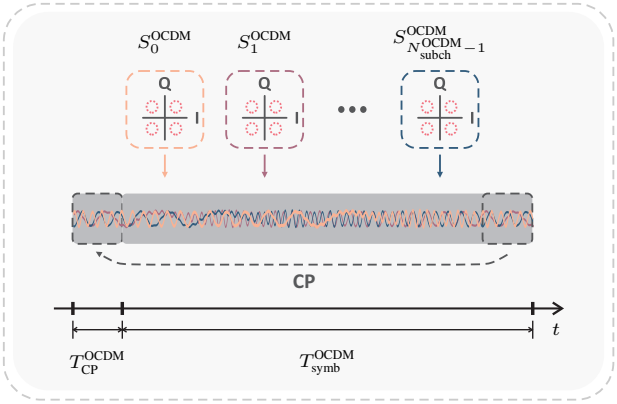

(b)

Fig. 13. OCDM transmit signal: (a) frame serial representation and (b) block representation.

$$s_m^{\text{OCDM}}(t) = \begin{cases} s_m^{\text{OCDM, w/o CP}}\left(t + T_{\text{symb}}^{\text{OCDM}} - T_{\text{CP}}^{\text{OCDM}} - mT_{\text{block}}^{\text{OCDM}}, t\right), & t \in \left[mT_{\text{block}}^{\text{OCDM}}, mT_{\text{block}}^{\text{OCDM}} + T_{\text{CP}}^{\text{OCDM}}\right) \\ s_m^{\text{OCDM, w/o CP}}(t - T_{\text{CP}}^{\text{OCDM}} - mT_{\text{block}}^{\text{OCDM}}, t), & t \in \left[mT_{\text{block}}^{\text{OCDM}} + T_{\text{CP}}^{\text{OCDM}}, (m+1)T_{\text{block}}^{\text{OCDM}}\right) \end{cases} \quad (18)$$

TABLE I
RADAR AND COMMUNICATION PERFORMANCE PARAMETERS OF THE SISO RADCOM SYSTEMS BASED ON CS, PMCW, OFDM, AND OCDM. EXCEPT FOR PMCW, WHICH ADOPTS BPSK MODULATION, ALL SCHEMES ARE ASSUMED TO ADOPT QPSK MODULATION.

Radar performance parameters				
	CS	**PMCW**	**OFDM**	**OCDM**
Range resolution	$\Delta R^{\mathrm{CS}} = \frac{c_0}{2B^{\mathrm{CS}}}$	$\Delta R^{\mathrm{PMCW}} = \frac{c_0}{2F_{\mathrm{s}}^{\mathrm{PMCW}}}$	$\Delta R^{\mathrm{OFDM}} = \frac{c_0}{2B^{\mathrm{OFDM}}}$	$\Delta R^{\mathrm{OCDM}} = \frac{c_0}{2B^{\mathrm{OCDM}}}$
Max. unamb. range	$R_{\mathrm{max,unamb}}^{\mathrm{CS}} = N_{\mathrm{chirp}}^{\mathrm{CS}} \frac{c_0}{2B^{\mathrm{CS}}}$	$R_{\mathrm{max,unamb}}^{\mathrm{PMCW}} = N_{\mathrm{PRBS}}^{\mathrm{PMCW}} \frac{c_0}{2F_{\mathrm{s}}^{\mathrm{PMCW}}}$	$R_{\mathrm{max,unamb}}^{\mathrm{OFDM}} = N_{\mathrm{subc}}^{\mathrm{OFDM}} \frac{c_0}{2B^{\mathrm{OFDM}}}$	$R_{\mathrm{max,unamb}}^{\mathrm{OCDM}} = N_{\mathrm{subch}}^{\mathrm{OCDM}} \frac{c_0}{2B^{\mathrm{OCDM}}}$
Max. tolerable range	Depends on required $G_{\mathrm{p}}^{\mathrm{CS}}$	No further restrictions	$R_{\mathrm{max,ISI}}^{\mathrm{OFDM}} = N_{\mathrm{CP}}^{\mathrm{OFDM}} \frac{c_0}{2B^{\mathrm{OFDM}}}$	$R_{\mathrm{max,ISI}}^{\mathrm{OCDM}} = N_{\mathrm{CP}}^{\mathrm{OCDM}} \frac{c_0}{2B^{\mathrm{OCDM}}}$
Relative radial velocity resolution	$\Delta v^{\mathrm{CS}} = \frac{c_0}{2f_{\mathrm{c}}\left(T_{\mathrm{chirp}}^{\mathrm{CS}}+T_{\mathrm{guard}}^{\mathrm{CS}}\right)M^{\mathrm{CS}}}$	$\Delta v^{\mathrm{PMCW}} = \frac{F_{\mathrm{s}}^{\mathrm{PMCW}} c_0}{2f_{\mathrm{c}}\left(N_{\mathrm{PRBS}}^{\mathrm{PMCW}} A^{\mathrm{PMCW}}\right)M^{\mathrm{PMCW}}}$	$\Delta v^{\mathrm{OFDM}} = \frac{B^{\mathrm{OFDM}} c_0}{2f_{\mathrm{c}}\left(N_{\mathrm{subc}}^{\mathrm{OFDM}}+N_{\mathrm{CP}}^{\mathrm{OFDM}}\right)M^{\mathrm{OFDM}}}$	$\Delta v^{\mathrm{OCDM}} = \frac{B^{\mathrm{OCDM}} c_0}{2f_{\mathrm{c}}\left(N_{\mathrm{subch}}^{\mathrm{OCDM}}+N_{\mathrm{CP}}^{\mathrm{OCDM}}\right)M^{\mathrm{OCDM}}}$
Max. unamb. relative radial velocity	$v_{\mathrm{max,unamb}}^{\mathrm{CS}} = \frac{c_0}{4f_{\mathrm{c}}\left(T_{\mathrm{chirp}}^{\mathrm{CS}}+T_{\mathrm{guard}}^{\mathrm{CS}}\right)}$	$v_{\mathrm{max,unamb}}^{\mathrm{PMCW}} = \frac{F_{\mathrm{s}}^{\mathrm{PMCW}} c_0}{4f_{\mathrm{c}} N_{\mathrm{PRBS}}^{\mathrm{PMCW}} A^{\mathrm{PMCW}}}$	$v_{\mathrm{max,unamb}}^{\mathrm{OFDM}} = \frac{B^{\mathrm{OFDM}} c_0}{4f_{\mathrm{c}}\left(N_{\mathrm{subc}}^{\mathrm{OFDM}}+N_{\mathrm{CP}}^{\mathrm{OFDM}}\right)}$	$v_{\mathrm{max,unamb}}^{\mathrm{OCDM}} = \frac{B^{\mathrm{OCDM}} c_0}{4f_{\mathrm{c}}\left(N_{\mathrm{subch}}^{\mathrm{OCDM}}+N_{\mathrm{CP}}^{\mathrm{OCDM}}\right)}$
Max. tolerable relative radial velocity	Limited by tolerable range-Doppler coupling	Depends on adopted PRBS	$v_{\mathrm{max,ICI}}^{\mathrm{OFDM}} = \frac{B^{\mathrm{OFDM}} c_0}{20 N_{\mathrm{subc}}^{\mathrm{OFDM}} f_{\mathrm{c}}}$	Not yet investigated
Processing gain	$G_{\mathrm{p}}^{\mathrm{CS}} = N_{\mathrm{chirp}}^{\mathrm{CS}} M^{\mathrm{CS}}$	$G_{\mathrm{p}}^{\mathrm{PMCW}} = N_{\mathrm{PRBS}}^{\mathrm{PMCW}} A^{\mathrm{PMCW}} M^{\mathrm{PMCW}}$	$G_{\mathrm{p}}^{\mathrm{OFDM}} = N_{\mathrm{subc}}^{\mathrm{OFDM}} M^{\mathrm{OFDM}}$	$G_{\mathrm{p}}^{\mathrm{OCDM}} = N_{\mathrm{subch}}^{\mathrm{OCDM}} M^{\mathrm{OCDM}}$
Communication performance parameters				
	CS	**PMCW**	**OFDM**	**OCDM**
Data rate	$\mathcal{R}_{\mathrm{QPSK}}^{\mathrm{CS}} = \frac{2}{T_{\mathrm{chirp}}^{\mathrm{CS}}+T_{\mathrm{guard}}^{\mathrm{CS}}}$	$\mathcal{R}_{\mathrm{BPSK}}^{\mathrm{PMCW}} = \frac{F_{\mathrm{s}}^{\mathrm{PMCW}}}{N_{\mathrm{PRBS}}^{\mathrm{PMCW}} A^{\mathrm{PMCW}}}$	$\mathcal{R}_{\mathrm{QPSK}}^{\mathrm{OFDM}} = \frac{2N_{\mathrm{subc}}^{\mathrm{OFDM}} \mathrm{B}^{\mathrm{OFDM}}}{N_{\mathrm{subc}}^{\mathrm{OFDM}}+N_{\mathrm{CP}}^{\mathrm{OFDM}}}$	$\mathcal{R}_{\mathrm{QPSK}}^{\mathrm{OCDM}} = \frac{2N_{\mathrm{subch}}^{\mathrm{OCDM}} \mathrm{B}^{\mathrm{OCDM}}}{N_{\mathrm{subch}}^{\mathrm{OCDM}}+N_{\mathrm{CP}}^{\mathrm{OCDM}}}$
E_{b}/N_0	$(E_{\mathrm{b}}/N_0)_{\mathrm{QPSK}}^{\mathrm{CS}} = \frac{P_{\mathrm{Tx}} N_{\mathrm{chirp}}^{\mathrm{CS}}}{\frac{1}{\left(N_{\mathrm{chirp}}^{\mathrm{CS}}\right)^2} \sum_{n=0}^{N_{\mathrm{chirp}}^{\mathrm{CS}}-1} \frac{N_0}{\lvert h_n^{\mathrm{CS}}\rvert^2}}$	$(E_{\mathrm{b}}/N_0)_{\mathrm{BPSK}}^{\mathrm{PMCW}} = \frac{P_{\mathrm{Tx}}(A^{\mathrm{PMCW}}-1) N_{\mathrm{PRBS}}^{\mathrm{PMCW}}}{\frac{1}{N_{\mathrm{PRBS}}^{\mathrm{PMCW}}} \sum_{n=0}^{N_{\mathrm{PRBS}}^{\mathrm{PMCW}}-1} \frac{N_0}{\lvert H_n^{\mathrm{PMCW}}\rvert^2}}$	$(E_{\mathrm{b}}/N_0)_{\mathrm{QPSK},n}^{\mathrm{OFDM}} = \frac{P_{\mathrm{Tx}} \lvert H_n^{\mathrm{OFDM}}\rvert^2}{N_0}$	$(E_{\mathrm{b}}/N_0)_{\mathrm{QPSK},n}^{\mathrm{OCDM}} = \frac{P_{\mathrm{Tx}}}{\frac{1}{N_{\mathrm{subch}}^{\mathrm{OCDM}}} \sum_{n=0}^{N_{\mathrm{subch}}^{\mathrm{OCDM}}-1} \frac{N_0}{\lvert H_n^{\mathrm{OCDM}}\rvert^2}}$
BER	$\mathrm{BER}_{\mathrm{QPSK}}^{\mathrm{CS}} = Q\left(\sqrt{2\,(E_{\mathrm{b}}/N_0)_{\mathrm{QPSK}}^{\mathrm{CS}}}\right)$	$\mathrm{BER}_{\mathrm{BPSK}}^{\mathrm{PMCW}} = Q\left(\sqrt{2\,(E_{\mathrm{b}}/N_0)_{\mathrm{BPSK}}^{\mathrm{PMCW}}}\right)$	$\mathrm{BER}_{\mathrm{QPSK},n}^{\mathrm{OFDM}} = Q\left(\sqrt{2\,(E_{\mathrm{b}}/N_0)_{\mathrm{QPSK},n}^{\mathrm{OFDM}}}\right)$	$\mathrm{BER}_{\mathrm{QPSK},n}^{\mathrm{OCDM}} = Q\left(\sqrt{2\,(E_{\mathrm{b}}/N_0)_{\mathrm{QPSK},n}^{\mathrm{OCDM}}}\right)$

reported in the literature so far.

The remaining processing steps after matched-filtering in the discrete-frequency domain are the same from the PMCW and OFDM case in Subsections III-B1 and III-C1, namely range and velocity windowing, row-wise DFTs for Doppler shift estimation, and column-wise IDFTs for time delay estimation. After the estimated Doppler shifts and time delays are translated into relative radial velocity and range estimates, respectively, a range-velocity radar image $\mathbf{I}^{\mathrm{OCDM}} \in \mathbb{C}^{N_{\mathrm{subch}}^{\mathrm{OCDM}} \times M^{\mathrm{OCDM}}}$ is ultimately obtained. According to [47], [92], the aforementioned radar image experiences a processing gain $G_{\mathrm{p}}^{\mathrm{OCDM}}$ and is associated with range resolution ΔR^{OCDM}, maximum unambiguous range $R_{\mathrm{max,unamb}}^{\mathrm{OCDM}}$, and maximum tolerable range $R_{\mathrm{max,ISI}}^{\mathrm{OCDM}}$, as well as relative radial velocity resolution, Δv^{OCDM} and maximum unambiguous relative radial velocity $v_{\mathrm{max,unamb}}^{\mathrm{OCDM}}$ values as shown in Table I based on [47], [92]. A restriction on maximum tolerable relative radial velocity for the considered OCDM-based RadCom system has not been accurately investigated in the literature yet and is therefore not shown in Table I.

2) Communication processing: Under the assumption that time, frequency and phase offsets from the second term in (1) have already been compensated via synchronization based on a preamble that can be defined by the Schmidl and Cox algorithm [104] as in the OFDM case from Subsection III-C2 [44], the remaining communication processing in the considered OCDM-based RadCom system starts with an element-wise multiplication of each block by the vector $\mathbf{\Gamma} \in \mathbb{C}^{N_{\mathrm{subch}}^{\mathrm{OCDM}} \times 1}$ [43], whose nth element, $n \in \{0, 1, \ldots, N_{\mathrm{subch}}^{\mathrm{OCDM}} - 1\}$, is expressed for even $N_{\mathrm{subch}}^{\mathrm{OCDM}}$ as

$$\Gamma_n = \mathrm{e}^{-\mathrm{j}\pi n^2 / N_{\mathrm{subch}}^{\mathrm{OCDM}}}. \tag{20}$$

Next, a fast-time, element-wise multiplication of each block by the vector $\mathbf{G}^{\mathrm{OCDM}} \in \mathbb{C}^{N_{\mathrm{subch}}^{\mathrm{OCDM}} \times 1}$ containing the multiplicative inverse of the estimate of the communication CFR $\mathbf{H}^{\mathrm{OCDM}} \in \mathbb{C}^{N_{\mathrm{subch}}^{\mathrm{OCDM}} \times 1}$ is performed, and column-wise IDFTs complete the communication processing. Together with the previously performed column-wise DFTs before the specific radar and communication processing steps, the multiplication by $\mathbf{\Gamma} \in \mathbb{C}^{N_{\mathrm{subch}}^{\mathrm{OCDM}} \times 1}$ and the IDFTs comprise a DFnT. The output discrete-Fresnel domain OCDM frame from the aforementioned processing steps undergoes P/S conversion, generating the modulated data stream $\mathbf{d}_{\mathrm{Rx}}^{\mathrm{OCDM}} \in \mathbb{C}^{(N_{\mathrm{subch}}^{\mathrm{OCDM}} M^{\mathrm{OCDM}}) \times 1}$.

The presented communication processing steps in the considered OFDM-based RadCom system ultimately yield the overall data rate denoted by $\mathcal{R}_{\mathrm{QPSK}}^{\mathrm{OCDM}}$, as well as energy per bit to noise power spectral density ratio $(E_{\mathrm{b}}/N_0)_{\mathrm{QPSK},n}^{\mathrm{OCDM}}$ and BER denoted by $\mathrm{BER}_{\mathrm{QPSK},n}^{\mathrm{OCDM}}$ for for the nth QPSK-modulated subchirp as presented in Table I, where $H_n^{\mathrm{OCDM}} \in \mathbb{C}$ is the nth element of $\mathbf{H}^{\mathrm{OCDM}}$.

3) Multiplexing for MIMO and multiuser scenarios: To enable MIMO or multiuser operation of N_{Tx} transmitters based on the transmission of orthogonal signals in OCDM-based RadCom systems, FDM and CDM approaches are usually adopted, being TDM disregarded for the same reasons as in the PMCW and OFDM cases from Subsections III-B3 and III-C3, respectively.

A typical FDM-based approach is the so-called frequency-shift precoding (FSP) [92], [124]. The use of FSP consists of allocating a set of $N_{\mathrm{subch}}^{\mathrm{OCDM}}/N_{\mathrm{Tx}}$ interleaved frequency tones to each of the N_{Tx} transmitters via a precoding, which is undone at the receiver side by selecting the associated frequency tones with the evaluated transmitter. This results in similar changes in both radar and

communication performances as in the OFDM case from Subsection III-C3, namely a reduction of the listed processing gain in Table I to $G_{\mathrm{p}}^{\mathrm{OCDM}} = (N_{\mathrm{subch}}^{\mathrm{OCDM}}/N_{\mathrm{Tx}})M^{\mathrm{OCDM}}$ and a reduction of the maximum unambiguous range to $R_{\mathrm{max,unamb}}^{\mathrm{OCDM}} = (N_{\mathrm{subch}}^{\mathrm{OCDM}}/N_{\mathrm{Tx}})c_0/(2B^{\mathrm{OCDM}})$. To avoid isolation loss among transmitters due to a similar effect to ICI in OFDM systems, an additional constraint on the maximum tolerable relative radial velocity for OCDM-based RadCom systems adopting FSP-based FDM as a multiplexing strategy is defined as $v_{\mathrm{max,FSP}}^{\mathrm{OCDM}} = B^{\mathrm{OCDM}}c_0/(20N_{\mathrm{subch}}^{\mathrm{OCDM}}f_{\mathrm{c}})$. As in the OFDM case, the communication performance is only affected in the multiuser case, where the achieved data rate assuming QPSK modulation is reduced by a factor of N_{Tx} to $\mathcal{R}_{\mathrm{QPSK}}^{\mathrm{OCDM}} = 2N_{\mathrm{subch}}^{\mathrm{OCDM}}\mathrm{B}^{\mathrm{OCDM}}/[N_{\mathrm{Tx}}(N_{\mathrm{subch}}^{\mathrm{OCDM}} + N_{\mathrm{CP}}^{\mathrm{OCDM}})]$.

A CDM-based approach for enabling MIMO or multiuser operation of OCDM-based RadCom systems is the use of uncorrelated OCDM symbols, which yields poor isolation among transmitters as described for the OFDM case in Subsection III-C [119]. Alternatively, the same outer coding described for CS, PMCW, and OFDM in Subsections III-A3, III-B3, and III-C3, respectively, can also be performed in the OCDM context [92], changing the required duration to transmit a block to $N_{\mathrm{Tx}}T_{\mathrm{block}}^{\mathrm{OCDM}}$ and consequently the maximum unambiguous relative radial velocity to $v_{\mathrm{max,unamb}}^{\mathrm{OCDM}} = B^{\mathrm{OCDM}}c_0/[4f_{\mathrm{c}}N_{\mathrm{Tx}}(N_{\mathrm{subch}}^{\mathrm{OCDM}} + N_{\mathrm{CP}}^{\mathrm{OCDM}})]$. Additionally, the outer-coding based CDM changes the listed processing gain in Table I to $G_{\mathrm{p}}^{\mathrm{OCDM}} = N_{\mathrm{Tx}}N_{\mathrm{subch}}^{\mathrm{OCDM}}M^{\mathrm{PMCW}}$, although the effectively experienced $G_{\mathrm{p}}^{\mathrm{OCDM}}$ tends to be the same as in the SISO case due to the necessary reduction of M^{PMCW} to keep $T_{\mathrm{frame}}^{\mathrm{OCDM}}$ constant. Finally, it is worth highlighting that, as in the previously described FSP-based FDM approach, the only experienced change in the communication performance is the reduction of the data rate by a factor of N_{Tx} in the multiuser case.

Alternative multiplexing strategies for OCDM-based RadCom systems include the so-called Fresnel-division multiplexing (FrDM), which consists of allocating different sets of orthogonal subchirps to different transmit channels. A possible FrDM approach is described in [94] for time-domain reflectometry (TDR) systems, but FrDM-based approaches that enable higher data rates have not yet been investigated.

IV. Comparative performance analysis

In this section, a comparative performance analysis of the RadCom modulation schemes presented in Section III is performed. In this sense, the influence of key parameters in RadCom on radar and communication performance parameters is discussed in Subsection IV-A. Assuming an HAD context, Subsection IV-B presents and discusses the parameterization of RadCom systems based on all four considered modulation schemes. Next, Subsections IV-C and IV-D discuss the influence of a same-modulation-scheme interferer on the radar and communication perfomances of the RadCom systems considered in the previous subsection, respectively. Finally, a similar scenario to the one discussed in Section IV-C is considered in a MIMO and multiuser context in Subsection IV-E, where introduced performance changes in the considered RadCom systems by the adoption of multiplexing schemes are discussed.

A. Radar and Communication Parameter Dependencies

To analyze the dependencies of radar and communication performance of RadCom systems based on CS, PMCW, OFDM, and OCDM modulation schemes on key signal parameters, an HAD context is assumed. Consequently, the physical parameters listed in Table II are adopted, which results in a range resolution of $0.15\,\mathrm{m}$ for all considered modulation schemes. Further assumptions include $N_{\mathrm{guard}}^{\mathrm{CS}} = N_{\mathrm{chirp}}^{\mathrm{CS}}/20$, as the pause between chirps is usually much shorter than the duration of a chirp in, e.g., CS-based radar systems. Additionally, $N_{\mathrm{CP}}^{\mathrm{OFDM}} = N_{\mathrm{subc}}^{\mathrm{OFDM}}/4$ and $N_{\mathrm{CP}}^{\mathrm{OCDM}} = N_{\mathrm{subch}}^{\mathrm{OCDM}}/4$ are adopted for the OFDM- and OCDM-based RadCom systems, respectively, which are typically considered values for the CP length in the literature. In order for the fraction of unused samples to be equal to $1/5$ as in the OFDM and OCDM cases, $A^{\mathrm{PMCW}} = 5$ is adopted for the PMCW-based RadCom system.

Based on the described assumptions and on the expressions in Table I, Fig. 14 shows the dependence of several parameters on the number of samples $N \in \mathbb{N}_+$ of a single obtained range profile after radar signal processing, which corresponds to the number of samples of a chirp after A/D conversion $N_{\mathrm{chirp}}^{\mathrm{CS}}$ in the CS case, the PRBS length $N_{\mathrm{PRBS}}^{\mathrm{PMCW}}$ in the PMCW case, the number of subcarriers $N_{\mathrm{subc}}^{\mathrm{OFDM}}$ in the OFDM case, and the number of subchirps $N_{\mathrm{subch}}^{\mathrm{OCDM}}$ in the OCDM case. For all modulation schemes, a direct proportion to the block duration and maximum unambiguous and tolerable ranges is observed in Figs.14a and 14b, respectively, while the maximum unambiguous and tolerable relative radial velocities are inversely proportional to N as shown in Fig.14c.

In terms of communication performance, both CS and PMCW RadCom systems experience data rate degradation along with increasing N as observed in Fig. 14d. This is explained by the fact that their block duration becomes longer, while the number of transmitted QPSK symbols in the CS case or BPSK symbols in the PMCW case remains equal to one. Conversely, the communication data rate is kept constant for increasing N values in both OFDM and OCDM RadCom schemes, which also yield higher data rates than the two aforementioned modulation schemes due to their multicarrier nature. Although the number of subcarriers or subchirps and consequently the total number of transmitted QPSK symbols increases along with N, the block duration also does, which leads to a fixed communication data rate. Assuming an AWGN channel with no attenuation and a noise power defined as in the noise contribution in (4), i.e., $k_{\mathrm{B}}\ B\ T_{\mathrm{therm}}\ NF$, the obtained E_{b}/N_0 values are shown in Fig.14e. In this figure, higher values are experienced for increasing N in both CS and PMCW modulation schemes due to the fact that P_{Tx} is integrated into the modulation symbol energy over a longer time. Although two bits per chirp are transmitted in the CS-based RadCom scheme due to the use of QPSK modulation, a higher E_{b}/N_0 than in its BPSK-based PMCW counterpart is experienced due to its higher number of usable samples per block and the reduced noise bandwidth by a factor of 10, since

TABLE II
ADOPTED PHYSICAL PARAMETERS FOR THE CONSIDERED SISO RADCOM SYSTEMS.

Physical parameters					
		CS	**PMCW**	**OFDM**	**OCDM**
Parameter	Transmission power	$P_{\mathrm{Tx}} = 0\,\mathrm{dBm}$			
	Antenna gains	$G_{\mathrm{Tx}} = G_{\mathrm{Rx}} = 10\,\mathrm{dB}$			
	Noise figure	$NF = 10\,\mathrm{dB}$			
	Carrier frequency	$f_{\mathrm{c}} = 79\,\mathrm{GHz}$			
	RF frequency bandwidth	$B^{\mathrm{CS}} = 1$ GHz	$B^{\mathrm{PMCW}} = 2$ GHz	$B^{\mathrm{OFDM}} = 1$ GHz	$B^{\mathrm{OCDM}} = 1$ GHz
	ADC sampling rate	$F_{\mathrm{s}}^{\mathrm{CS}} = 100\,\mathrm{MHz}$	$F_{\mathrm{s}}^{\mathrm{PMCW}} = 1\,\mathrm{GHz}$	$F_{\mathrm{s}}^{\mathrm{OFDM}} = 1\,\mathrm{GHz}$	$F_{\mathrm{s}}^{\mathrm{OCDM}} = 1\,\mathrm{GHz}$

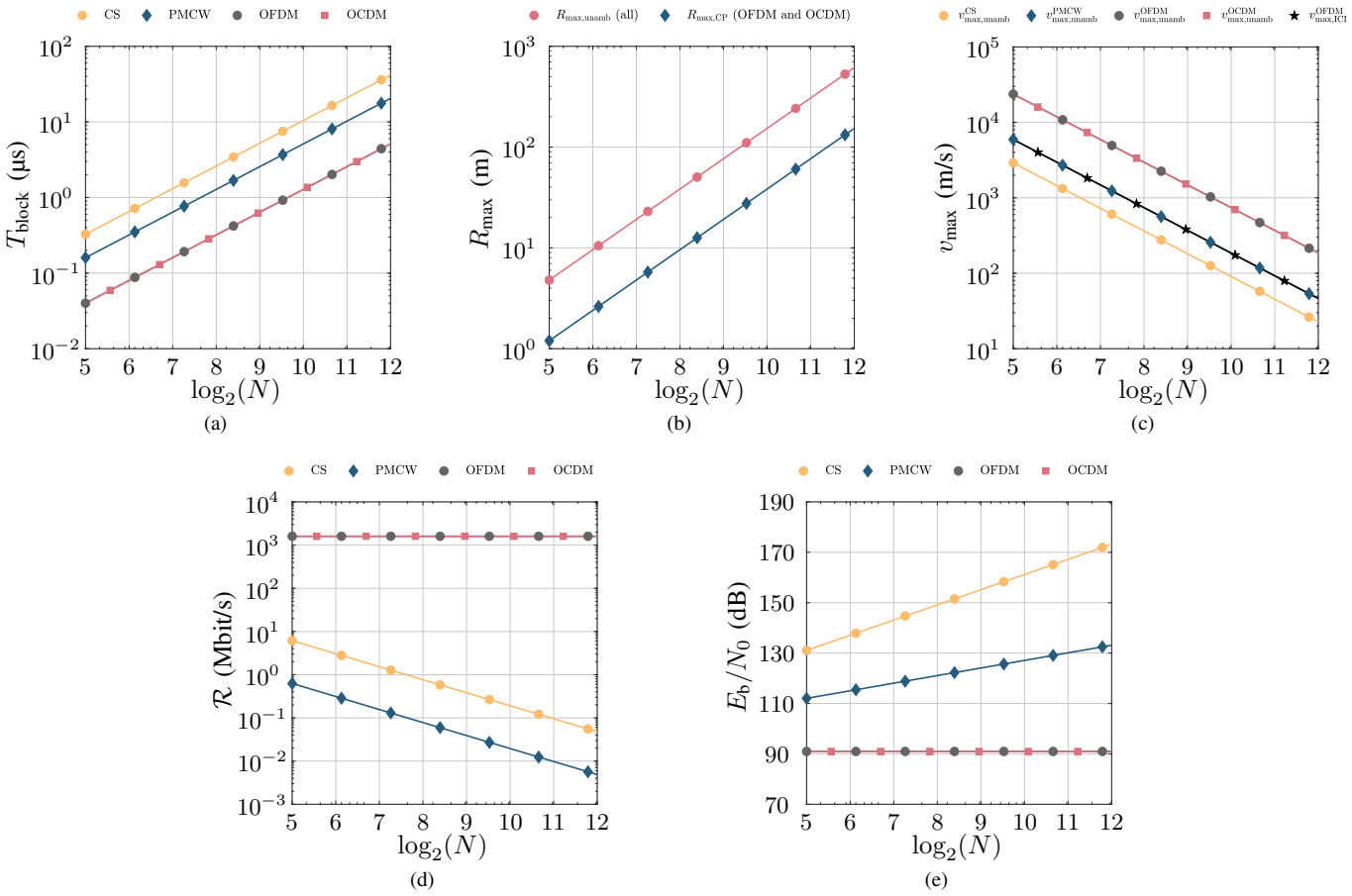

Fig. 14. Dependence of block duration and radar and communication performance parameters on the number of usable samples within a block $N \in \{32, 64, 128, 256, 512, 1024, 2040, 4096\}$, which corresponds to $N_{\mathrm{chirp}}^{\mathrm{CS}}$, $N_{\mathrm{PRBS}}^{\mathrm{PMCW}}$, $N_{\mathrm{subc}}^{\mathrm{OFDM}}$, and $N_{\mathrm{subch}}^{\mathrm{OCDM}}$ in RadCom systems based on CS, PMCW, OFDM, and OCDM, respectively. (a) shows the resulting block duration in µs. (b) shows the achieved maximum unambiguous range in m, which follows the function of N for all modulation schemes. (c) shows the maximum unambiguous relative radial velocity in m/s for all considered modulation schemes, as well as the maximum tolerable relative radial velocity for OFDM due to ICI. (d) shows the achieved data rate in Mbit/s. (e) shows the achieved E_{b}/N_0 in the considered AWGN channel.

the parameters from Table II result in $F_{\mathrm{s}}^{\mathrm{CS}} = F_{\mathrm{s}}^{\mathrm{PMCW}}/10$. In the OFDM and OCDM RadCom systems, a lower, constant E_{b}/N_0 is experienced. The lower E_{b}/N_0 is experienced due to the fact that the total transmission power P_{Tx} is divided over multiple subcarriers or subchirps. Furthermore, the fact that E_{b}/N_0 remains constant over increasing N values can be similarly explained as in the data rate case. While the power per subcarrier or subchirp is reduced by a certain factor with increasing N, the block duration is increased by the same factor, being therefore integrated into the same energy.

Considering the block parameter dependencies depicted in Fig. 14 and aiming for typical parameterization of all RadCom modulation schemes in an HAD context, which must cover a maximum range of at least 70 m and a maximum relative radial velocity of at least 50 m/s as described in Subsection IV-B, $N_{\mathrm{chirp}}^{\mathrm{CS}} = 1000$, $N_{\mathrm{PRBS}}^{\mathrm{PMCW}} = 1023$, $N_{\mathrm{subc}}^{\mathrm{OFDM}} = 2048$, $N_{\mathrm{subch}}^{\mathrm{OCDM}} = 2048$ are fixed for the considered RadCom systems based on CS, PMCW, OFDM, and OCDM, respectively. Based on the assumed parameters, the dependence of the frame duration and the remaining radar performance parameters on the number of blocks $M \in \mathbb{N}_+$ is shown in Fig. 15. In RadCom systems based on CS, PMCW, OFDM, and OCDM, M is ex-

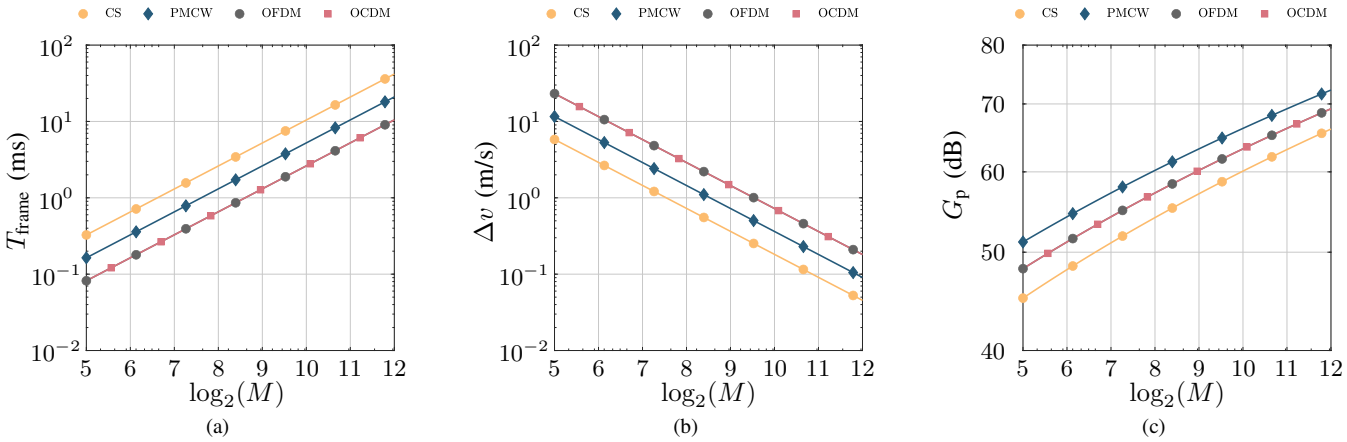

Fig. 15. Dependence of frame duration and radar performance parameters on the number of blocks $M \in \{32, 64, 128, 256, 512, 1024, 2040, 4096\}$, which corresponds to M^{CS}, M^{PMCW}, M^{OFDM}, and M^{OCDM} in RadCom systems based on CS, PMCW, OFDM, and OCDM, respectively. (a) shows the resulting frame duration in ms. (b) shows the achieved relative radial velocity resolution in m/s. (c) shows the processing gain in dB for all considered modulation schemes.

pressed by M^{CS}, M^{PMCW}, M^{OFDM}, and M^{OCDM}, respectively. In this context, Fig. 15a shows the resulting frame duration. For typical HAD applications, the frame duration should be below $20\,\text{ms}$, which yields appropriate relative radial velocity resolution and processing gain in all considered modulation schemes as shown in Figs. 15b and 15c.

Furthermore, the aforementioned fixed values for the N parameters result in the complementary cumulative distribution functions (CCDFs) of the RF PAPR for all considered RadCom modulation schemes shown in Fig. 16. The attained results were obtained by calculating the peak-to-mean envelope power ratio (PMEPR) [125], i.e., the PAPR of the complex-baseband equivalent of the transmit signals expressed in (9), (11), (14), and (19), assuming an oversampling factor of 20 to capture fast variations of signals. Since f_{c} is much higher than the bandwidth in all considered cases, the PAPRs of the RF signals are finally obtained by adding 3.0 dB to the results from the aforementioned PAPR calculation for oversampled complex-baseband equivalents of signals [126]. Both CS and PMCW yield a fixed PAPR of nearly 3.0 dB due to CW characteristic of their transmit waveforms, which does not change for other combinations of chirp duration $T_{\text{chirp}}^{\text{CS}}$, frequency bandwidth B^{CS}, as well as for $N_{\text{chirp}}^{\text{CS}} = T_{\text{chirp}}^{\text{CS}} F_{\text{s}}^{\text{CS}}$ in the CS case or PRBS lengths $N_{\text{PRBS}}^{\text{PMCW}}$ in the PMCW case. The worst observed PAPR in Fig. 16, with probability 0.99 of being higher than 11.5 dB, is attained by both OFDM and OCDM due to their similar transmitter structure [43]. For higher number of subcarriers $N_{\text{subc}}^{\text{OFDM}}$ and subchirps $N_{\text{subch}}^{\text{OCDM}}$ in OFDM and OCDM systems, respectively, increasing PAPR values are expected. For the sake of conciseness, the reader is referred to [43], [95], [127] for an extended discussion on PAPR in OFDM- and OCDM-based systems.

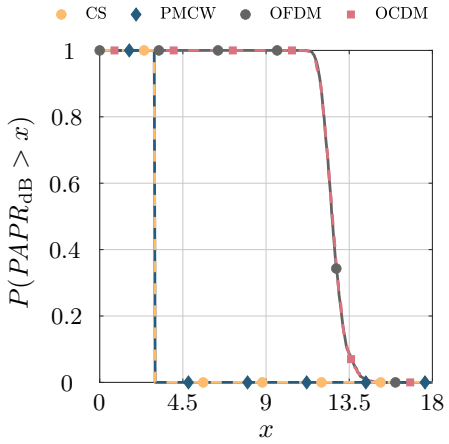

Fig. 16. Simulated RF PAPR performance based on the carrier frequency $f_{\text{c}} = 79\,\text{GHz}$ from Table II and assuming $N_{\text{chirp}}^{\text{CS}} = 1000$, $N_{\text{PRBS}}^{\text{PMCW}} = 1023$, $N_{\text{subc}}^{\text{OFDM}} = 2048$, and $N_{\text{subch}}^{\text{OCDM}} = 2048$.

B. Joint Radar-Communication System Parameterization

In this section, a comparative performance analysis of the RadCom modulation schemes presented in Section III is performed. Since CS- and PMCW-based RadCom systems are primarily used for radar sensing, offering low-data-rate communication capabilities simply as an additional feature, a radar-centric parameterization of RadCom systems is performed aiming to satisfy typical mid-range HAD requirements, which comprise a maximum range of 70 m with a resolution of up to 0.2 m, and a maximum relative radial velocity of 50 m/s with a resolution of up to 0.2 m/s. In this context, the physical parameters from Table II are further considered and additionally adopted waveform parameters for the considered RadCom modulation schemes are listed in Table III.

The attained radar and communication performance parameters by the SISO RadCom systems with parameters from Table III are listed in Table IV. As a proof of concept, the system-on-a-chip (SoC) platform Zynq UltraScale+ RFSoC ZCU111 from Xilinx, Inc. was used to emulate SISO RadCom systems based on the considered modulation schemes and adopted parameters together with the radar target simulator (RTS) described in [109] and used in [108], [128], [129], which receives transmitted signals by the RadCom system and

TABLE III
ADOPTED SIGNAL PARAMETERS FOR THE CONSIDERED SISO RADCOM SYSTEMS.

Signal parameters					
		CS	**PMCW**	**OFDM**	**OCDM**
Block parameters	Samples	$N_{\text{chirp}}^{\text{CS}} = 1000$ $N_{\text{guard}}^{\text{CS}} = 20$	$N_{\text{PRBS}}^{\text{PMCW}} = 1023$ $A^{\text{PMCW}} = 5$	$N_{\text{subc}}^{\text{OFDM}} = 2048$ $N_{\text{CP}}^{\text{OFDM}} = 512$	$N_{\text{subch}}^{\text{OCDM}} = 2048$ $N_{\text{CP}}^{\text{OCDM}} = 512$
	Time duration	$T_{\text{chirp}}^{\text{CS}} = 10.00\,\mu\text{s}$ $T_{\text{guard}}^{\text{CS}} = 0.20\,\mu\text{s}$ $T_{\text{block}}^{\text{CS}} = 10.20\,\mu\text{s}$	$T_{\text{PRBS}}^{\text{PMCW}} = 1.02\,\mu\text{s}$ $T_{\text{block}}^{\text{PMCW}} = 5.11\,\mu\text{s}$	$T_{\text{symb}}^{\text{OFDM}} = 2.05\,\mu\text{s}$ $T_{\text{CP}}^{\text{OFDM}} = 0.51\,\mu\text{s}$ $T_{\text{block}}^{\text{OFDM}} = 2.56\,\mu\text{s}$	$T_{\text{symb}}^{\text{OCDM}} = 2.05\,\mu\text{s}$ $T_{\text{CP}}^{\text{OCDM}} = 0.51\,\mu\text{s}$ $T_{\text{block}}^{\text{OCDM}} = 2.56\,\mu\text{s}$
Frame parameters	Samples	$M^{\text{CS}} = 1024$	$M^{\text{PMCW}} = 2048$	$M^{\text{OFDM}} = 4096$	$M^{\text{OCDM}} = 4096$
	Time duration	$T_{\text{frame}}^{\text{CS}} = 10.45$ ms	$T_{\text{frame}}^{\text{PMCW}} = 10.48$ ms	$T_{\text{frame}}^{\text{OFDM}} = 10.49$ ms	$T_{\text{frame}}^{\text{OCDM}} = 10.49$ ms

TABLE IV
RESULTING RADAR AND COMMUNICATION PERFORMANCE PARAMETERS FOR THE CONSIDERED SISO RADCOM SYSTEMS.

Radar performance parameters				
	CS	**PMCW**	**OFDM**	**OCDM**
Range resolution	$\Delta R^{\text{CS}} = 0.15\,\text{m}$	$\Delta R^{\text{PMCW}} = 0.15\,\text{m}$	$\Delta R^{\text{OFDM}} = 0.15\,\text{m}$	$\Delta R^{\text{OCDM}} = 0.15\,\text{m}$
Max. unamb. range	$R_{\text{max,unamb}}^{\text{CS}} = 150\,\text{m}$	$R_{\text{max,unamb}}^{\text{PMCW}} = 153.45\,\text{m}$	$R_{\text{max,unamb}}^{\text{OFDM}} = 307.20\,\text{m}$	$R_{\text{max,unamb}}^{\text{OCDM}} = 307.20\,\text{m}$
Max. tolerable range	—	—	$R_{\text{max,ISI}}^{\text{OFDM}} = 76.80\,\text{m}$	$R_{\text{max,ISI}}^{\text{OCDM}} = 76.80\,\text{m}$
Relative radial velocity resolution	$\Delta v^{\text{CS}} = 0.18\,\text{m/s}$	$\Delta v^{\text{PMCW}} = 0.18\,\text{m/s}$	$\Delta v^{\text{OFDM}} = 0.18\,\text{m/s}$	$\Delta v^{\text{OCDM}} = 0.18\,\text{m/s}$
Max. unamb. relative radial velocity	$v_{\text{max,unamb}}^{\text{CS}} = 93.08\,\text{m/s}$	$v_{\text{max,unamb}}^{\text{PMCW}} = 185.60\,\text{m/s}$	$v_{\text{max,unamb}}^{\text{OFDM}} = 370.85\,\text{m/s}$	$v_{\text{max,unamb}}^{\text{OCDM}} = 370.85\,\text{m/s}$
Max. tolerable relative radial velocity	—	—	$v_{\text{max,ICI}}^{\text{OFDM}} = 92.71\,\text{m/s}$	—
Processing gain	$G_{\text{p}}^{\text{CS}} = 60.10\,\text{dB}$	$G_{\text{p}}^{\text{PMCW}} = 69.23\,\text{dB}$	$G_{\text{p}}^{\text{OFDM}} = 69.24\,\text{dB}$	$G_{\text{p}}^{\text{OCDM}} = 69.24\,\text{dB}$
Communication performance parameters				
	CS	**PMCW**	**OFDM**	**OCDM**
Data rate	$\mathcal{R}_{\text{QPSK}}^{\text{CS}} = 196.08\,\text{kbit/s}$	$\mathcal{R}_{\text{BPSK}}^{\text{PMCW}} = 195.50\,\text{kbit/s}$	$\mathcal{R}_{\text{QPSK}}^{\text{OFDM}} = 1.60\,\text{Gbit/s}$	$\mathcal{R}_{\text{QPSK}}^{\text{OCDM}} = 1.60\,\text{Gbit/s}$

modifies them according to adjustable range, relative radial velocity, and attenuation factors depending on, e.g., range and RCS. In the considered measurement setup, the transmitters and the receivers of both RadCom and RTS have I/Q channels. To avoid unwanted reflections of the surrounding, the DACs of the RadCom transmitter are directly connected to the corresponding ADCs of the RTS and the DACs of RTS transmitter are directly connected to the ADCs of the RadCom receiver. The region of interest of the obtained radar images from measurements with a single point target with RCS $\sigma_{\text{RCS}} = 20\,\text{dBsm}$ at an emulated range of 25.5 m and relative radial velocity of 30 m/s is shown in Fig. 17. For those images, rectangular windowing in range and velocity directions was considered. A slightly higher sidelobe floor is observed for the OCDM-based RadCom system, while the remaining modulation schemes yield a similarly lower sidelobe level. This is explained by the influence of the modulated QPSK symbols onto the OCDM signal, which is not removed by the correlation processing at the receiver side and ultimately biases the range sidelobes. Since a DFT-based Doppler shift estimation is performed in all considered RadCom systems, the sidelobe level decreases at the same ratio for all modulation schemes when moving away from the estimated target velocity along the relative radial velocity direction.

Although only slight differences are observed in the radar images shown in Fig. 17, where typical range and relative radial velocity values are assumed, an increase in the latter parameter may induce Doppler shifts that impose non-negligible degradation to the radar images that strongly depends on the adopted modulation scheme. Aiming to quantify the Doppler-shift robustness of the radar sensing performed by RadCom systems based on each of the four considered modulation schemes, peak power loss ratio (PPLR), peak-to-sidelobe level ratio (PSLR), and integrated-sidelobe level ratio (ISLR) of their range ambiguity functions were evaluated along Doppler shifts associated with relative radial velocities from 0 m/s to the maximum tolerable value of 92.71 m/s in the OFDM scheme. The simulation results, which assume an oversampling factor of 20 to account for the influence of sidelobes on point targets that do not exactly fall onto a single range bin, are shown in Fig. 18. The PPLR results shown in Fig. 18a serve as a measure of SNR loss, expressing the ratio between the main lobe power under the evaluated Doppler shift and the one under no Doppler shift [116]. An analysis of the obtained results reveals that PMCW yields the highest PPLR degradation along with increasing relative radial velocities, which is caused by both the degradation of the MLS periodic autocorrelation function (PACF) and the incoherent accumulation effect under increasing Doppler shifts, which is described in further detail in [130]. A maximum PPLR degradation of 0.14 dB is observed in both OFDM and OCDM cases and, as expected, no PPLR degradation is experience in the CS

This is the author's version of an article that has been published in the IEEE TRANSACTIONS ON MICROWAVE THEORY AND TECHNIQUES. Changes were made to this version by the publisher prior to publication. The final version of record is available at https://doi.org/10.1109/TMTT.2021.3126887

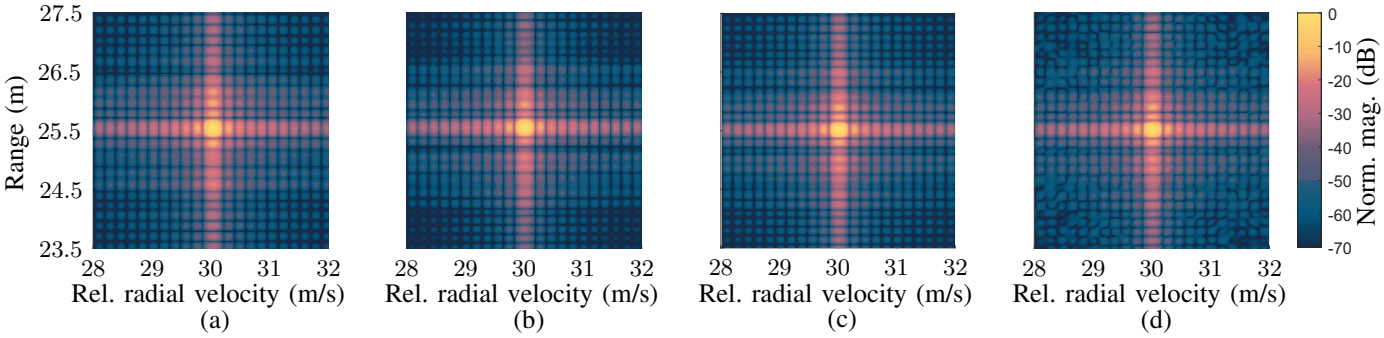

Fig. 17. Obtained range-velocity radar images from measurements with RadCom systems based on: (a) CS, (b) PMCW, (c) OFDM, and (d) OCDM modulation schemes.

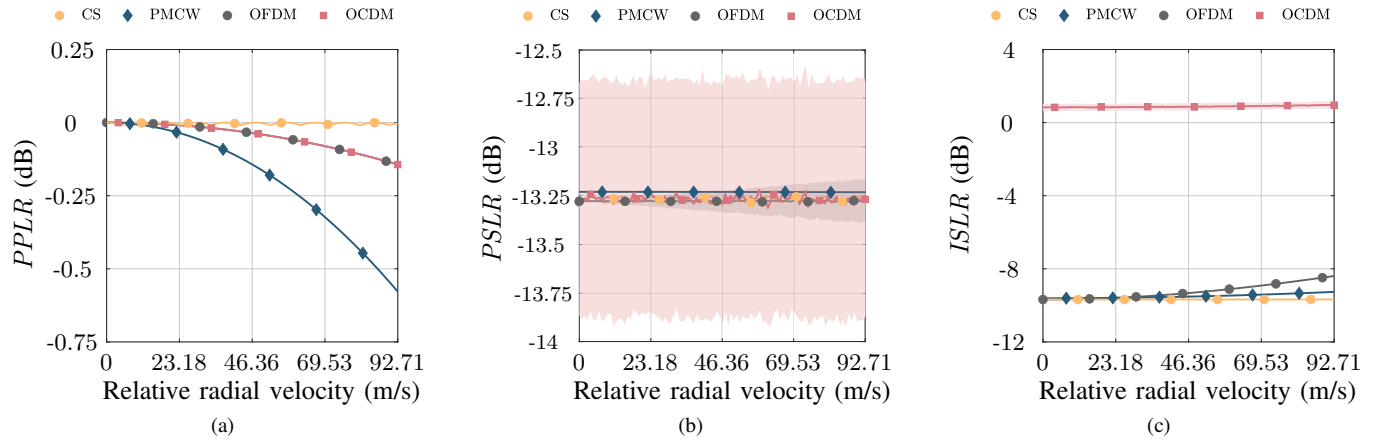

Fig. 18. Simulated Doppler-shift tolerance: range (a) PPLR, (b) PSLR, and (c) ISLR. The continuous lines represent the mean value of the calculated parameters and the shading in the background represents the standard deviation.

case. For all modulation schemes, the calculated PPLR values present negligible standard deviation. In their turn, the PSLR and ISLR express the ratio between the peak powers of the highest sidelobe and the main lobe and the ratio between the integrated sidelobe and main lobe powers, respectively [125]. Both metrics serve as parameters to predict the radar sensing performance in multi-target scenarios, since high sidelobes associated with a strong target detection may not only mask weaker target reflections, but also be erroneously detected as targets. As shown in Fig. 18b, all modulation schemes present roughly the mean PSLR value along all evaluated relative radial velocities. In terms of standard deviation of the PSLR, both CS and PMCW present negligible values, while increasing values are observed for both OFDM and OCDM. The high standard deviation values experiences in the OCDM-based RadCom system are explained by the dependence of the obtained range profiles on the transmit QPSK symbols. The Doppler-shift robustness analysis is finally completed with the ISLR results shown in Fig. 18c. The attained ISLR values in the CS-based RadCom system remain unaltered over all considered velocities due to its known robustness, while ISLR degradations of 0.12 dB and 0.35 dB at 92.71 m/s are observed in the OCDM and PMCW cases, respectively, w.r.t. the values attained at 0 m/s. Although a small ISLR degradation is experienced in the OCDM case, high ISLR values are attained for all considered velocities due to the aforementioned absence of compensation for the influence of transmit QPSK symbols on the correlation-based OCDM radar processing. Lastly, the most severe ISLR degradation is observed in the OFDM case, where the experienced ICI at the highest considered velocity yields a 1.31 dB ISLR degradation w.r.t. the static case. As in the PPLR case, negligible standard deviation of the calculated ISLRs is observed. If other parameterizations of the SISO RadCom systems are adopted, attention must be drawn to the fact that increasing PRBS length $N_{\text{PRBS}}^{\text{PMCW}}$ and number of accumulations A^{PMCW} in the PMCW case, as well as increasing numbers of subcarriers $N_{\text{subc}}^{\text{OFDM}}$ and subchirps $N_{\text{subch}}^{\text{OCDM}}$ in the OFDM and OCDM cases, respectively, lead to more severe degradation of PPLR, PSLR, and ISLR values along increasing relative radial velocities if both the carrier frequency and the frequency bandwidth are kept constant.

The comparative performance analysis in this subsection is finally completed with a simulative BER analysis, whose results assuming a 4-path Rayleigh channel are shown in Fig. 19. For the RadCom systems based on OFDM and OCDM, mean BER results were obtained for all $N_{\text{subc}}^{\text{OFDM}}$ subcarriers and $N_{\text{subch}}^{\text{OCDM}}$ subchirps, respectively. The simulated BER performance results are represented in the form of curves in Fig. 19 and agree with the calculated BER performance results based on the closed-form E_{b}/N_0 and BER

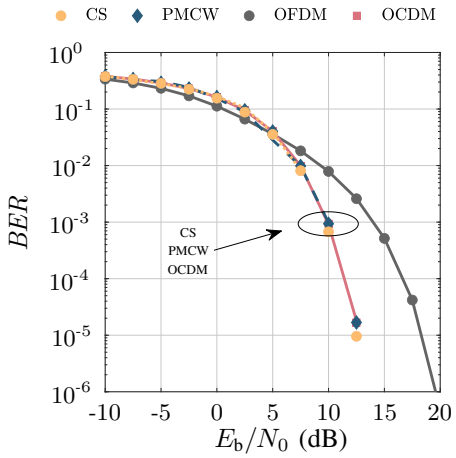

Fig. 19. Simulated BER performance in a 4-path Rayleigh channel.

expressions from Table I, which in turn are represented in the form of markers. Due to their spread-spectrum nature, RadCom systems based on CS, PMCW, and OCDM schemes yield virtually the same BER performance, outperforming their OFDM counterpart for E_b/N_0 higher than 5 dB in the considered communication channel. A slightly performance improvement for increasing E_b/N_0 can be observed in the CS due to its unique experienced communication channel, which becomes irrelevant for usual E_b/N_0 and BER values. If the same transmit power P_{Tx} is assumed for all considered RadCom systems, very high E_b/N_0 values will be attained by CS and PMCW, since they only carry 2 bits and 1 bit per block, respectively. This results in the fact that symbols may be correctly demodulated in those modulation schemes even under negative SNR regime, since very high processing gains are yielded by the RadCom systems based on CS and PMCW. In their turn, OFDM and OCDM yield much higher data rates as listed in Table IV, while having considerably lower E_b/N_0 values since 2 bits are transmitted per subcarrier and subchirp, respectively. This indicates that OCDM yields the best communication performance among the four considered modulation schemes, achieving the same data rate and spectral efficiency as OFDM while also presenting sufficiently robust BER performance.

C. Influence of Interference on Radar Performance

Still considering the parameters from Tables III and II, as well as their resulting radar and communication performance parameters from Table IV, the influence of a RadCom interferer on both radar and communication performances of a victim RadCom system is analyzed assuming that both adopt the same modulation scheme, but transmit different payload data.

For the analysis of radar performance under interference, it is assumed that the interferer and victim RadCom systems are at the same position and that the same considered point target for the measurements with the RTS, which has RCS $\sigma_{RCS} = 20\,\mathrm{dBsm}$, range of 25.5 m and relative radial velocity of 30 m/s, is present in the scenario. Additionally, it is assumed that there is no coupling between the receiver of the victim RadCom system and the both the victim and interferer RadCom transmitters. Consequently, the victim RadCom receives both the reflection of its own signal and the one of the signal transmitted by the RadCom interferer off the point target, being also impaired by AWGN. Although this scenario is not realistic, it allows evaluating the sole influence of the adopted modulation scheme on the experienced interference in a worst-case scenario and has already been assumed in the literature [117].

Given the assumed scenario, the simulated radar images keeping the aforementioned parameters and adding an interfering signal with power such that the victim RadCom experiences a signal-to-interference ratio (SIR) before signal processing of $-25\,\mathrm{dB}$ are shown in Fig. 20. In this image only the worst case in the considered scenario was considered for CS, namely the one where there is full time and frequency overlap between the interfering and victim RadCom signals. For PMCW, both the use of the same MLS for the RadCom interferer and the RadCom victim and the use of orthogonal MLSs as described in Subsection III-B3 are considered, which are henceforth occasionally referred to as the worst and best cases in the considered scenario, respectively. While only a higher noise floor is observed for PMCW with orthogonal MLSs, OFDM and OCDM, a stripe along the relative radial velocity axis at the point target range and its corresponding range sidelobes is observed in the radar images obtained by both CS and PMCW with same MLS for the RadCom interferer and the RadCom victim. This is explained by the fact that the correlation with an orthogonal MLS in the best PMCW case, symbol division in the OFDM case, and the PCCF in the OCDM case turn the interfering signal into a pseudonoise, therefore experiencing the full range processing gain that is proportional to $N_{\mathrm{subc}}^{\mathrm{OFDM}}$ and $N_{\mathrm{subch}}^{\mathrm{OCDM}}$, respectively. Conversely, the mixing procedure to originate the signal containing the beat frequencies in the CS RadCom system and the correlation with the same MLS in the worst PMCW case do not contribute to the experienced processing gain w.r.t. the interfering signal. In fact, only the DFTs for relative radial velocity estimation are able to transform the interfering signal contribution to the already estimated range cells into pseudonoise, being the effective processing gains w.r.t. the interfering signal in the CS and the worst PMCW cases around $10\log_{10} N_{\mathrm{chirp}}^{\mathrm{CS}} = 39.14\,\mathrm{dB}$ and $10\log_{10} A^{\mathrm{PMCW}} N_{\mathrm{PRBS}}^{\mathrm{PMCW}} = 37.10\,\mathrm{dB}$ lower than the listed values in Table 17. Considering the reduced noise bandwidth by a factor of 10 in the considered CS RadCom system, this would result in expected dynamic range reductions for the considered point target w.r.t. the interfering signal and noise of around $39.14\,\mathrm{dB}$ and $37.10\,\mathrm{dB}$ in the worst CS and PMCW cases, respectively, w.r.t. their OFDM and OCDM counterparts. The aforementioned values, however, only hold with the simplified assumption that the resulting pseudonoise from the interfering signal after radar signal processing is Gaussian.

Considering SIR values before radar signal processing that range from $-90\,\mathrm{dB}$ to $30\,\mathrm{dB}$, Fig. 21 shows the achieved dynamic range for the considered point target with the adopted signal and system parameters. The calculated dynamic range values can be described as the ratio between the point tar-

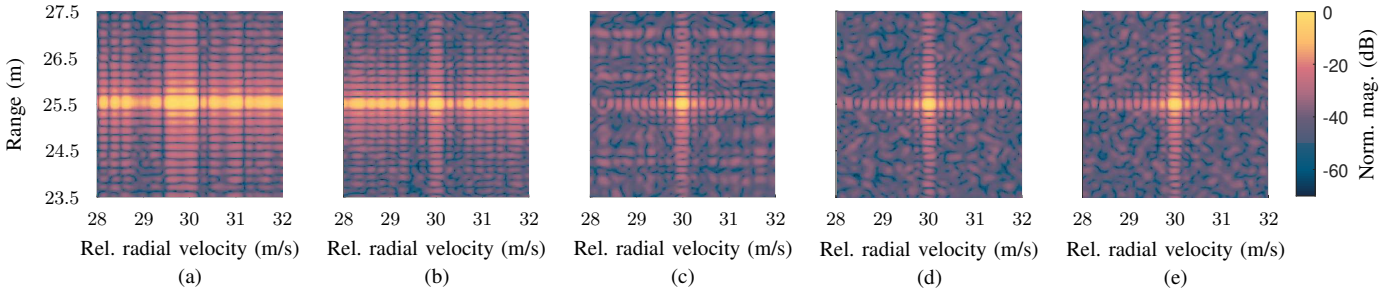

Fig. 20. Simulated range-velocity radar images under influence of a same-modulation-scheme interferer: (a) CS with full time and frequency overlap of interfering and victim RadCom signals, (b) PMCW with same PRBS for interferer and victim RadCom systems, (c) PMCW with orthogonal PRBSs for interferer and victim RadCom systems, (d) OFDM, and (e) OCDM. In all subfigures, same-modulation-scheme interferers and $SIR = -25\,\mathrm{dB}$ before radar signal processing were assumed.

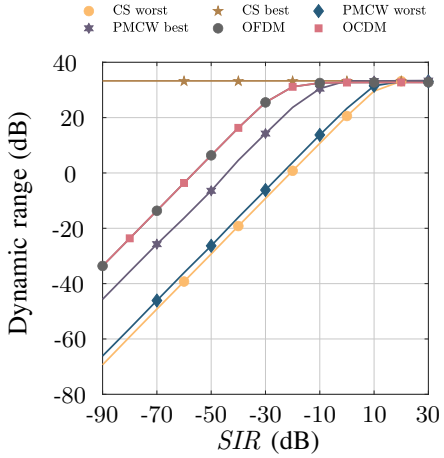

Fig. 21. Simulated dynamic range as a function of SIR w.r.t. same-modulation-scheme interfering signal before radar signal processing for RadCom systems based on all considered modulation schemes and parameterization. In this figure, CS worst represents the case with full overlap in time and frequency of the interfering and victim RadCom signals. In its turn, CS best represents the case where the interfering signal is shifted w.r.t. to the victim signal in time so that no observable beat frequencies are generated, therefore yielding no inteference. Similarly, PMCW worst represents the case where the interferer and victim RadCom systems use the same PRBS, whereas PMCW best represents the case where orthogonal PRBSs are adopted.

get contribution and the peak of the joint contribution of interference and noise in the radar image, and the ultimately presented results are the average dynamic ranges over multiple simulations. In addition to the considered cases in Fig. 20, the CS case where the interfering signal is shifted w.r.t. to the victim signal in time so that the resulting beat frequencies lie outside the observable range allowed by the adopted sampling frequency $F_\mathrm{s}^\mathrm{CS} = 100\,\mathrm{MHz}$, therefore yielding no inteference and being henceforth referred to as the best CS case. In practice, intermediate cases to the aforementioned case and the previously mentioned one with full time and frequency overlap of the interfering and victim RadCom signals are observed and can be detected and compensated for. For the sake of conciseness, those cases are not considered here and the reader is referred to [131]–[134] for further details. At the low SIR regime in Fig. 21, the achieved dynamic range by both OFDM and OCDM RadCom systems is around $35.67\,\mathrm{dB}$, $32.70\,\mathrm{dB}$, and $12.26\,\mathrm{dB}$ higher than in the worst CS, worst PMCW, and best PMCW cases, respectively. The aforementioned numbers indicate that the experienced dynamic ranges in the worst CS and PMCW cases are around $4\,\mathrm{dB}$ higher than originally predicted, which is explained by the fact that simply performing a DFT along the same range cells transforms the QPSK or BPSK modulation symbols of the interfering signal into a pseudonoise that follows a non-Gaussian distribution. In its turn, the reduced dynamic range in the best PMCW is explained by the considerably high sidelobes resulting from the PCCF between the orthogonal PRBSs [40]. Furthermore, the presented results in Fig. 21 show that negligible dynamic range losses are observed in the best PMCW, OFDM and OCDM cases for SIR values higher than around $-20\,\mathrm{dB}$, while SIRs of $20\,\mathrm{dB}$ or higher are demanded in the worst CS and PMCW cases. For low SIR regime, SIC can be performed by iteratively decoding signals from present interferers in the scenario, reconstructing them and subtracting their contributions from the overall received signal similarly to what is described in [64].

D. Influence of Interference on Communication Performance

For evaluating the influence of an interfering signal of the same modulation scheme on the communication performance of a victim RadCom receiver, the signal parameters from Table III are further considered, yielding the listed data rates in Table IV. Similarly to Subsection IV-C, it is assumed that the RadCom transmitter transmitting the signal of interest and the RadCom interferer adopt the same modulation scheme and are at the same position, therefore experiencing the same channel CIR which is assumed to be the same of the adopted Rayleigh channel in Subsection IV-B. Furthermore, as in Subsection IV-C, both the interference-free and worst case are considered for CS, and the cased assuming the use of same or orthogonal MLSs are considered for PMCW.

The simulated BER performances of all considered RadCom modulation schemes in the described scenario are presented in Fig. 22, where BER versus E_b/N_0 curves for SIRs ranging from $-10\,\mathrm{dB}$ to $20\,\mathrm{dB}$ are considered alongside with the interference-free case. The achieved results show that an SIR of $20\,\mathrm{dB}$ results in nearly the same BER performance as in

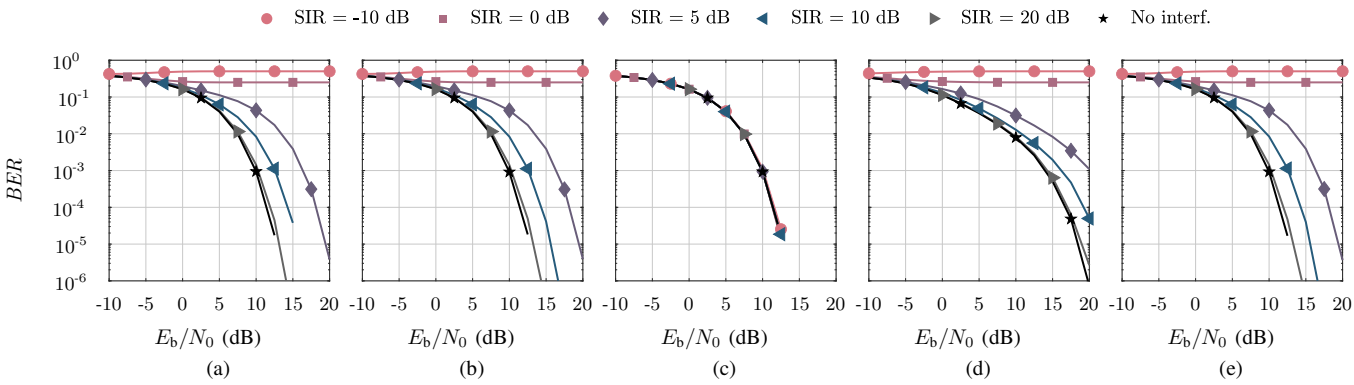

Fig. 22. Simulated BER performance under interference with RadCom systems based on: (a) CS, (b) PMCW with same PRBS, (c) PMCW with orthogonal PRBSs, (c) OFDM, and (d) OCDM modulation schemes. In all subfigures, same-modulation-scheme interferers and different SIR levels before communication signal processing were assumed.

the interference-free case for all four modulation schemes, except in the PMCW case where orthogonal sequences are assigned to the interferer and victim RadCom systems. As in the radar case from Subsection IV-C, a better performance is achieved in the aforementioned case w.r.t. its counterpart with same MLSs for the RadCom interferer and the RadCom victim. This is explained by the yielded isolation of the RadCom victim's signal w.r.t. the interfering one with the use of orthogonal MLSs, which already assumes a value of $24.81\,\mathrm{dB}$ at the lowest considered SIR value of $-10\,\mathrm{dB}$ and therefore makes the influence of the interfering signal at all considered SIR values negligible. Additionally, it can be observed that CS, PMCW, and OCDM RadCom systems still tend to outperform their OFDM counterpart for reasonable SIR values, while all modulation schemes present equally poor performance for lower SIR values than $5\,\mathrm{dB}$. This also includes a lower communication performance degradation due to interference compared to the RadCom systems based on OFDM in the considered scenario. To compensate for SIR values that may yield non-negligible performance degradation, which can either be caused by interference of an external RadCom system as so far considered or by reflections off radar targets of the signal transmitted by the same RadCom device whose receiver is evaluated, iterative SIC can also be performed following, e.g., a similar approach as the radar-oriented one in [64] as mentioned in Subsection IV-C.

E. Analysis of Multiplexing Schemes for MIMO Operation

As discussed in Subsections III-A3, III-B3, III-C3, and III-D3 for RadCom systems based on the CS, PMCW, OFDM, and OCDM modulation schemes, respectively, the use of multiplexing schemes for enabling MIMO or multiuser operation may change some of the signal parameters, as well as some of the radar and communication performance parameters. Assuming $N_{\mathrm{Tx}} = 4$ transmitters and adjusting the necessary parameters to keep the same frame durations from Table III, the effects of each multiplexing scheme on the aforementioned parameters is discussed as follows.

Based on the discussion on multiplexing strategies for CS-based RadCom systems in Subsection III-A3, the use of TDM changes the listed $T_{\mathrm{block}}^{\mathrm{CS}}$ and M^{CS} parameters in Table III to $T_{\mathrm{block}}^{\mathrm{CS}} = 40.80\,\mu\mathrm{s}$ and $M^{\mathrm{CS}} = 256$, respectively. Consequently, the maximum unambiguous relative radial velocity and the processing gain listed in Table IV are changed to $v_{\mathrm{max,unamb}}^{\mathrm{CS}} = 23.27\,\mathrm{m/s}$ and $G_{\mathrm{p}}^{\mathrm{CS}} = 54.10\,\mathrm{dB}$, respectively, and the data rate in a multiuser scenario is reduced to $\mathcal{R}_{\mathrm{QPSK}}^{\mathrm{CS}} = 49.02\,\mathrm{kb/s}$. In case FDM is used, the only differences are w.r.t. the listed parameters in Table III, namely the total occupied RF bandwidth becomes $B^{\mathrm{CS}} + (N_{\mathrm{Tx}} - 1)F_{\mathrm{s}}^{\mathrm{CS}}/2 = 1.15\,\mathrm{GHz}$ and the required ADC sampling rate becomes $N_{\mathrm{Tx}}F_{\mathrm{s}}^{\mathrm{CS}} = 400\,\mathrm{MHz}$. Finally, if CDM based on outer coding is adopted, the altered signal parameters are $T_{\mathrm{block}}^{\mathrm{CS}} = 40.80$ and $M^{\mathrm{CS}} = 256$, which result in a reduction of the maximum unambiguous relative radial velocity and of the communication data rate in a multiuser scenario, assuming the same aforementioned values in the TDM case. Unlike the TDM case, however, the processing gain $G_{\mathrm{p}}^{\mathrm{CS}}$ remains the same as the one listed in Table IV for the considered SISO-CS RadCom system.

Regarding PMCW-based RadCom systems, the use of orthogonal PRBSs as a CDM strategy produces neither changes in the signal parameters nor in the radar and communication ones as discussed in Subsection III-B3, being the only difference the reduced dynamic range even under absence of Doppler shifts. If, however, CDM based on outer coding is adopted, then the required duration to transmit a block becomes $T_{\mathrm{block}}^{\mathrm{PMCW}} = 20.44\,\mu\mathrm{s}$ and the number of transmitted blocks becomes $M^{\mathrm{PMCW}} = 512$ so that $T_{\mathrm{frame}}^{\mathrm{PMCW}}$ is kept the same as listed in Table III. Consequently, the maximum unambiguous relative radial velocity is changed to $v_{\mathrm{max,unamb}}^{\mathrm{PMCW}} = 46.40\,\mathrm{m/s}$, and the achieved data rate assuming BPSK modulation in a multiuser scenario is reduced to $\mathcal{R}_{\mathrm{BPSK}}^{\mathrm{PMCW}} = 48.88\,\mathrm{kb/s}$.

According to the discussion in Subsection III-C3, the parameters listed in Table III for the SISO case are kept if interleaved FDM is adopted in the considered OFDM-based RadCom system. However, as the number of assigned subcarriers to each of the $N_{\mathrm{Tx}} = 4$ transmitter is equal to $N_{\mathrm{subc}}^{\mathrm{OFDM}}/N_{\mathrm{Tx}} = 512$, changes are observed w.r.t. the radar parameters listed in Table IV for the SISO case. Those changes are the reduced maximum unambiguous range $R_{\mathrm{max,unamb}}^{\mathrm{OFDM}} = 76.80\,\mathrm{m}$ and the reduced processing gain $G_{\mathrm{p}}^{\mathrm{OFDM}} = 63.24\,\mathrm{dB}$. Furthermore, in

a multiuser scenario, the achieved data rate assuming QPSK modulation is also reduced to $\mathcal{R}_{\text{QPSK}}^{\text{OFDM}} = 400\,\text{Mb/s}$.

Following the discussion in Subsection III-D3, the use of FSP as an FDM approach in the considered OCDM-based RadCom system yields similar changes in the signal, radar and communication performance parameters as for the interleaved FDM in the OFDM case w.r.t. to the listed parameters for the SISO case in Tables III and IV. Those are a reduced maximum unambiguous range $R_{\text{max,unamb}}^{\text{OCDM}} = 76.80\,\text{m}$, a reduced processing gain $G_{\text{p}}^{\text{OCDM}} = 63.24\,\text{dB}$, and a data rate $\mathcal{R}_{\text{QPSK}}^{\text{OCDM}} = 400\,\text{Mb/s}$ in a multiuser scenario. Additionally, as discussed in Subsection III-D3, an upperbound $v_{\text{max,FSP}}^{\text{OCDM}} = 92.71\,\text{m/s}$ on the maximum tolerable relative radial velocity is set to ensure that only tolerable isolation losses among the transmitters are experienced. If, instead, outer coding is adopted as a CDM approach, the required duration to transmit a block is increased to $T_{\text{block}}^{\text{OCDM}} = 10.24\,\mu\text{s}$ and the number of transmitted blocks decreased to $M^{\text{OCDM}} = 1024$ to keep $T_{\text{frame}}^{\text{OCDM}}$ constant. This results in a reduced maximum unambiguous relative radial velocity $v_{\text{max,unamb}}^{\text{OCDM}} = 92.71\,\text{m/s}$ and in a reduction by a factor of $N_{\text{Tx}} = 4$ of the achieved data rate, which yields the same mentioned value in the FSP-based FDM case.

Besides the changes in the signal parameters, as well as the ones in the radar and communication performance parameters, the choice for a specific multiplexing scheme affects the robustness of the channel isolation against increasing Doppler shifts. To perform a comparative analysis among different modulation and multiplexing schemes, it is assumed that all $N_{\text{Tx}} = 4$ transmitters and a single receiver are at the same position and that there is no coupling between any of the transmitters and the aforementioned receiver. Additionally, it is assumed that a single point target with RCS $\sigma_{\text{RCS}} = 20\,\text{dBsm}$ is at a range of $25.5\,\text{m}$ in front of them as already assumed in the assumed scenarios in Subsections IV-B and IV-C. Considering that no constraints on maximum unambiguous or tolerable range are violated, Fig. 23 presents the mean achieved dynamic range by all $N_{\text{Tx}} = 4$ transmitters assuming the same parameters from Subsection IV-C. The achieved dynamic range results are calculated as the ratio between the point target contribution to the obtained radar image and the peak of the joint transmitter-to-transmitter interference and noise contribution. The presented results in Fig. 23 for velocities up to $92.71\,\text{m s}$, which corresponds to the maximum tolerable value in the OFDM-based RadCom system, show that most combinations of modulation and multiplexing schemes suffer nearly negligible dynamic range degradation for the whole considered velocity range. The only two exceptions are CS and PMCW with CDM based on outer coding, which present severe dynamic range loss even for low relative radial velocities. The poorer performance in the aforementioned cases is explained by their rather long block durations of respectively $T_{\text{block}}^{\text{CS}} = 40.80\,\mu\text{s}$ and $T_{\text{block}}^{\text{PMCW}} = 20.44\,\mu\text{s}$, which makes the sum of $N_{\text{Tx}} = 4$ repetitions of the original block for decoding non-coherent due to Doppler-shift-induced phase rotations, leading to decreased power of the point target contribution to the receive signal w.r.t. to noise similarly to what is discussed in [130].

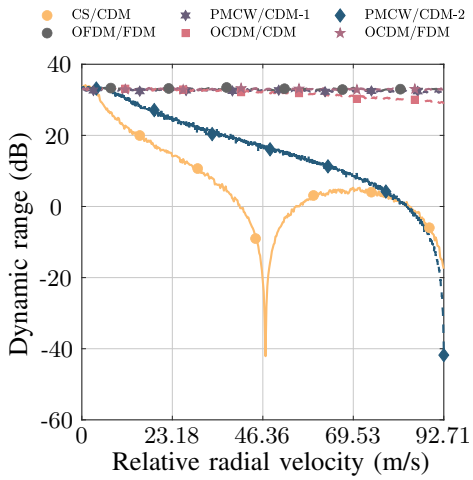

Fig. 23. Simulated dynamic range as a function of the point target radial relative velocity for RadCom systems based on all considered modulation schemes. In the PMCW case, CDM-1 represents the CDM approach based on orthogonal PRBS, while CDM-2 represents the CDM approach based on outer coding.

V. Conclusion

This article has presented an overview of widely known RadCom modulation schemes, i.e., CS, PMCW, OFDM, and OCDM. After a literature review on state-of-the-art research on RadCom enablement, thorough descriptions of RadCom systems based on the aforementioned modulation schemes as well as of parameters for efficiently assessing both radar and communication aspects of the overall system performance have been presented. Finally, a comparative performance analysis covering radar and communication performance parameter dependencies, a case study on a radar-centric RadCom system parameterization in a mid-range HAD scenario, interference analysis, and considerations on MIMO and multiuser operation has been carried out to validate the presented discussion.

In this context, information present in RadCom literature and novel contributions were combined to show that radar-centric RadCom systems based on CS and PMCW modulation schemes can achieve satisfactory radar performance and can be used for reliable, low-data-rate communication in applications such as traffic coordination and interference avoidance among RadCom sensors. Furthermore, it was shown that OFDM achieves considerably higher data rates than the two aforementioned modulation schemes, while also offering simultaneous high unambiguous range and relative radial velocity values. It was also was pointed out that the OCDM scheme achieves superior communication performance over all its counterparts, while demanding further investigation on alternative radar processing approaches to circumvent the undesired range sidelobes yielded by the correlation-based processing reported in the literature. Additionally, a comparative interference analyses focusing on radar and communication and addressing particular aspects of all considered was performed, which indicated the need for multiplexing scheme to avoid dynamic range reduction. Finally, it was shown that multiplexing schemes based on OFDM and OCDM tend to achieve overall better performance than their CS and PMCW counterparts in terms of channel isolation in MIMO or multiuser operation due

to multicarrier nature of the two first modulation schemes, which yields higher waveform orthogonality and enables more effective multiplexing strategies.

REFERENCES

[1] T. S. Rappaport et al., "Wireless communications and applications above 100 GHz: Opportunities and challenges for 6G and beyond," *IEEE Access*, vol. 7, pp. 78 729–78 757, Jun. 2019.

[2] C. de Lima et al., "Convergent communication, sensing and localization in 6G systems: An overview of technologies, opportunities and challenges," *IEEE Access*, vol. 9, pp. 26 902–26 925, Jan. 2021.

[3] S. Quan, W. Qian, J. Guq, and V. Zhang, "Radar-communication integration: An overview," in *2014 IEEE 7th Int. Conf. Adv. Infocomm Technol.*, Nov., pp. 98–103.

[4] A. R. Chiriyath, B. Paul, and D. W. Bliss, "Radar-communications convergence: Coexistence, cooperation, and co-design," *IEEE Trans. Cognitive Commun. Netw.*, vol. 3, no. 1, pp. 1–12, Mar. 2017.

[5] L. Zheng, M. Lops, Y. C. Eldar, and X. Wang, "Radar and communication coexistence: An overview: A review of recent methods," *IEEE Signal Process. Mag.*, vol. 36, no. 5, pp. 85–99, Sep. 2019.

[6] T. Wild, V. Braun, and H. Viswanathan, "Joint design of communication and sensing for beyond 5G and 6G systems," *IEEE Access*, vol. 9, pp. 30 845–30 857, Feb. 2021.

[7] J. A. Zhang et al., "An overview of signal processing techniques for joint communication and radar sensing," *IEEE J. Sel. Topics Signal Process.*, vol. 15, no. 6, pp. 1295–1315, Sep. 2021.

[8] L. Han and K. Wu, "Joint wireless communication and radar sensing systems - state of the art and future prospects," *IET Microw., Antennas & Propag.*, vol. 7, no. 11, pp. 876–885, Aug. 2013.

[9] J. A. Zhang et al., "Enabling joint communication and radar sensing in mobile networks – a survey," arXiv preprint arXiv:2006.07559 [eess.SP], Jan. 2021.

[10] R. Thomä, T. Dallmann, S. Jovanoska, P. Knott, and A. Schmeink, "Joint communication and radar sensing: An overview," in *2021 15th European Conf. Antennas Propag.*, Mar., pp. 1–5.

[11] O. Kanhere, S. Goyal, M. Beluri, and T. S. Rappaport, "Target localization using bistatic and multistatic radar with 5G NR waveform," arXiv preprint arXiv:2103.03426 [cs.IT], Mar. 2021.

[12] Z. Feng, Z. Fang, Z. Wei, X. Chen, Z. Quan, and D. Ji, "Joint radar and communication: A survey," *China Commun.*, vol. 17, no. 1, pp. 1–27, Jan. 2020.

[13] S. Mazahir, S. Ahmed, and M.-S. Alouini, "A survey on joint communication-radar systems," Oct. 2020.

[14] A. Hassanien, M. G. Amin, E. Aboutanios, and B. Himed, "Dual-function radar communication systems: A solution to the spectrum congestion problem," *IEEE Signal Process. Mag.*, vol. 36, no. 5, pp. 115–126, Sep. 2019.

[15] F. Liu, C. Masouros, A. P. Petropulu, H. Griffiths, and L. Hanzo, "Joint radar and communication design: Applications, state-of-the-art, and the road ahead," *IEEE Trans. Commun.*, vol. 68, no. 6, pp. 3834–3862, Jun. 2020.

[16] D. Ma, N. Shlezinger, T. Huang, Y. Liu, and Y. C. Eldar, "Joint radar-communication strategies for autonomous vehicles: Combining two key automotive technologies," *IEEE Signal Process. Mag.*, vol. 37, no. 4, pp. 85–97, Jul. 2020.

[17] Y. Luo, "Signal processing for joint communication and radar sensing techniques in autonomous vehicular networks," Ph.D. dissertation, Dep. Eng. Inf. Technol., Univ. Technol. Sydney, Australia, 2019.

[18] C. Sturm and W. Wiesbeck, "Waveform design and signal processing aspects for fusion of wireless communications and radar sensing," *Proc. IEEE*, vol. 99, no. 7, pp. 1236–1259, Jul. 2011.

[19] A. Gameiro, D. Castanheira, J. Sanson, and P. P. Monteiro, "Research challenges, trends and applications for future joint radar communications systems," *Wireless Pers. Commun.*, vol. 100, pp. 81–96, Mar. 2018.

[20] R. M. Mealey, "A method for calculating error probabilities in a radar communication system," *IEEE Trans. Sp. Electron. and Telemetry*, vol. 9, no. 2, pp. 37–42, Jun. 1963.

[21] C. Sturm, T. Zwick, and W. Wiesbeck, "An OFDM system concept for joint radar and communications operations," in *VTC Spring 2009 - IEEE 69th Veh. Technol. Conf.*, pp. 1–5.

[22] C. Waldschmidt, J. Hasch, and W. Menzel, "Automotive radar - from first efforts to future systems," *IEEE J. Microw.*, vol. 1, no. 1, pp. 135–148, 2021.

[23] S. M. Patole, M. Torlak, D. Wang, and M. Ali, "Automotive radars: A review of signal processing techniques," *IEEE Signal Process. Mag.*, vol. 34, no. 2, pp. 22–35, Mar. 2017.

[24] S. Dwivedi, A. N. Barreto, P. Sen, and G. Fettweis, "Target detection in joint frequency modulated continuous wave (FMCW) radar-communication system," in *2019 16th Int. Symp. Wireless Commun. Syst.*, Aug., pp. 277–282.

[25] S. Dwivedi, M. Zoli, A. N. Barreto, P. Sen, and G. Fettweis, "Secure joint communications and sensing using chirp modulation," in *2020 2nd 6G Wireless Summit*, Mar., pp. 1–5.

[26] C. Aydogdu, M. F. Keskin, N. Garcia, H. Wymeersch, and D. W. Bliss, "RadChat: Spectrum sharing for automotive radar interference mitigation," *IEEE Trans. Intell. Transp. Syst.*, vol. 22, no. 1, pp. 416–429, Jan. 2021.

[27] C. Aydogdu, M. F. Keskin, and H. Wymeersch, "Automotive radar interference mitigation via multi-hop cooperative radar communications," in *2020 17th European Radar Conf.*, Jan., pp. 270–273.

[28] G. Hakobyan and B. Yang, "High-performance automotive radar: A review of signal processing algorithms and modulation schemes," *IEEE Signal Process. Mag.*, vol. 36, no. 5, pp. 32–44, Sep. 2019.

[29] F. Roos, J. Bechter, C. Knill, B. Schweizer, and C. Waldschmidt, "Radar sensors for autonomous driving: Modulation schemes and interference mitigation," *IEEE Microw. Mag.*, vol. 20, no. 9, pp. 58–72, Sep. 2019.

[30] C. Aydogdu et al., "Radar interference mitigation for automated driving: Exploring proactive strategies," *IEEE Signal Process. Mag.*, vol. 37, no. 4, pp. 72–84, Jul. 2020.

[31] F. Engels, P. Heidenreich, M. Wintermantel, L. Stacker, M. Al Kadi, and A. M. Zoubir, "Automotive radars signal processing: Research directions and practical challenges," *IEEE J. Sel. Topics Signal Process. (Early Access)*, pp. 1–1, 2021.

[32] Z. Geng, "Evolution of netted radar systems," *IEEE Access*, vol. 8, pp. 124 961–124 977, Jul. 2020.

[33] F. Bozorgi, P. Sen, A. N. Barreto, and G. Fettweis, "RF front-end challenges for joint communication and radar sensing," in *2021 1st IEEE Inter. Online Symp. Joint Commun. Sens.*, Feb., pp. 1–6.

[34] A. N. Barreto, T. M. Pham, S. George, P. Sen, and G. Fettweis, "Analysis of a chirp-based waveform for joint communications and radar sensing (JC&S) using non-linear components," in *2021 15th European Conf. Antennas Propag.*, Mar., pp. 1–5.

[35] B. Nuss, L. Sit, M. Fennel, J. Mayer, T. Mahler, and T. Zwick, "MIMO OFDM radar system for drone detection," in *2017 18th Int. Radar Symp.*, Jun., pp. 1–9.

[36] O. Kanhere and T. S. Rappaport, "Position location for futuristic cellular communications: 5G and beyond," *IEEE Commun. Mag.*, vol. 59, no. 1, pp. 70–75, Jan. 2021.

[37] C. B. Barneto et al., "Radio-based sensing and environment mapping in millimeter-wave 5G and beyond networks," arXiv preprint arXiv:2102.11593 [eess.SP], Feb. 2021.

[38] M. Kronauge and H. Rohling, "New chirp sequence radar waveform," *IEEE Trans. Aerosp. Electron. Syst.*, vol. 50, no. 4, pp. 2870–2877, Oct. 2014.

[39] V. Giannini et al., "A 79 GHz phase-modulated 4 GHz-BW CW radar transmitter in 28 nm CMOS," *IEEE J. Solid-State Circuits*, vol. 49, no. 12, pp. 2925–2937, Dec. 2014.

[40] *Millimeter-Wave Radar SoC Integration in CMOS*, ser. The Cambridge RF and Microwave Engineering Series. Cambridge University Press, 2019, pp. 162–192.

[41] G. L. Stuber, J. R. Barry, S. W. McLaughlin, Ye Li, M. A. Ingram, and T. G. Pratt, "Broadband MIMO-OFDM wireless communications," *Proc. IEEE*, vol. 92, no. 2, pp. 271–294, Nov. 2004.

[42] T. Hwang, C. Yang, G. Wu, S. Li, and G. Ye Li, "OFDM and its wireless applications: A survey," *IEEE Trans. on Veh. Technol.*, vol. 58, no. 4, pp. 1673–1694, Aug. 2009.

[43] X. Ouyang and J. Zhao, "Orthogonal chirp division multiplexing," *IEEE Trans. Commun.*, vol. 64, no. 9, pp. 3946–3957, Sep. 2016.

[44] X. Ouyang, "Digital signal processing for fiber-optic communication systems," Ph.D. dissertation, Dept. Elect. Electron. Eng., Univ. College Cork, Ireland, 2017.

[45] C. B. Barneto, S. D. Liyanaarachchi, M. Heino, T. Riihonen, and M. Valkama, "Full duplex radio/radar technology: The enabler for advanced joint communication and sensing," *IEEE Wireless Commun.*, vol. 28, no. 1, pp. 82–88, Feb. 2021.

[46] B. Schweizer et al., "The fairy tale of simple all-digital radars: How to deal with 100 Gbit/s of a digital millimeter-wave MIMO radar on an FPGA [application notes]," *IEEE Microw. Mag.*, vol. 22, no. 7, pp. 66–76, Jul. 2021.

[47] L. Giroto de Oliveira, M. B. Alabd, B. Nuss, and T. Zwick, "An OCDM radar-communication system," in *2020 14th European Conf. Antennas Propag.*, Mar., pp. 1–5.

[48] B. Nuss, J. Mayer, S. Marahrens, and T. Zwick, "Frequency comb OFDM radar system with high range resolution and low sampling rate," *IEEE Trans. Microw. Theory Tech.*, vol. 68, no. 9, pp. 3861–3871, May 2020.

[49] B. Nuss, L. G. de Oliveira, and T. Zwick, "Frequency comb MIMO OFDM radar with nonequidistant subcarrier interleaving," *IEEE Microw. Wireless Compon. Lett.*, vol. 30, no. 12, pp. 1209–1212, Oct. 2020.

[50] D. Schindler, B. Schweizer, C. Knill, J. Hasch, and C. Waldschmidt, "MIMO-OFDM radar using a linear frequency modulated carrier to reduce sampling requirements," *IEEE Trans. Microw. Theory Tech.*, vol. 66, no. 7, pp. 3511–3520, Mar. 2018.

[51] C. Pfeffer, R. Feger, and A. Stelzer, "A stepped-carrier 77-GHz OFDM MIMO radar system with 4 GHz bandwidth," in *2015 European Radar Conf.*, Sep., pp. 97–100.

[52] B. Schweizer, C. Knill, D. Schindler, and C. Waldschmidt, "Stepped-carrier OFDM-radar processing scheme to retrieve high-resolution range-velocity profile at low sampling rate," *IEEE Trans. Microw. Theory Tech.*, vol. 66, no. 3, pp. 1610–1618, Mar. 2018.

[53] D. Schindler, B. Schweizer, C. Knill, J. Hasch, and C. Waldschmidt, "An integrated stepped-carrier OFDM MIMO radar utilizing a novel fast frequency step generator for automotive applications," *IEEE Trans.s Microw. Theory Tech.*, vol. 67, no. 11, pp. 4559–4569, Jun. 2019.

[54] C. Knill, B. Schweizer, S. Sparrer, F. Roos, R. F. H. Fischer, and C. Waldschmidt, "High range and doppler resolution by application of compressed sensing using low baseband bandwidth OFDM radar," *IEEE Trans. Microw. Theory Tech.*, vol. 66, no. 7, pp. 3535–3546, Jun. 2018.

[55] W. Scheiblhofer, R. Feger, A. Haderer, S. Scheiblhofer, and A. Stelzer, "In-chirp FSK communication between cooperative 77-GHz radar stations integrating variable power distribution between ranging and communication system," *Int. J. Microw. Wireless Technol.*, vol. 8, no. 4-5, pp. 825–832, 2016.

[56] M. Kucharski, A. Ergintav, W. A. Ahmad, M. Krstić, H. J. Ng, and D. Kissinger, "A scalable 79-GHz radar platform based on single-channel transceivers," *IEEE Trans. Microw. Theory Tech.*, vol. 67, no. 9, pp. 3882–3896, Sep. 2019.

[57] H. J. Ng, R. Hasan, and D. Kissinger, "A scalable four-channel frequency-division multiplexing MIMO radar utilizing single-sideband delta-sigma modulation," *IEEE Trans. Microw. Theory Tech.*, vol. 67, no. 11, pp. 4578–4590, Nov. 2019.

[58] H. J. Ng, M. Kucharski, W. Ahmad, and D. Kissinger, "Multi-purpose fully differential 61- and 122-GHz radar transceivers for scalable MIMO sensor platforms," *IEEE J. Solid-State Circuits*, vol. 52, no. 9, pp. 2242–2255, Sep. 2017.

[59] B. Nuss, A. Diewald, J. Schoepfel, D. Martini, N. Pohl, and T. Zwick, "76GHz OFDM radar demonstrator with real-time processing for automotive applications," in *2020 IEEE MTT-S Int. Conf. Microw. Intell. Mobility*, Nov., pp. 1–4.

[60] B. Farley, J. McGrath, and C. Erdmann, "An all-programmable 16-nm RFSoC for digital-RF communications," *IEEE Micro*, vol. 38, no. 2, pp. 61–71, Mar./Apr. 2018.

[61] S. Kumar, K. V. Mishra, S. Gautam, M. R. Bhavani Shankar, and B. Ottersten, "Interference mitigation methods for coexistence of radar and communication," in *2021 15th European Conf. Antennas Propag.*, Mar., pp. 1–4.

[62] M. F. Keskin, C. Aydogdu, and H. Wymeersch, "Stepped-carrier OFDM V2V resource allocation for sensing and communication convergence," in *2020 14th European Conf. on Antennas Propag.*, Mar., pp. 1–5.

[63] Y. L. Sit, "MIMO OFDM radar-communication system with mutual interference cancellation," Ph.D. dissertation, Inst. Radio Freq. Eng. Electron., Karlsruhe Inst. Technol., Germany, 2017.

[64] Y. L. Sit, B. Nuss, and T. Zwick, "On mutual interference cancellation in a MIMO OFDM multiuser radar-communication network," *IEEE Trans. Veh. Technol.*, vol. 67, no. 4, pp. 3339–3348, Dec. 2018.

[65] M. L. Rahman, J. A. Zhang, X. Huang, Y. J. Guo, and R. W. Heath, "Framework for a perceptive mobile network using joint communication and radar sensing," *IEEE Trans. Aerosp. Electron. Syst.*, vol. 56, no. 3, pp. 1926–1941, Jun. 2020.

[66] Z. Ni, J. A. Zhang, K. Yang, X. Huang, and T. A. Tsiftsis, "Waveform optimization with multiple performance metrics for broadband joint communication and radar sensing," arXiv preprint arXiv:2011.10943 [eess.SP], Nov. 2020.

[67] F. Liu, L. Zhou, C. Masouros, A. Li, W. Luo, and A. Petropulu, "Toward dual-functional radar-communication systems: Optimal waveform design," *IEEE Trans. Signal Process.*, vol. 66, no. 16, pp. 4264–4279, Aug. 2018.

[68] J. A. Zhang, X. Huang, Y. J. Guo, J. Yuan, and R. W. Heath, "Multibeam for joint communication and radar sensing using steerable analog antenna arrays," *IEEE Trans. Veh. Technol.*, vol. 68, no. 1, pp. 671–685, Jan. 2019.

[69] Y. Luo, J. A. Zhang, X. Huang, W. Ni, and J. Pan, "Multibeam optimization for joint communication and radio sensing using analog antenna arrays," *IEEE Trans. Veh. Technol.*, vol. 69, no. 10, pp. 11 000–11 013, Oct. 2020.

[70] M. Heino, C. B. Barneto, T. Riihonen, and M. Valkama, "Design of phased array architectures for full-duplex joint communications and sensing," in *2021 15th European Conf. Antennas Propag.*, Mar., pp. 1–5.

[71] S. H. Dokhanchi, B. S. Mysore R, M. Kobayashi, and B. Ottersten, "Multicasting precoder design for vehicular joint radar-communication systems," in *2021 1st IEEE Int. Online Symp. Joint Commun. Sens.*, Feb., pp. 1–6.

[72] S. D. Liyanaarachchi, C. Baquero Barneto, T. Riihonen, M. Heino, and M. Valkama, "Joint multi-user communication and MIMO radar through full-duplex hybrid beamforming," in *2021 1st IEEE Int. Online Symp. Joint Commun. Sens.*, Feb., pp. 1–5.

[73] M. Heino et al., "Recent advances in antenna design and interference cancellation algorithms for in-band full duplex relays," *IEEE Communications Magazine*, vol. 53, no. 5, pp. 91–101, May 2015.

[74] C. B. Barneto, S. D. Liyanaarachchi, T. Riihonen, L. Anttila, and M. Valkama, "Multibeam design for joint communication and sensing in 5G new radio networks," in *ICC 2020 - 2020 IEEE Int. Conf. Commun.*, Jun., pp. 1–6.

[75] A. M. Elbir, K. V. Mishra, and S. Chatzinotas, "Terahertz-band joint ultra-massive MIMO radar-communications: Model-based and model-free hybrid beamforming," arXiv preprint arXiv:2103.00328 [eess.SP], Feb. 2021.

[76] M. Temiz, E. Alsusa, and M. W. Baidas, "Optimized precoders for massive mimo ofdm dual radar-communication systems," *IEEE Trans. Commun. (Early Access)*, pp. 1–1, Mar. 2021.

[77] A. Hassanien, M. G. Amin, Y. D. Zhang, and F. Ahmad, "Dual-function radar-communications: Information embedding using sidelobe control and waveform diversity," *IEEE Trans. Signal Process.*, vol. 64, no. 8, pp. 2168–2181, Apr. 2016.

[78] Z. Geng, R. Xu, H. Deng, and B. Himed, "Fusion of radar sensing and wireless communications by embedding communication signals into the radar transmit waveform," *IET Radar, Sonar & Navigation*, vol. 12, pp. 632–640(8), Jun. 2018.

[79] M. B. Alabd, B. Nuss, C. Winkler, and T. Zwick, "Partial chirp modulation technique for chirp sequence based radar communications," in *2019 16th European Radar Conf.*, Oct., pp. 173–176.

[80] U. Kumbul, N. Petrov, F. van der Zwan, C. S. Vaucher, and A. Yarovoy, "Experimental investigation of phase coded FMCW for sensing and communications," in *2021 15th European Conf. Antennas Propag.*, Mar., pp. 1–5.

[81] M. B. Alabd, L. G. de Oliveira, B. Nuss, W. Wiesbeck, and T. Zwick, "Time-frequency shift modulation for chirp sequence based radar communications," in *2020 IEEE MTT-S Int. Conf. Microw. Intell. Mobility*, Nov., pp. 1–4.

[82] T. M. Pham, A. N. Barreto, and G. P. Fettweis, "Efficient communications for overlapped chirp-based systems," *IEEE Wireless Commun. Lett.*, vol. 9, no. 12, pp. 2202–2206, Dec. 2020.

[83] C. Davis, M. Hegde, W. E. Stark, A. Eshraghi, M. Goldenberg, and M. Ali, "Vehicle radar system with a shared radar and communication system," Patent WO 2017/187 331 A1, 11 2, 2017. [Online]. Available: https://patentscope.wipo.int/search/en/detail.jsf?docId=WO2017187331

[84] S. H. Dokhanchi, M. R. B. Shankar, Y. A. Nijsure, T. Stifter, S. Sedighi, and B. Ottersten, "Joint automotive radar-communications waveform design," in *2017 IEEE 28th Annu. Int. Symp. Pers., Indoor, Mobile Radio Commun.*, Oct., pp. 1–7.

[85] S. H. Dokhanchi, B. S. Mysore, K. V. Mishra, and B. Ottersten, "A mmWave automotive joint radar-communications system," *IEEE Trans. Aerosp. Electron. Syst.*, vol. 55, no. 3, pp. 1241–1260, Jun. 2019.

[86] K. V. Mishra, M. R. Bhavani Shankar, V. Koivunen, B. Ottersten, and S. A. Vorobyov, "Toward millimeter-wave joint radar communications: A signal processing perspective," *IEEE Signal Process. Mag.*, vol. 36, no. 5, pp. 100–114, Sep. 2019.

[87] Y. Liu, G. Liao, J. Xu, Z. Yang, and Y. Zhang, "Adaptive OFDM integrated radar and communications waveform design based on infor-

mation theory," *IEEE Commun. Lett.*, vol. 21, no. 10, pp. 2174–2177, Jul. 2017.

[88] C. Shi, F. Wang, S. Salous, and J. Zhou, "Low probability of intercept-based optimal OFDM waveform design strategy for an integrated radar and communications system," *IEEE Access*, vol. 6, pp. 57 689–57 699, Oct. 2018.

[89] C. B. Barneto et al., "Full-duplex OFDM radar with LTE and 5G NR waveforms: Challenges, solutions, and measurements," *IEEE Trans. Microw. Theory Tech.*, vol. 67, no. 10, pp. 4042–4054, Oct. 2019.

[90] S. D. Liyanaarachchi, C. B. Barneto, T. Riihonen, and M. Valkama, "Joint OFDM waveform design for communications and sensing convergence," in *ICC 2020 - 2020 IEEE Int. Conf. Commun.*, Jun., pp. 1–6.

[91] ——, "Experimenting joint vehicular communications and sensing with optimized 5G NR waveform," in *2021 IEEE 93rd Veh. Technol. Conf.: VTC2021-Spring*, Apr., pp. 1–5.

[92] L. Giroto de Oliveira, B. Nuss, M. B. Alabd, Y. Li, L. Yu, and T. Zwick, "MIMO-OCDM-based joint radar sensing and communication," in *2021 15th European Conf. Antennas Propag.*, Mar., pp. 1–5.

[93] K. M. Braun, "OFDM radar algorithms in mobile communication networks," Ph.D. dissertation, Commun. Eng. Lab, Karlsruhe Inst. Technol., Germany, 2014.

[94] L. Giroto de Oliveira, M. de Lima Filomeno, H. V. Poor, and M. Vidal Ribeiro, "Orthogonal chirp-division multiplexing for power line sensing via time-domain reflectometry," *IEEE Sensors J.*, vol. 21, no. 2, pp. 955–964, Jan. 2021.

[95] M. S. Omar and X. Ma, "Performance analysis of OCDM for wireless communications," *IEEE Trans. Wireless Commun. (Early Access)*, vol. 20, no. 7, pp. 4032–4043, Feb. 2021.

[96] L. Giroto de Oliveira, G. Ribeiro Colen, A. J. Han Vinck, and M. Vidal Ribeiro, "Resource allocation in HS-OFDM-based PLC systems: A tutorial," *J. Commun. Inf. Sys.*, vol. 33, no. 1, pp. 308–321, Oct. 2018.

[97] R. Bomfin, M. Chafii, and G. Fettweis, "Low-complexity iterative receiver for orthogonal chirp division multiplexing," in *2019 IEEE Wireless Commun. and Netw. Conf. Workshop*, Apr., pp. 1–6.

[98] M. S. Omar and X. Ma, "The effects of narrowband interference on OCDM," in *2020 IEEE 21st Inter. Workshop Signal Process. Advances in Wireless Commun.*, May 2020, pp. 1–5.

[99] X. Ouyang, C. Antony, F. Gunning, H. Zhang, and Y. L. Guan, "Discrete Fresnel transform and its circular convolution," arXiv preprint arXiv:1510.00574 [cs.IT], Oct. 2015.

[100] L. Gaudio, M. Kobayashi, G. Caire, and G. Colavolpe, "On the effectiveness of otfs for joint radar parameter estimation and communication," *IEEE Trans. Wireless Commun.*, vol. 19, no. 9, pp. 5951–5965, Jun. 2020.

[101] J. Sanson, A. Gameiro, D. Castanheira, and P. P. Monteiro, "24 GHz QAM-FBMC radar with communication system (RadCom)," in *2018 Asia-Pacific Microw. Conf.*, Nov., pp. 678–680.

[102] J. B. Sanson, D. Castanheira, A. Gameiro, and P. P. Monteiro, "Non-orthogonal multicarrier waveform for radar with communications systems: 24 GHz GFDM radcom," *IEEE Access*, vol. 7, pp. 128 694–128 705, Sep. 2019.

[103] G. Huang, Y. Ding, S. Ouyang, and V. Fusco, "Index modulation for OFDM RadCom systems," *The J. Eng.*, vol. 2021, no. 2, pp. 61–72, Jan. 2021.

[104] T. M. Schmidl and D. C. Cox, "Robust frequency and timing synchronization for OFDM," *IEEE Trans. Commun.*, vol. 45, no. 12, pp. 1613–1621, Dec. 1997.

[105] W. Van Thillo, V. Giannini, D. Guermandi, S. Brebels, and A. Bourdoux, "Impact of ADC clipping and quantization on phase-modulated 79 GHz CMOS radar," in *2014 11th European Radar Conf.*, Oct. 2014, pp. 285–288.

[106] Texas Instruments. AWR 1843 single-chip 77- to 79-GHz FMCW radar sensor. [Online]. Available: https://www.ti.com/lit/ds/symlink/awr1843.pdf?ts=1617610069077

[107] V. Winkler, "Range doppler detection for automotive FMCW radars," in *2007 European Microw. Conf.*, Oct., pp. 1445–1448.

[108] A. Diewald, T. Antes, B. Nuss, M. Pauli, and T. Zwick, "Range Doppler migration synthesis for realistic radar target simulation," in *2021 IEEE Topical Conf. on Wireless Sensors and Sensor Netw.*, Jan., pp. 1–3.

[109] A. Diewald, T. Antes, B. Nuss, and T. Zwick, "Implementation of range Doppler migration synthesis for radar target simulation," in *2021 IEEE 93rd Veh. Technol. Conf.: VTC2021-Spring*, Apr., pp. 1–5.

[110] J. Bechter, F. Roos, and C. Waldschmidt, "Compensation of motion-induced phase errors in TDM MIMO radars," *IEEE Microw. Wireless Compon. Lett.*, vol. 27, no. 12, pp. 1164–1166, Sep. 2017.

[111] S. Häfner and R. Thomä, "Compensation of motion-induced phase errors and enhancement of Doppler unambiguity in TDM-MIMO systems by model-based estimation," *IEEE Sensors Lett.*, vol. 4, no. 10, pp. 1–4, Sep. 2020.

[112] Y. L. Sit, G. Li, S. Manchala, H. Afrasiabi, C. Sturm, and U. Lubbert, "BPSK-based MIMO FMCW automotive-radar concept for 3D position measurement," in *2018 15th European Radar Conf.*, Sep. 2018.

[113] A. Bourdoux, U. Ahmad, D. Guermandi, S. Brebels, A. Dewilde, and W. Van Thillo, "PMCW waveform and MIMO technique for a 79 GHz CMOS automotive radar," in *2016 IEEE Radar Conf.*, May, pp. 1–5.

[114] D. Guermandi et al., "A 79-GHz 2×2 MIMO PMCW radar SoC in 28-nm CMOS," *IEEE J. Solid-State Circuits*, vol. 52, no. 10, pp. 2613–2626, Oct. 2017.

[115] O. Bialer, A. Jonas, and T. Tirer, "Code optimization for fast chirp FMCW automotive MIMO radar," *IEEE Trans. Veh. Technol.*, vol. 70, no. 8, pp. 7582–7593, Jul. 2021.

[116] J. Overdevest, F. Jansen, F. Uysal, and A. Yarovoy, "Doppler influence on waveform orthogonality in 79 GHz MIMO phase-coded automotive radar," *IEEE Trans. Veh. Technol.*, vol. 69, no. 1, pp. 16–25, Jan. 2020.

[117] C. Sturm, Y. L. Sit, M. Braun, and T. Zwick, "Spectrally interleaved multi-carrier signals for radar network applications and multi-input multi-output radar," *IET Radar, Sonar & Navigation*, vol. 7, no. 3, pp. 261–269, Mar. 2013.

[118] G. E. A. Franken, H. Nikookar, and P. V. Genderen, "Doppler tolerance of OFDM-coded radar signals," in *2006 European Radar Conf.*, Sep., pp. 108–111.

[119] B. Nuss, J. Mayer, and T. Zwick, "Limitations of MIMO and multi-user access for OFDM radar in automotive applications," in *2018 IEEE MTT-S Int. Conf. Microw. Intell. Mobility*, Apr., pp. 1–4.

[120] C. Knill, F. Embacher, B. Schweizer, S. Stephany, and C. Waldschmidt, "Coded OFDM waveforms for MIMO radars," *IEEE Trans. Veh. Technol.*, pp. 1–1, Apr. 2021.

[121] X. Ouyang, O. A. Dobre, Y. L. Guan, and J. Zhao, "Chirp spread spectrum toward the Nyquist signaling rate – orthogonality condition and applications," *IEEE Signal Process. Lett.*, vol. 24, no. 10, pp. 1488–1492, 2017.

[122] R. Bomfin, M. Chafii, and G. Fettweis, "A novel iterative receiver design for CP-free transmission under frequency-selective channels," *IEEE Commun. Lett.*, vol. 24, no. 3, pp. 525–529, Dec. 2020.

[123] M. S. Omar and X. Ma, "Spectrum design for orthogonal chirp division multiplexing transmissions," *IEEE Wireless Commun. Lett.*, vol. 9, no. 11, pp. 1990–1994, Nov. 2020.

[124] ——, "Designing OCDM-based multi-user transmissions," in *2019 IEEE Global Commun. Conf.*, Dec., pp. 1–6.

[125] G. Lellouch, A. K. Mishra, and M. Inggs, "Design of OFDM radar pulses using genetic algorithm based techniques," *IEEE Trans. Aerosp. Electron. Syst.*, vol. 52, no. 4, pp. 1953–1966, Aug. 2016.

[126] J. L. G. Monsalve, "GreenOFDM a new method for OFDM PAPR reduction," Ph.D. dissertation, École doctorale Électronique, Électrotechnique, Automatique et Traitement du Signal, Communauté Université Grenoble Alpes, France, 2019.

[127] X. Ouyang and J. Zhao, "Orthogonal chirp division multiplexing for coherent optical fiber communications," *J. Lightw. Technol.*, vol. 34, no. 18, pp. 4376–4386, Aug. 2016.

[128] A. Diewald et al., "Radar target simulation for vehicle-in-the-loop testing," *Vehicles*, vol. 3, no. 2, pp. 257–271, May 2021.

[129] A. Diewald, B. Nuss, M. Pauli, and T. Zwick, "Arbitrary angle of arrival in radar target simulation," *IEEE Trans. Microw. Theory Tech. (Early Access)*, pp. 1–1, Aug. 2021.

[130] L. Giroto de Oliveira et al., "Doppler shift tolerance of accumulation and outer coding in MIMO-PMCW radar," *IEEE Microw. Wireless Compon. Lett.*, in press, https://doi.org/10.1109/LMWC.2021.3123691.

[131] T. Schipper, S. Prophet, M. Harter, L. Zwirello, and T. Zwick, "Simulative prediction of the interference potential between radars in common road scenarios," *IEEE Trans. Electromagn. Compat.*, vol. 57, no. 3, pp. 322–328, Jun. 2015.

[132] C. Fischer, H. L. Blöcher, J. Dickmann, and W. Menzel, "Robust detection and mitigation of mutual interference in automotive radar," in *2015 16th Int. Radar Symp.*, Jun. 2015, pp. 143–148.

[133] K. Hahmann, S. Schneider, and T. Zwick, "Evaluation of probability of interference-related ghost targets in automotive radars," in *2018 IEEE MTT-S Int. Conf. Microw. Intell. Mobility*, Apr. 2018, pp. 1–4.

[134] K. Hahmann, S. Schneider, , and T. Zwick, "Analysis of interference between vast numbers of automotive radars considering stochastic temporal conditions," *Progress In Electromagnetics Research M*, vol. 94, pp. 131–142, Jul. 2020.

This is the author's version of an article that has been published in the IEEE TRANSACTIONS ON MICROWAVE THEORY AND TECHNIQUES. Changes were made to this version by the publisher prior to publication. The final version of record is available at https://doi.org/10.1109/TMTT.2021.3126887

Lucas Giroto de Oliveira (Graduate Student Member, IEEE) received the B.Sc. and M.Sc. degrees in electrical engineering with a major in electronic systems from the Federal University of Juiz de Fora, Juiz de Fora, Brazil, in 2017 and 2019, respectively. He is currently pursuing the Dr.-Ing. (Ph.D.E.E.) degree at the Karlsruhe Institute of Technology (KIT), Karlsruhe, Germany.

He was with the Digital Communications Group, University of Duisburg-Essen, Duisburg, Germany, from 2015 to 2016, with a Science without Borders (CsF) scholarship funded by Coordenação de Aperfeiçoamento de Pessoal de Nível Superior (CAPES), Brazil. Since 2019, he has been a Research Associate with the Institute of Radio Frequency Engineering and Electronics (IHE), KIT. His research interests are in the areas of signal processing, digital communication, and their applications to integrated radar sensing and communication systems and radar networks.

Mr. Giroto de Oliveira was a recipient of the Research Grant for Doctoral Programmes in Germany from the German Academic Exchange Service (DAAD) from April 2019 to March 2021.

Benjamin Nuss (Graduate Student Member, IEEE) received the B.Sc. and M.Sc. degrees in electrical engineering and information technology from the Karlsruhe Institute of Technology (KIT), Karlsruhe, Germany, in 2012 and 2015, respectively, and the Dr.-Ing. (Ph.D.E.E) degree from KIT, in 2021.

He is currently working as a Group Leader for radar systems at the Institute of Radio Frequency Engineering and Electronics (IHE). The focus of his work is on the development of efficient future radar waveforms and interference mitigation techniques for multiuser scenarios. His current research interests include orthogonal frequency-division multiplexing-based multiple-input multiple-output radar systems for future automotive applications and drone detection.

Mohamad Basim Alabd (Graduate Student Member, IEEE) received the B.Sc. and M.Sc. degrees in electronics and telecommunications from Al-Baath University, Homs, Syria, in 2010 and 2014, respectively.

He was a Research Associate with the Chair of Information Systems, Innovation & Value Creation (WI1), Friedrich-Alexander-Universität Erlangen-Nürnberg, Nuremberg, Germany. From 2010 to 2014, he was with Syrian Telecommunication Company, Homs, and worked there in different positions. He has been a Research Associate with the Institute of Radio Frequency Engineering and Electronics (IHE), Karlsruhe Institute of Technology, Karlsruhe, Germany, since 2017. His current research interests include chirp sequence (CS) joint radar-communication and orthogonal frequency-division multiplexing-based multiple-input?multiple-output radar systems for future automotive applications.

Axel Diewald (Graduate Student Member, IEEE) received the B.Sc. and M.Sc. degrees in electrical engineering and information technology from the Karlsruhe Institute of Technology (KIT), Karlsruhe, Germany, in 2015 and 2017, respectively, where he is currently pursuing the Ph.D. degree in electrical engineering (EE) at the Institute of Radio Frequency Engineering and Electronics (IHE).

His main research interests include digital radar target simulation for the purpose of automotive radar sensor validation and realistic target modeling.

Mario Pauli (Senior Member, IEEE) received the Dipl.-Ing. (M.S.E.E.) degree in electrical engineering from the University of Karlsruhe, Karlsruhe, Germany, in 2003, and the Dr.-Ing. (Ph.D.E.E.) degree from the Karlsruhe Institute of Technology (KIT), Karlsruhe, in 2011.

He was a Lecturer for radar and smart antennas of the Carl Cranz Series for Scientific Education. In 2002, he spent four months at the IBM Thomas J. Watson Research Center, Yorktown Heights, NY, USA, working on time- and frequency-domain measurement systems for the characterization of the 60-GHz indoor radio channel. From 2004 to 2011, he was a Research Assistant with the Institut für Höchstfrequenztechnik und Elektronik (IHE), University of Karlsruhe. Since 2011, he has been a Senior Researcher and a Lecturer with the Institute of Radio Frequency Engineering and Electronics (IHE), KIT. He is currently a Co-Founder and the Managing Director of PKTEC GmbH, Schutterwald, Germany, and a Co-Founder of Wellenzahl Radar- und Sensortechnik GmbH & Company KG, Karlsruhe. His current research interests include radar and sensor systems, radar cross section (RCS) measurements, antennas, and millimeter-wave packaging.

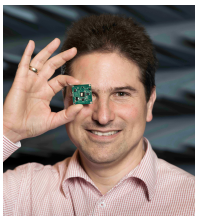

Thomas Zwick (Fellow, IEEE) received the Dipl.-Ing. (M.S.E.E.) and Dr.-Ing. (Ph.D.E.E.) degrees from the Universität Karlsruhe (TH), Karlsruhe, Germany, in 1994 and 1999, respectively.

From 1994 to 2001, he was a Research Assistant with the Institut für Höchstfrequenztechnik und Elektronik (IHE), TH. In February 2001, he joined IBM as Research Staff Member at the IBM Thomas J. Watson Research Center, Yorktown Heights, NY, USA. From October 2004 to September 2007, he was with Siemens AG, Lindau, Germany. During that period, he managed the RF development team for automotive radars. In October 2007, he became a Full Professor with the Karlsruhe Institute of Technology (KIT), Karlsruhe. He is currently the Director of the Institute of Radio Frequency Engineering and Electronics (IHE), KIT. He is a co-editor of three books and the author or a co-author of 120 journal articles, over 400 contributions at international conferences, and 15 granted patents. His research topics include wave propagation, stochastic channel modeling, channel measurement techniques, material measurements, microwave techniques, millimeter-wave antenna design, wireless communication, and radar system design.

Dr. Zwick has been a member of the Heidelberg Academy of Sciences and Humanities since 2017. Since 2019, he has been a member of acatech (German National Academy of Science and Engineering). His research team received over ten best paper awards at international conferences. In 2013, he was the General Chair of the International Workshop on Antenna Technology (iWAT 2013) in Karlsruhe and the IEEE MTT-S International Conference on Microwaves for Intelligent Mobility (ICMIM) in Heidelberg in 2015. He was the TPC Chair of the European Microwave Conference (EuMC) 2013 and the General TPC Chair of the European Microwave Week (EuMW) 2017. In 2023, he will be the General Chair of EuMW in Berlin. He has served on the technical program committees (TPC) of several scientific conferences. From 2008 to 2015, he was the president of the Institute for Microwaves and Antennas (IMA). He was selected as a Distinguished IEEE Microwave Lecturer for the 2013-2015 period with his lecture on "QFN Based Packaging Concepts for Millimeter-Wave Transceivers." In 2019, he became the Editor-in-Chief of the IEEE MICROWAVE AND WIRELESS COMPONENTS LETTERS.